UAV-Assisted mmWave and THz-Enabled Hybrid Heterogeneous Network

By

Adil Ali Raja

NUST201590310PSEECS0515F

Supervisor

Dr. Syed Ali Hassan

Department of Electrical Engineering

A thesis submitted in partial fulfillment of the requirements for the degree of

In

School of Electrical Engineering and Computer Science,

National University of Sciences and Technology (NUST),

Islamabad, Pakistan.

(2021)

Approval

It is certified that the contents and form of the thesis entitled "**UAV-Assisted mmWave and THz-Enabled Hybrid Heterogeneous Network**" submitted by **Adil Ali Raja** have been found satisfactory for the requirement of the degree.

Advisor: **Dr. Syed Ali Hassan**

Signature: _____

Date: _____

Committee Member 1: **Dr. Hassaan Khaliq Qureshi**

Signature: _____

Date: _____

Committee Member 2: **Dr. Fahd Ahmed Khan**

Signature: _____

Date: _____

Committee Member 3: **Dr. Shahryar Saleem (Air University)**

Signature: _____

Date: _____

Abstract

Heterogeneous networks (HetNets) are becoming a promising solution for future wireless systems to satisfy the high data rate requirements. Specifically, with the advent of millimeter wave (mmWave) and TeraHertz (THz) communication, there is a need to redesign and analyze the conventional cellular systems. Unmanned Aerial Vehicles (UAVs) are becoming an integral part of communication framework in an HetNet owing to its fast mobility and quick deployment in crowdy or disastrous hit areas. UAVs can be deployed to offload heavy traffic in scenarios such as a football match in a stadium or to provide infrastructure if existing communication infrastructure get destroyed such as by an earthquake or a storm. This research focuses on the analysis of SINR and rate coverage probabilities in a HetNet comprising of above mentioned technologies. This research also considered wireless backhauling to the core network by replacing cumbersome wired channels to the core. This research also introduces a stochastic geometry framework for the analysis of downlink coverage probability in a multi-tier HetNet consisting of macro-base station (MBS) operating at sub-6 GHz, mmWave small BSs and unmanned aerial vehicles (UAVs) operating at 28 GHz and THz frequencies enabled BSs. The effectiveness of the HetNet is analyzed on various performance metrics including association and coverage probabilities for different network parameters.

The analytical expressions for the coverage probability for each tier have been derived in this research. Monte Carlo simulations are performed to evaluate the significance of the model. It has been shown that the mmWave and THz-enabled cells provide significant improvement in the achievable data rates because of their high available bandwidth, however, they have a degrading effect on the coverage probabilities due to their high propagation losses. It has also been shown that UAVs due to its mobile deployment provide better coverage to end users where signals from the conventional MBS does not have enough strength. This research also highlight a suitable combination of tier densities required to achieve the QoS requirements.

Dedication

I dedicate this thesis to my late mother, my father and my family and friends.

List of Publications

- A. A. Raja, H. Pervaiz, S. A. Hassan, S. Garg, M. S. Hossain and M. J. Piran, ”Coverage Analysis of mmWave and THz-Enabled Aerial and Terrestrial Heterogeneous Networks,” in IEEE Transactions on Intelligent Transportation Systems, doi: 10.1109/TITS.2021.3086958. (Impact Factor: 6.492)

- A. A. Raja, M. A. Jamshed, H. Pervaiz and S. A. Hassan, ”Performance Analysis of UAV-assisted Backhaul Solutions in THz enabled Hybrid Heterogeneous Network,” IEEE INFOCOM 2020 - IEEE Conference on Computer Communications Workshops (INFOCOM WKSHPS), 2020, pp. 628-633, doi: 10.1109/INFOCOMWKSHPS50562.2020.9163026.

Certificate of Originality

I hereby declare that this submission is my own work and to the best of my knowledge it contains no materials previously published or written by another person, nor material which to a substantial extent has been accepted for the award of any degree or diploma at NUST SEECS or at any other educational institute, except where due acknowledgement has been made in the thesis. Any contribution made to the research by others, with whom I have worked at NUST SEECS or elsewhere, is explicitly acknowledged in the thesis.

I also declare that the intellectual content of this thesis is the product of my own work, except for the assistance from others in the project's design and conception or in style, presentation and linguistics which has been acknowledged.

Author Name: **Adil Ali Raja**

Signature: _____

Acknowledgment

I would like to express my gratitude to my supervisor Dr. Syed Ali Hassan who guided and helped me in every phase throughout my degree. I would also like to especially thank Dr. Haris Pervez whose guidance throughout my research phase is a key factor that I am able to write this thesis.

I also want to thank my colleagues at Information Processing and Transmissions Lab, who are always available to guide me during my research.

Lastly, I acknowledge the support of my family especially my wife for constant prayers and moral support. I also want to thank my friends especially Usman Haider who are always there to guide and motivate me throughout my PhD.

Table of Contents

List of Figures

List of Tables

Chapter 1

Introduction

In today's world, the mobile communication is used to connect everything everywhere and is not limited to only connect people [2–4]. The existing technologies needed a sudden revamp in order to cope with such significant requirements which give rise to HetNets and 5G and beyond technologies [5], [6]. To meet all these advancements, achieving high data rate is a pivotal factor [7], [8]. 5G and beyond technologies make use of mmWave and TeraHertz(THz) band to provide such high data rate requirements [9–11]. To furthur enhance the performance of networks 3rd Generation Partnership Project (3GPP) have included Heterogeneous networks (HetNets) to mitigate the coverage holes issue and also to provide communication in disaster hit and overly crowded areas [12], [13].

1.1 Heterogeneous Networks

The communication in the world has changed dramatically over the course of several decades. The transition from downloading a single image file in minutes to a

complete movie in seconds has become possible thanks to the emergence of new generations of communication. Now people wants to have lightning fast speed at all times everywhere. This gave rise to the need of Heterogeneous networks comprising of different technologies such as mmWave, THz communication [14–25] and also the use of UAVs. UAVs are most suitable for areas requiring immediate assistance and overly crowded spaces. UAV with its dynamic placement is able to give a good connection to the user by having a good line of sight (LoS) connection [26], [27].

1.2 Millimeter wave Communication

Communication which takes place in 30 GHz-300 GHz frequency band is referred as Millimeter wave (mmWave) communication.

1.2.1 Motivation behind mmWave Communication

The importance of this band to be used as a communication spectrum arises due to the emergence and usage of applications requiring extremely intensive bandwidth. Bandwidth of 270 GHz available in mmWave frequency range greatly reduces the load on microwave frequency band. Technologies such as Wi-Fi are becoming heavily overloaded by users due to its unlicensed band with a carrier frequency of 2.4 GHz frequency. To accommodate high data traffic, bands operating at higher frequencies are the viable solution.

1.2.2 Advantages of mmWave Communication

High Frequency Spectrum availability

To accommodate ever increasing data traffic, frequency regions having high bandwith emerge as a potential solution. Millimeter wave frequency bands provide such high unused bandwidths.

Large Antenna Arrays

Antenna size directly depends upon the carrier wavelength. High carrier frequencies have a shorter wavelength resulting in reduced antenna sizes. Smaller antenna sizes make the usage of large antenna arrays in a smaller physical dimension possible. Millimeter wave communication can utilize these large antenna arrays for high beamforming gains.

1.2.3 Issues in mmWave Communication

The operating frequencies of mmWave communication are very high such as 28 GHz and 73 GHz. At such high frequencies, transmitted signals encounter a different propagation environment than signals communicating in sub-6 GHz band. Some of the factors that the signal faces during transmission are:

Attenuation

Signals experience severe attenuation while propagating through mmWave spectrum due to oxygen absorption. Absorption of signals resulting in attenuation is different at different carrier frequencies. Some frequency windows have very high

signal attenuation while the absorption in other windows are comparatively less severe.

Diffraction

Owing to the short wavelengths, signals propagating at mmWave frequency band suffers from poor diffraction while experiencing blockages in the communication path.

1.2.4 Some solutions for limitations in mmWave Communication

Selective frequency windows for Communication

As the signals experience different oxygen absorptions resulting in attenuation at different frequency windows, proper selection of frequency windows can mitigate the effect of attenuation on the signals in mmWave communication.

Highly Directive Beams

Owing to the smaller wavelengths at mmWave frequency bands, the attenuation can be significantly reduced by making use of highly directive beams from large antenna arrays.

1.3 UAV Communication

1.3.1 Classification of UAVs

UAVs are classified according to the height it can achieve. Low altitude Platforms (LAP) can attain height upto 5 km, Medium Altitude Platform (MAP) can achieve height between 5 km to 10 km and High Altitude Platform (HAP) can attain height more than 10 kms.

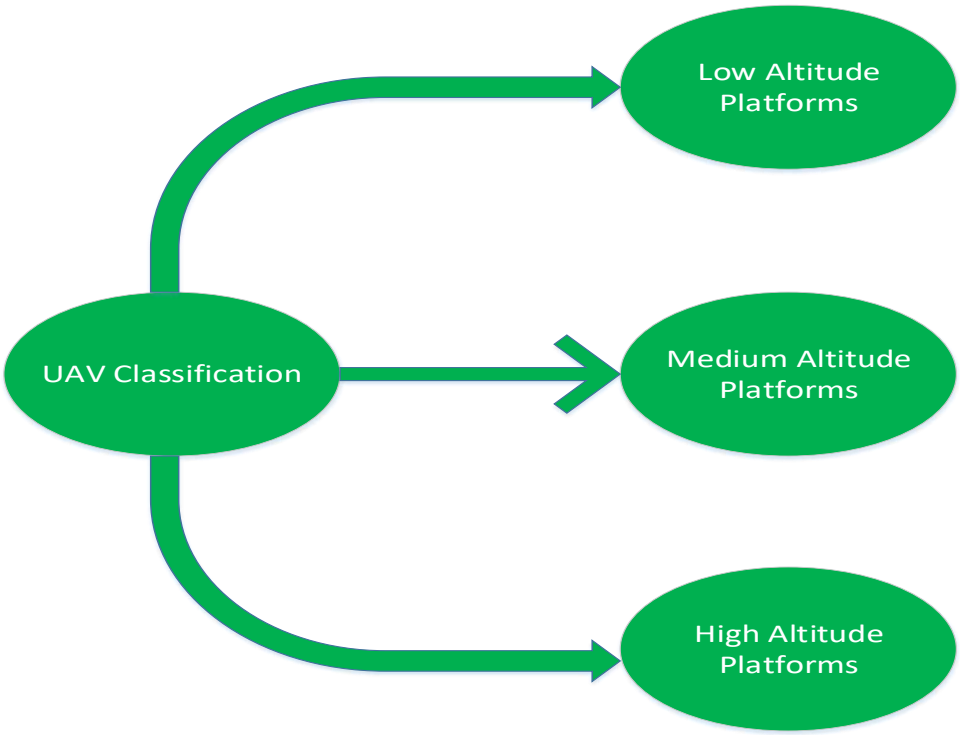

Figure 1.1: UAV Classification

1.3.2 Advantages of UAVs over Terrestrial Networks

UAVs provide several advantages over terrestrial networks such as:

- Better line of sight availability
- Quick and mobile deployment to any location
- Group of UAVs can relay the traffic from remote areas to the desired location

1.3.3 Applications of UAV Networks

UAVs are found to be useful in various applications such as:

Delivery systems

UAVs are useful to deliver daily life consumables to remote areas where normal transportation is not cost feasible. It is also quite helpful in delivering products to the residents of hilly areas.

Emergency Response Systems

Due to its flying capabilities, it is the best choice to provide emergency assistance kit containing first aid items to the patients. It avoids jam packed highways and could be life saving in the emergency situations.

Tracking and Imaging

UAVs are now becoming the first choice for imaging and tracking. It is used by the firefighters to assess the situation of the fires in the forests. It is used by the law enforcement agencies to have the real time video of the crime scene and to track the cars or person in a crime scene. UAVs can be used for images of the

battleground without indulging the military personnel hence act as another eye in the battle field.

Agriculture

UAVs are also used in the agriculture field to spray seeds to the cultivation land. Recently, they are used in Pakistan to kill swarms of Locusts.

Internet of Things

UAVs are often used to collect data from the IoT sensors located in the field. This data can be further relayed to the core network through a swarm of coordinated UAVs.

Wireless Communication

UAVs are becoming essential integral of any Heterogeneous communication network due to its mobility and fast deployment. They can provide communication if the existing infrastructure get destroyed in a disaster or the conventional infrastructure is not cost effective at any place such as remotely less crowded areas. They are also very useful in overly crowded areas such as cricket stadium during matches. They can be placed quickly to the overcrowded region to offload traffic from BS.

1.4 TeraHertz Communication

The communication which takes place in 0.1 THz -10 THz frequency band is referred as TeraHertz (THz) communication. With the emergence of Internet of

Things (IoTs), Device-to-Device Communication (D2D), Autonomous Vehicles, etc. data rate requirements rise to a new level. Existing wireless infrastructure is not able to cope with such high data rates. Researchers are looking for new avenues to fulfill the very high data requirements and to make these emerging technologies a reality.

The propagation channel of THz frequency band is quite different from sub-6 GHz and mmWave frequency band. Path loss is not limited to distance but also to the molecular absorption of the signals. Different frequency ranges in the THz frequency band have a different absorption behaviour. In some windows, absorption is quite severe while others have a nominal absorption. In the literature, researchers have also indicated several THz frequency windows which are suitable for THz communication.

1.5 Thesis Motivation

The evolution of wireless generations is directly related to the need for high data rates. This is the evolution from sending simple text messages to downloading a few kbytes image and from there to download full high definition movie in seconds. As the technology is evolving to fully autonomous systems, the data rate requirements to make these technologies a reality is sky rocketing. From paying house hold utility bills, to buy groceries or food, to make transactions for businesses, all are now possible from mobile phones. Millions of people are streaming movies from Netflix and videos from youtube, uploading their photos and videos on instagram and sharing their daily routines on social media. All of that need a lot of bandwidth to support fast downloading and uploading. Technologies like au-

tonomous vehicles, virtual reality, robotics all need very fast communication. The basic motivation behind all this evolution of generations is to satisfy the high data rate demands of the users to make these technologies a reality and provide comfort to the human race. Likewise the motivation behind this thesis is to propose a HetNet environment which can provide better SINR coverage and rate coverage to the users in different environments.

1.6 Research Gap

A lot of work has been carried out in the stochastic modeling of different cellular networks over the years and is discussed in detail in literature review. In [28–30] rate and coverage analysis of the millimeter wave cellular networks have been carried out. In some other research works UAV aided networks have been studied. In [31, 32] analysis for the coverage probabilities have been performed in an environment where UAVs are operating on millimeter wave frequencies. Several works considered a HetNet environment such as in [33], a HetNet composed of sub-6 GHz and THz cells is considered and interference and coverage analysis has been performed. In [34], a HetNet consisting of sub-6 GHz MIMO enabled BS, sub-6 GHz small cells and mmWave SBSs have been considered and coverage analysis of the HetNet has been performed. All the above mentioned work have either considered a single tier environment for the coverage and rate analysis or a HetNet composed of either sub-6 GHz and mmWave BSs or sub-6 GHz and THz small cells. Moreover to the best of our knowledge, the previous work done for coverage and rate analysis in HetNets did not considered a HetNet composed of sub-6 GHz MBS, UAVs and small cells operating on mmWave frequencies and

small cells operating on THz frequencies. This is the first work that explored and provided a detailed insight into the coverage and rate analysis of such a robust HetNet.

1.7 Thesis Contribution

The major contributions of this thesis work are given below:

- In this first phase, performance analysis of the hybrid heterogeneous network consisting of MBS and UAVs operating at sub-6 GHz and THz SCs operating at 0.3 THz has been evaluated. Simulations are done considering bandwith proportions for both the the fronthaul and backhaul links. Rate and coverage probabilities have been found in different network configurations like various densities of THz small cells, different allocations for fronthaul and backhaul links and for various biased values. It has been observed that the THz SCs provide very high data rates to the associated users while MBS and UAVs operating at sub-6 GHz band provides better SINR coverage. UAVs are also helpful to provide better coverage to the cell edge users.

- In the second phase, a detailed stochastic analysis of sub-6GHz, mmWave, THz communication and UAVs have been conducted. A HetNet comprising of sub-6 GHz MBS, small cells and UAVs operating at mmWave frequencies and small cells operating at THz frequencies is considered. User association probabilities for various small cell densities have been derived. The effect of biasness on the user association to a specific tier has also been

observed. SINR and rate coverage probabilities for various bias factors are depicted. The effect of UAV transmit powers on UAV association probability and SINR coverage probability of the HetNet is also analyzed. Rate coverage probabilities for different TSC densities and THz bandwidths have also been depicted. We have also shown the effect of sub-6 GHz UAVs and mmWave UAVs on the SINR and rate coverage probabilities by changing the proportion of sub-6 GHz UAVs w.r.t. mmWave UAVs in the HetNet. It has been observed that HetNet can be configured in a way to provide better rate coverage by making use of THz Small cells and better SINR coverage by using sub-6 GHz BSs.

1.8 Thesis Organization

The organization of the thesis is as follows: Chapter 2 give an insight into mmWave and THz communication. Chapter 3 provides literature review of all the technologies involved in HetNets comprising of mmWave, THz and UAVs. In Chapter 4 UAV-asssisted backhaul solutions in THz enabled Hybrid Heterogeneous Networks has been presented. Chapter 5 considers a Heterogeneous Network comprising of mmWave and THz-enabled Aerial and Terrestrial networks and depicts the coverage analysis. At last, Chapter 6 give conclusions and future directions to the research.

Chapter 2

Millimeter Wave and TeraHertz Communication

2.1 Millimeter Wave Communication

With the introduction of Internet of Things [35–42], self-less driving cars, device to device (D2D) communication [43–51] and other emerging technologies, demand in high data rates rise to a significant level. This high data rate requirement cannot be achieved by already over burdened sub-6 GHz band. By communicating in mmWave band, this burdened can be reduced sufficiently. But communication in millimeter wave frequency band is not very easy as in sub-6 GHz due to high path loss. Millimeter wave communication provides a greater bandwidth which significantly helps in limited bandwidth problem face in sub-6 GHz band.

The introduction of Internet of Things (IoTs), smart cities, self driving cars, virtual reality, augmented reality, telesurgery etc. drive the need for very high data rates. Sub-6 GHz band alone due to limited bandwidth is not able to satisfy all the

data rate requirements. This creates a need to have a spectrum having very high bandwidth. Millimeter wave band operating at 28 GHz and 73 GHz frequencies provide a very high bandwidth at these frequencies.

2.2 Millimeter Wave communication in Physical Layer

There are different aspects and challenges that need to be addresses in physical layer. Some of the aspects are depicted in Fig. 2.1.

2.2.1 Channel Modeling

Severe signal attenuation during propagation in mmWave Communication led to the research of proper channel modeling. Several indoor and outdoor channel models have been presented in the literature. Different scenarios such as:

- Offices
- Shopping malls
- Street canyons
- Indoor environment
- Short-range outdoor environment
- Urban dense environment
- Urban microcells
- Urban macrocells

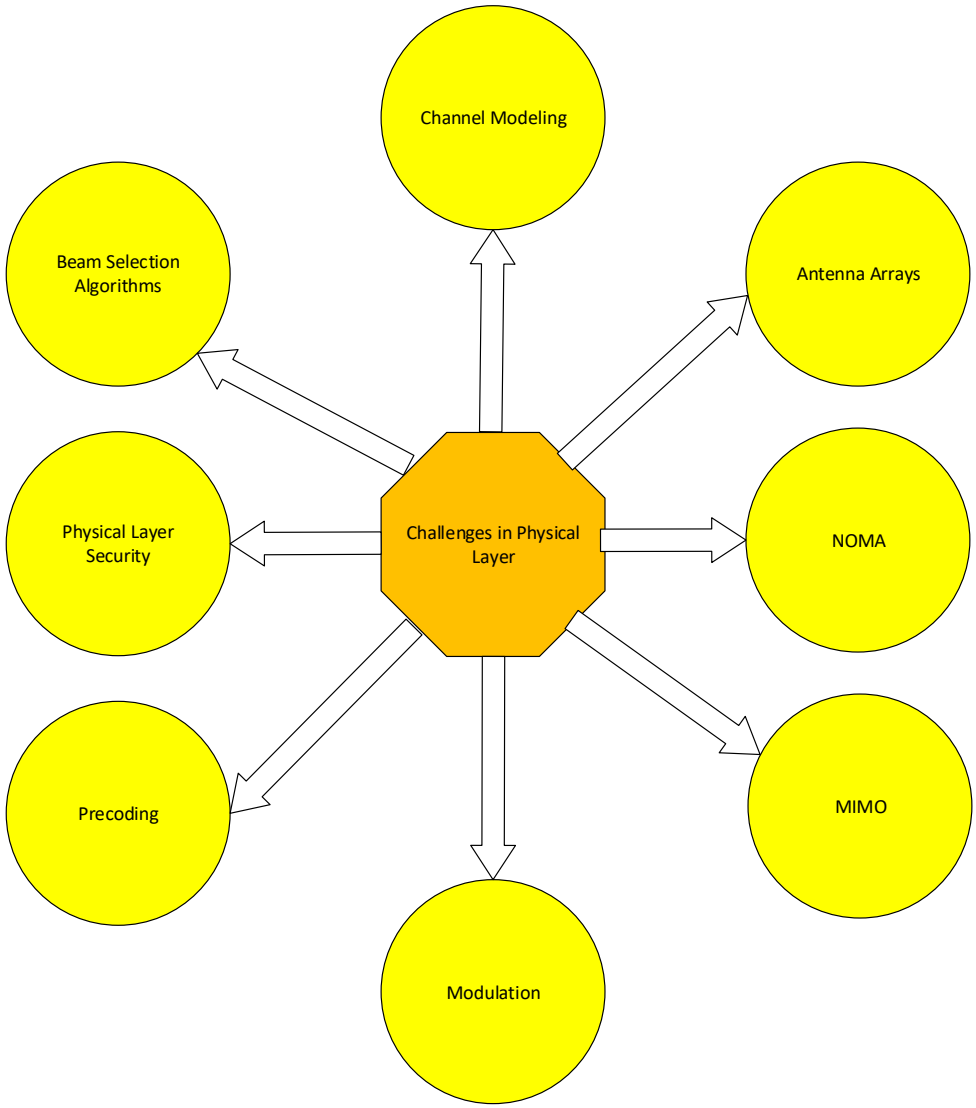

Figure 2.1: Challenges in mmWave Physical Layer [1]

have been considered in the literature to evaluate parameters such as:

- Path loss
- Shadowing
- LoS Probability

- Delay Spread
- Excess Delay
- RMS Delay
- Power Angle Profiles
- Power Delay Profiles
- Polarization
- Angular Dispersion
- Outage
- Attenuation

at 6 GHz, 28 GHz, 60 GHz, 73 GHz,and 100 GHz frequencies.

2.2.2 Physical Layer Security

Physical layer security is also of greater concern in mmWave frequency band as reflectors can allow an eavesdropper to wiretap the data from high gain beam. So the protection of data from eavesdropper needs essential transmission techniques in mmWave communication [34].

2.2.3 NOMA

Improved spectrum efficiency can be achieved by Non Orthogonal Multiple Access technique as it employ power multiplexing. Other advantages that the NOMA access technique provides are:

- Increased Fairness
- Low latency
- Improved Throughput
- Greater Reliability
- Massive Connectivity

2.2.4 Antenna Arrays

Another aspect of physical layer in mmWave communication is the design of the antenna arrays. Very short wavelengths in mmWave communication allow the design of smaller antennas and possibility of high gains using beamforming. This smaller size not only reduces the cost of the antennas but also allow to place more number of antennas in a compact physical area. Wavelengths offered in the mmWave communication at different frequencies are given in the table. Conventional mmWave antennas are categorized into five types as shown in Fig. 2.2 [52].

Table 2.1: Millimeter Wavelengths

Parameter	**Value**
28 GHz	10.7 mm
60 GHz	5 mm
300 GHz	1 mm

2.2.5 MIMO

Multiplexing gains that are provided by MIMO significantly contribute to high energy and spectral efficiency. Beamforming with high gains and MIMO sig-

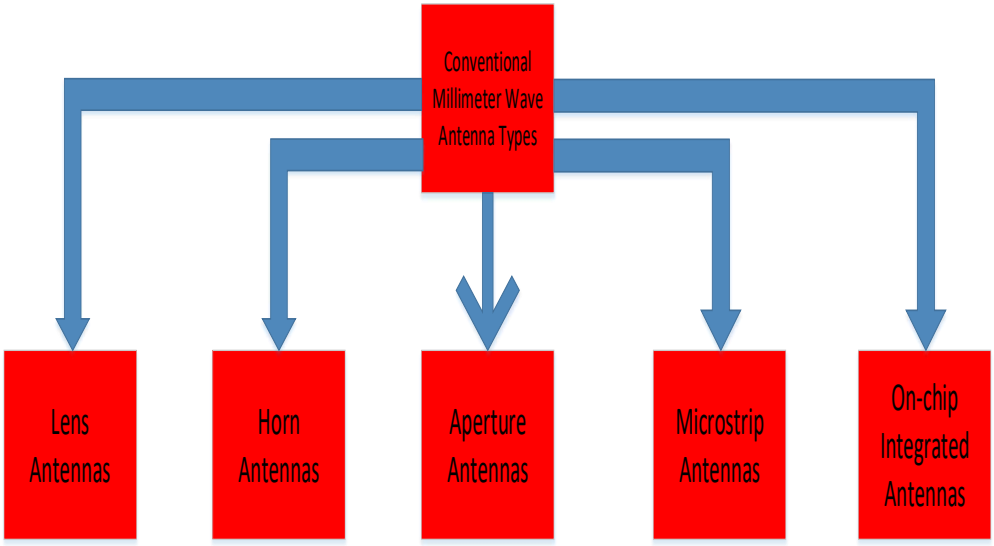

Figure 2.2: Conventional Millimeter Wave Antenna Types

nificantly contributes in compensating severe attenuation experienced by signals operating on mmWave frequencies.

2.2.6 Beam Selection Algorithm

Beamforming is generaly employed to compensate high penetration losses by use of large antenna arrays [53, 54]. Several beamforming methods are available as shown in Fig. 2.3.

Digital Beamforming

In digital beamforming, every element of the antenna array have a separate RF stream. This type of beamforming is quite costly to implement in mmWave communication systems.

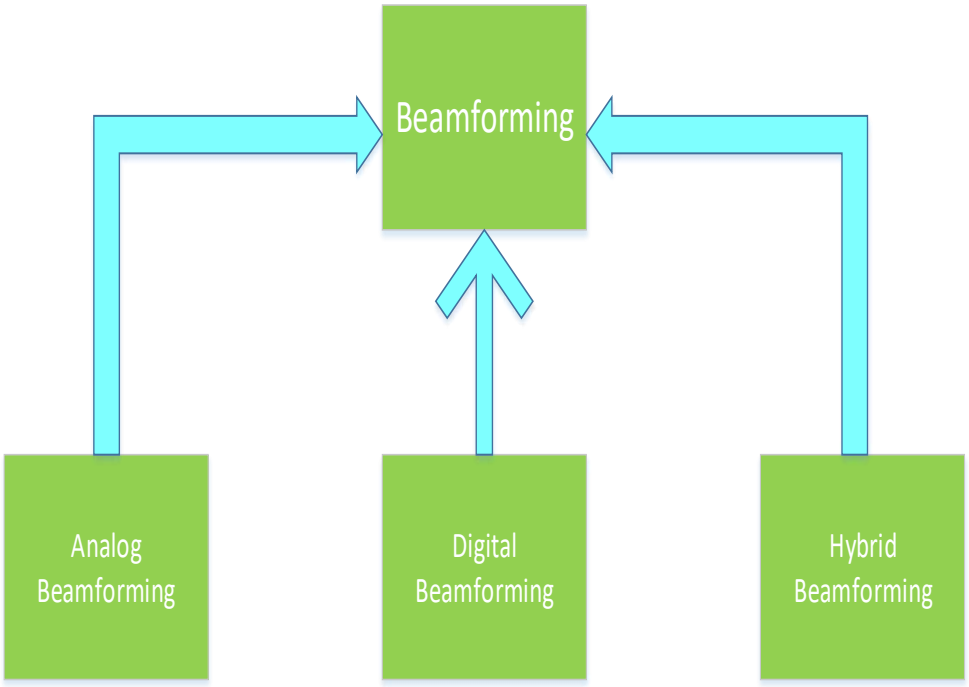

Figure 2.3: Types of Beamforming

Analog Beamforming

In analog beamforming, all the elements of the antenna array utilize a common RF stream. This technique has been explored in MIMO based mmWave OFDM systems.

Hybrid Analog/Digital Beamforming

This type of beamforming make use of digital phase shifters, after that processed signals pass through analog beamforming. This beamforming is also commonly used in mmWave communication systems.

2.2.7 Precoding

To improve spectral efficiency in mmWave communication systems, beamforming with multiple data streams known as precoding can be employed. There are different types of precoding having different characteristics, namely

- Analog Precoding
- Digital Precoding
- Hybrid Precoding

2.2.8 Modulation

Its a very hot research topic in mmWave communication systems to determine which type of moduation is best suited for mmWave communication. OFDM has been widely employed in mmWave communication systems to increase the spectral efficiency but issues such as high Peak to average power ratio (PAPR) resulting in higher power consumption, the complexity of the amplifiers and the redundancy in the cyclic prefix results in the utilization of other techniques. Several candidate modulation schemes for mmWave communication is presented in Fig. 2.4.

2.3 Technologies incorporating mmWave Communications

Millimeterwave communication can be a potential candidate for several Technologies such as given in Fig. 2.5.

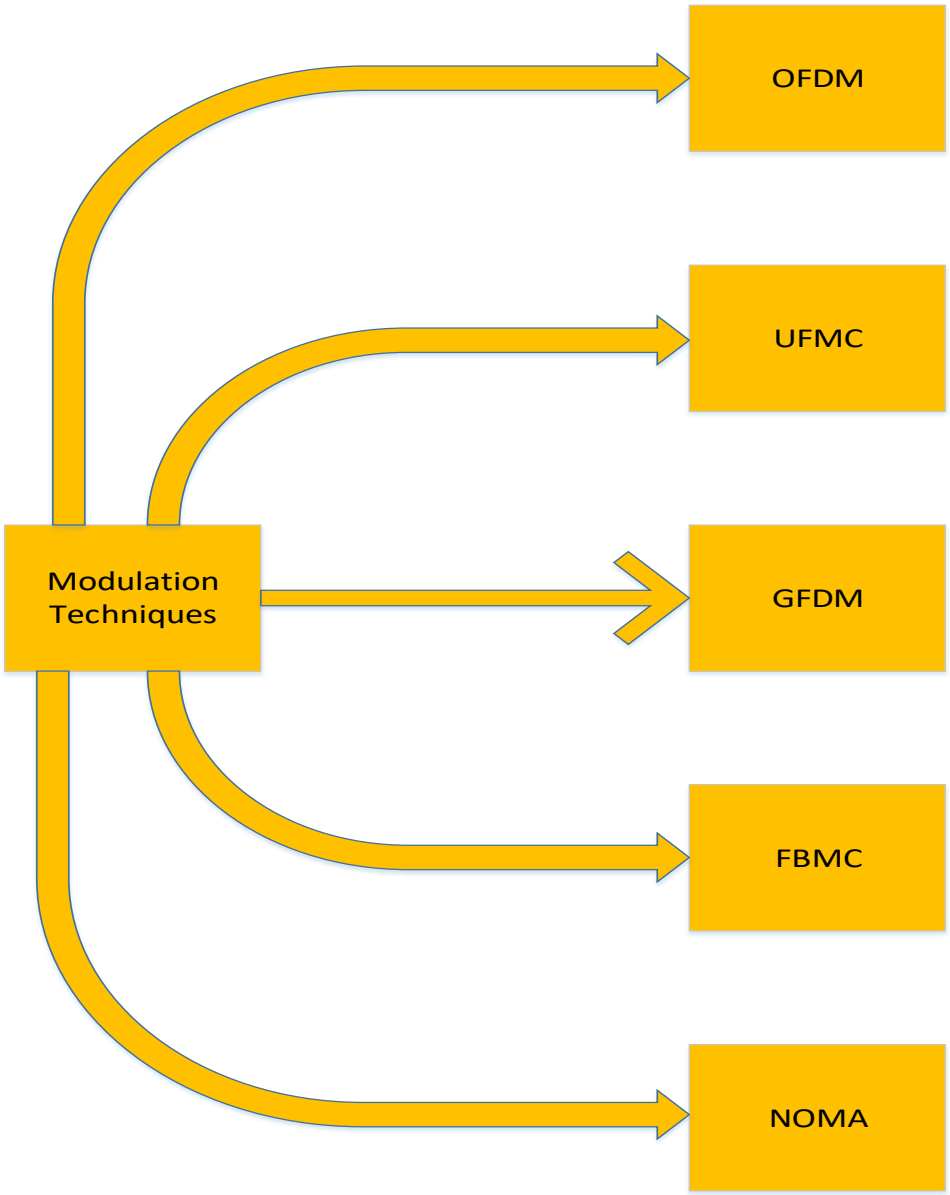

Figure 2.4: Modulation types in mmWave Communication

2.3.1 Tracking and Imaging

Emerging technologies such as Robots and Unmanned Aerial Vehicles needs tracking. Robots and UAVs can be used for imaging purposes. Communication at

Figure 2.5: Technologies and Millimeter Wave Communication

mmWave frequencies such as 60 GHz can provide several benefits such as interference reduction by highly directed beams. Small antennas designed at such high frequencies can be compactly packed in small devices.

2.3.2 Satellite Communication

Satellite communication services such as HDTV broadcast and also the introduction of satellite internet such as by Starlink or Blue Origin, requires a huge bandwidth. Federal Communication Commission allocate several bands for fixed,

mobile, inter-satellite communication ranging from 30 GHz to 275 GHz which are in mmWave frequencies.

2.3.3 Smart Devices

Recently, use of smart wearable devices are at peak to measure vital signs such as heart rate, temperature, etc. These vital signs and other fitness parameters such as number of steps, distance covered etc. are measured using sensors in the wearable devices. Data generated by hundreds of people in close vicinity required a high bandwidth. Millimeter Wave communication can play a significant role to accommodate such high data rates. Factors such as interference between signal from different devices and how to mitigate it is also a prospective research area.

2.3.4 5G mmWave Communication

Every ten years, a need arises to have a new generation of mobile communication subject to the increased demand in the downlink and uplink data rates. To cater these demands, 5G mobile communication needs unused spectrum to cater very high speed data communication. This spectrum is provided by mmWave frequency bands such as 28 GHz and 73 GHz.

2.3.5 Internet of Things

With the evolution of internet, immense number of devices needs internet to connect and transmit its data to cloud. Each of these devices need bandwidth to share their data. Existing frequency bands are already overloaded so mmWave unused

frequency band is a viable solution to accommodate Internet of Things (IoT) devices.

2.3.6 Device to Device Communication

Device to Device communication works on the principle that the nodes communicate with each other directly without the need of the BS. This greatly reduces the latency. In mmWave communication, owing to the large antenna arrays providing highly directed beams, D2D devices can operate effectively without interfering with each other.

2.3.7 Machine to Machine Communication

Machine to Machine Communication relies on sensors to collect data from the machines and some wireless technology to send this data to control different machine functions. M2M communication generates a large amount of data so mmWave frequency range can provide huge bandwidth to cater the data transmission requirements between machines.

2.3.8 Autonomous Vehicles

Vehicles are the most common mode of transportation. To make travel easier, vehicular industry implement advanced technologies into their vehicles such as cruise control, collision detection and internet services in the vehicle. The concept of autonomous vehicles and self driving cars is also materializing now a days by the advancements in wireless communications. The wireless technologies that are being employed for vehicular networks are

- ZigBee
- Bluetooth
- Ultra Wide Band (RFID)
- RFID
- 60 GHz mmWave frequency band

A vehicular network comprises of various V2X components such as:

- Vehicle to Vehicle (V2V)
- Vehicle to Internet (V2I)
- Vehicle to Sensor (V2S)
- Vehicle to Road Infrastructure (V2R)

All these wireless communications require a huge bandwidth. Millimeter wave unused spectrum can be utilized for such high bandwidth requirements.

2.4 THz Communication

The high data rate requirements in 6G led to the option of considering communication in THz frequency band ranging from 0.1 THz to 10 THz. Communication at such high frequencies experience very high losses in terms of propagation and molecular absorption. The high available bandwidth at these frequencies make this band a hotspot for researchers.

2.5 Applications of THz Communication

THz communication due to its high data rates evolve as a potential candidate for several applications such as 6G communication, secure military communication, personal area networks and applications pertaining to systems for monitoring health etc.

2.5.1 6G communication

Humankind in the last few decades seen an evolution in the wireless communication. This evolution results due to an enormous increased in data communication. Data hungry application requires a large bandwidth to support high data rates. THz communications provides such a high bandwidth.

2.5.2 Secure Military Communication

TeraHertz due to its limited range because of its high propagation and molecular absorption losses need huge antenna arrays to steer beams to a specific direction. The communication through beamforming is quite helpful as it is more difficult for the eavesdropper to tap a very narrow beam.

2.5.3 Personal Area Network

THz communication due to its limited range is mostly suitable for Personal Area Networks. THz frequencies can provide very fast data transfers upto Tbps between personal devices.

2.5.4 Systems for Monitoring Health

THz systems are quite helpful in communicating data in health systems used to monitor different vital signs of humans with the help of the sensors. Data can be transferred from the sensors to the mobile phone or some other communicating device.

2.6 Challenges in THz band communication

THz communications pose several challenges in order to get benefit from its huge bandwidth potential.

2.6.1 Transceiver Design

Communication at THz frequencies experience very high propagation and molecular losses. To overcome such losses new transceiver designs are required which provide high power and are also very highly sensitive. Various technologies such as plasma wave and photonic [55, 56], graphene [57], silicon germanium [58], indium phosphide and gallium nitride [59] have been proposed to develop transceivers for THz devices.

2.6.2 Channel Modeling

Due to very high molecular absorption losses, channel models designed for low frequencies are not adaptable to THz frequencies. Work has been done for channel modeling mostly in 300 GHz range [18, 60]. In channel modeling, both LoS and NLoS links pose several challenges.

Channel Modeling in LoS Propagation

In [61], for the THz range of 0.1-10 THz authors have developed a LoS propagation model. They have also proposed several transmission windows where the effect of molecular absorption loss is quite less.

Channel Modeling in NLoS Propagation

NLoS communication due to presence of obstacles also presents several challenges. Different surfaces produce different scattering, reflection and diffraction in THz frequency range and their characterization is also necessary.

2.6.3 TeraHertz Communication Windows

Communication at THz frequencies is highly prone to molecular absorption losses in addition to high propagation losses. The amount of molecular absorption varies at different frequencies. At some frequencies it is more severe than at other frequencies. Researchers have studied, observed and presented several frequency windows in THz band in which the effect of molecular absorption is much less [62].

2.7 Conclusions

In this chapter, a brief introduction to mmWave and THz communication is presented. Different aspects especially related to physical layer of mmWave communication such as security, channel modeling, MIMO, NOMA, precoding and beamforming have been covered. This chapter also gives insight into some of the

technologies incorporating mmWave communications such as satellite communication, 5G communication, M2M, D2D and Internet of Things. This chapter also gives a brief introduction of THz communication and its windows. Several applications of THz band and also its challenges have been briefly discussed at the end of the chapter.

Chapter 3

Literature Review

This chapter presents the background and literature review of different technologies used in this thesis such as unmanned aerial vehicles (UAVs) communication, mmWave communication and THz communication. State of the art work in Heterogeneous network comprising of above mentioned technologies is also presented in this chapter.

3.1 UAVs Communication

Unmanned aerial vehicles (UAVs), used as aerial networks is becoming an integral part of any communication system. Features such as high mobility, flexible and dynamic deployment and ability to vary heights make UAVs adaptable to various network deployment scenarios [63–68]. UAVs are highly suitable for providing coverage in scenarios involving disaster hit areas or highly crowded regions such as sports events or musical concerts due to its quick mobility and dynamic deployment [69–73]. Use of UAVs as communication platform comes with several

constraints such as flight time of UAVs due to its limited battery life [74–79]. Researchers are working on key challenges such as path planning, UAV 3D placements, energy conservation in UAVs etc [80–84].

UAVs with their ability to provide quick and infrastructure-less deployment for fulfilling high demand for data rates give them pivotal importance in next-generation networks [85–94]. Recent work on UAVs has focused on multiple avenues; such as its deployment in scenarios of infrastructure damage, for package delivery and traffic surveillance [88]. The ability to change the altitude is a differentiating aspect of UAV from the terrestrial base station based networks. In [95], the authors introduced a framework to compute the optimal height of UAVs which gives the maximum coverage probability and also proposed an environmental and UAV height dependent geometric line-of-sight (LoS) model. In [96], the authors investigate the efficient deployment of UAVs to provide coverage to users and used the circle packing theory to determine the 3D-locations of UAVs to maximize the coverage area and lifetime of UAVs. Moreover, the study focuses on the aspects of mitigating the interference by adjusting the altitude of UAVs based on antenna beamwidth. Recently, the use of UAVs in providing a backhaul opens up new horizons for various applications. In a recent study [97], the use of UAVs in backhauling the network traffic to the core network has been considered. The authors in [94] investigated the optimal positioning of UAVs to backhaul the data between the core network and the small cells. The authors in [98] studied and analyzed various quality-of-service (QoS) metrics for a coexisting network of sub-6GHz and mmWave UAVs. Numerous studies in analytical framework for coverage analysis of elevated base stations has been conducted [99–101]. A lot of work has also been done in mmWave-aided networks. In [102], the authors provided an analysis

for rate, coverage and energy efficiency using tools from stochastic geometry in a mmWave-aided multi-tier network. In [34], physical layer security has been analyzed in a massive MIMO HetNet. The coverage and rate analysis for mmWave networks has been extensively studied in [28–30].

3.2 Heterogeneous Networks

Traditional base stations (BSs) due to their low frequency bands (sub-6 GHz) and limited bandwidth are unable to cope with very high demand for data rates. This demand raises the need to have small cells operating at high frequencies such as millimeter (mmWave) and TeraHertz (THz) frequencies. On the other hand, the need for infrastructure-less networks such as unmanned aerial vehicles (UAVs) also gained importance as they can be utilized to serve over-crowded places or regions where terrestrial networks are unable to provide coverage. The integration of the above mentioned technologies has now become the focus of research to meet the ever increasing demand of ultra high data rates. This has given rise to so-called heterogeneous networks (HetNets), which offer attractive solutions by amalgamating technologies operating at diverse frequency bands where each band has its own coverage area, offered data rate, and operating power values.

The cellular network is facing a technological shift, to overcome the high data rate requirements of ever-growing connected devices and the evolved multimedia applications. The wireless network needs to be flexible to accommodate the different requirements of each user by allowing the coexistence of different infrastructure and hence supports heterogeneity. The use of heterogeneous networks (HetNets) was evolved by the deployment of a small cell with lower transmit power to

overcome the challenges faced by a traditional macro base station (MBS) [103]. With the advancement in the cellular network and the incorporation of various technologies, i.e., unmanned aerial vehicles (UAVs) and frequency bands such as sub6-GHz, millimeter (mm)Wave [104–111] and Terahertz (THz), the HetNets are becoming popular [112–116]. For instance, the use of UAVs and THz-based communications has emerged as effective integration for the wireless network to provide seamless coverage and to equip users with high bandwidth.

3.3 Communication in THz frequency band

Recently, the use of THz band to achieve high data rates has been explored in various studies. In [117], the authors surveyed the challenges in THz communication and provided an in-depth analysis of THz networks. THz band imposes several challenges such as limited coverage area due to high molecular absorption losses and high path loss. In [118], the authors discussed the problems associated with distance limitation at THz frequencies. The molecular absorption losses varies significantly with the choice of frequency windows in THz band. In [62], the authors studied the impact of various THz frequency windows for THz communication.

The exploration of the THz band to enable THz communication is considered as a new frontier with immense opportunities in providing huge bandwidth options. THz band addresses the issue of spectrum scarcity and also enables various new applications. In [117], the authors provide an in-depth insight of THz (0.1-10THz) communication and surveyed the challenges in designing such devices. They also discussed the high-speed transceiver architectures, problems related to

propagation, different modulation schemes, capacity aspects and other challenges encountered to perform a successful communication by using THz frequencies. Moreover, the use of high frequencies, i.e., THz, also imposes challenges in the form of high path loss and molecular absorption, which limits the coverage area. The authors in [118], provided four different directions to tackle the distance limitation problem in THz communication, such as reflect-arrays, ultra massive multiple-input-multiple-output (MIMO) communication, distance-aware physical layer design, and intelligent surfaces. The authors in [62], worked on the THz window selection process to find the best window, which is least affected by the molecular absorption loss.

3.4 Coverage and Rate Analysis in Heterogeneous Networks

Rise in HetNet deployment raises the need for analytical framework to perform coverage and rate analysis [119]. In [120], the authors performed the coverage and rate analysis on a device-to-device (D2D) and UAV communication network. The authors in [31,32,121,122], provided the analytical framework for coverage analysis for UAV-aided mmWave wireless networks. In [33], the authors derived the coverage probability for a hybrid THz and radio frequency (RF) wireless network. The authors in [123] computed the coverage probability in a network, where BSs can either operate on THz or sub-6GHz frequencies. In [124], the authors considered an interference regime in a THz only network and computed the mean interference.

3.5 Backhaul Solutions in Heterogeneous Networks

With an increase in the number of small cells operating at very high frequencies, the existing backhaul solutions formed by the combination of point-to-point (P2P) microwave links and the optical fiber are not feasible, in terms of the cost associated with them. In [125], the authors provide an insight into the baseband signal processing for optical and wireless backhaul links. Their work addresses the blending of coherent fiber technology with wireless THz transceiver architectures. Higher costs are involved in licensing bandwidths for the deployment of P2P links and non-affordability of laying optical fibers when an increased number of small cells are involved. This makes the unlicensed THz enabled backhauling solution a preferred choice. The use of the THz band eliminates the licensing cost and the price associated with costly fiber layout is waived [126]. The coexistence of hybrid technologies has the potential to serve and provide data rates that could not be possible through existing terrestrial wireless infrastructure.

3.6 Conclusions

In this chapter, literature review has been conducted on UAV communication, mmWave communication, Heterogeneous Networks and THz communication. Several works have been discussed covering the rate and coverage analysis either in single tier networks comprising of either sub-6 GHz, mmWave, THz or UAV communication or a HetNet of different configurations such as composed of sub-6 GHz and THz SBSs or a HetNet comprising of sub-6 GHz and mmWave small cells. To the best of our knowlege, no work has been done on coverage and rate

analysis of a HetNet composed of sub-6 GHz BSs, mmWave SBSs, THz SBSs and UAVs. Our work is the first one to provide detailed coverage and rate analysis of such a HetNet.

Chapter 4

UAV-Assisted Hybrid Heterogeneous Network

The coexistence of hybrid technologies has the potential to serve and provide data rates that could not be possible through existing terrestrial wireless infrastructure. To the best of our knowledge, limited research has been done in the integration of UAVs with small cells and none of the work has focused on the performance analysis of a HetNet having a combination of THz, and microwave base station with a layer of UAVs.

This chapter present a three-tier hybrid heterogeneous network consisting of MBS in tier 1 and UAVs in tier 2, both operating at sub-6 GHz band, with multiple small cells operating at THz frequency band constitute the tier 3. The small cells operating on the THz band with wireless backhaul capability can serve the users along with backhauling the traffic to the core network. On the other hand, the small cells operating on the THz band without wireless backhaul capability can serve the users whereas it can utilize the neighboring MBS, UAVs or THz enabled

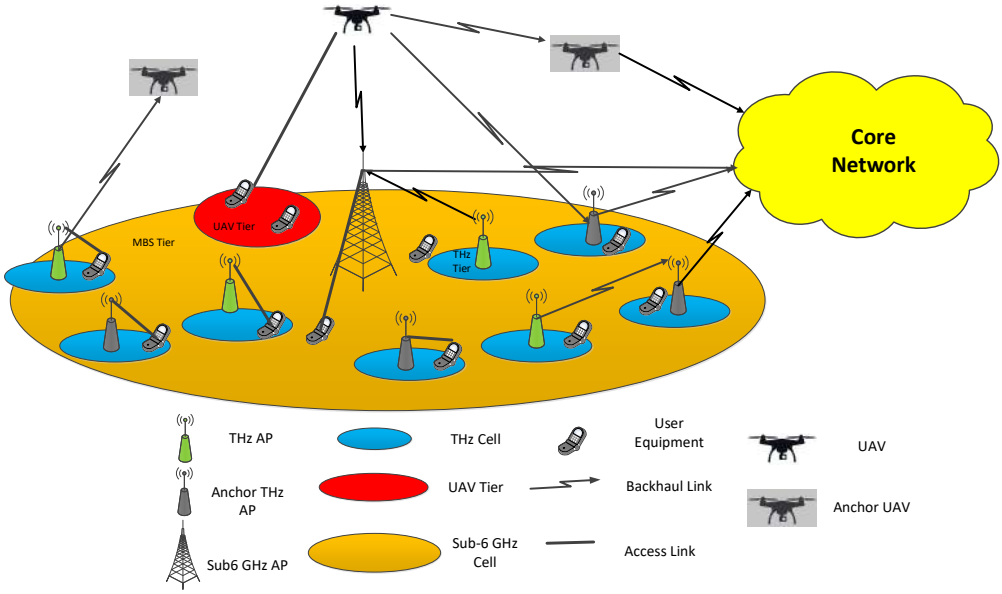

Figure 4.1: Graphical description of the system model of a multi-tier hybrid HetNet comprising of a MBS, multiple THz enabled small cells, and multiple UAVs.

small cells for backhauling the traffic to the core network.

A detailed system performance analysis of the proposed multi-tier hybrid HetNet is carried out to demonstrate the coverage and rate probability trends subject to the available capacity of the wireless backhaul links. The simulation results also demonstrate that the users can be offloaded from the traditional cellular infrastructure such as sub-6 GHz MBS to the small cells operating on THz bands and UAVs operating on sub-6 GHz band.

4.1 System Model

We consider a multi-tier hybrid HetNet scenario comprising of a MBS with S THz enabled small-cells and U UAVs, serving K users, as depicted in Fig. 4.1. The MBS and UAVs are operating at sub 6-GHz frequency bands whereas the small

cells are operating at THz frequency band. It is also assumed that each MBS is equipped with the backhaul capabilities to backhaul their traffic to the core network via fiber links whereas only one third of the UAVs labeled as Anchor UAVs are equipped with the backhaul capabilities. It is also considered that some of the small cells operating on THz frequency band have their own backhaul capabilities labeled as Anchor THz Access Points whereas the remaining small cells labeled as THz Access Points and UAVs can utilize the MBS, Anchor UAVs or Anchor THz Access points to backhaul their trafiic to the core network. It is also assumed that the base stations (BS) belonging to any tier with their own backhaul capabilities can satisfy the capacity requirements for the users in the access link. The BS of a tier can distribute their available spectrum resources for the both backhaul and access links. We assume that the BS of a tier j can allocate the proportion of spectrum resources (α_j) for the access links and remaining portion of spectrum resources ($1-\alpha_j$) for the backhaul links, respectively.

We have considered a multi-tier HetNet comprising of three tiers. The macro cell operating at sub-6 GHz constitute tier 1, small cells operating at THz band constitute tier 2 and UAVs operating at sub-6 GHz band constitute tier 3, respectively. It is assumed that the location of BSs follow a two dimensional homogeneous Poisson point process (HPPP) with intensity Φ_j and density λ_j where $j \in \{\text{MBS}, \text{SC}, \text{UAV}\}$. Using the Nakagami fading model, the envelope of the fading has the probability density function (PDF) given as [127]

$$|g| \sim f_{|g|}\left(x, \mu_q\right) \triangleq \frac{\mu_q^{\mu_q} x^{\mu_q - 1} \exp\{-\mu_q x\}}{\gamma\left(\mu_q\right)}, \forall x > 0, \tag{4.1}$$

where μ_q is the Nakagami fading parameter wherein $q \in \{L_m, N_m\}$ and $\gamma\left(\mu_q\right)$ is

the gamma function. Here L_m and N_m represent the LoS and NLoS propagation environments, respectively, and the Nakagami parameter is characterized for each environment differently. The small scale fading between the BS and the typical user is considered to be independent Nakagami fading with Nakagami fading parameter μ_{L_m} and μ_{N_m} for LoS and NLoS links, respectively. Both μ_{L_m} and μ_{N_m} are considered as positive integers [127]. It is important to highlight that for the sub-6 GHz network, g is assumed to be Nakagami fading with $\mu_q = 1$ [127]. The path loss model for MBS tier operating at sub-6 GHz band at the separating distance d is given by

$$\mathrm{PL}_{\mathrm{MBS}} = 20\log\left(\frac{4\pi f_c^{\mathrm{MBS}}}{c}\right) + 10\beta\log(d) + \chi, \tag{4.2}$$

where f_c^{MBS} is the carrier frequency, c is the speed of the light, d is the separating distance between the MBS and the user, β is the path loss exponent and χ accounts for shadowing in sub-6 GHz band. To compute path loss model for UAVs, we use geometric model given in [95] to derive the line-of-sight (LoS) probability denoted by P_{LoS} between the user and UAV. This model incorporates elevation angle, ϕ_{UAV}, for sub-6 GHz band UAVs. The elevation angle ϕ_{UAV}, can be computed as

$$\phi_{\mathrm{UAV}} = \arctan\left(\frac{h}{x}\right), \tag{4.3}$$

where h represents the height of the UAV and x is the horizontal distance between UAV and user. The LoS probability (P_{LoS}) between user and UAV can be calcu-

lated similar to [95] as follows

$$P_{\mathrm{LOS}} = \frac{1}{1 + a\exp\left[-b\left(\phi_{\mathrm{UAV}} - a\right)\right]}, \tag{4.4}$$

where the parameters a and b are dependent upon environment in region of interest (RoI). The non-line of Sight (NLoS) probability is given by

$$P_{\mathrm{NLoS}} = 1 - P_{\mathrm{LoS}} \tag{4.5}$$

By using the aforementioned calculated LoS and NLoS probabilities, we can compute the average path loss of a UAV operating at sub-6 GHz band as

$$\mathrm{PL}_{\mathrm{UAV}} = \mathrm{FSPL} + P_{\mathrm{LoS}} \times \mathrm{PL}_{\mathrm{LoS}}^{\mathrm{UAV}} + P_{\mathrm{NLoS}} \times \mathrm{PL}_{\mathrm{NLoS}}^{\mathrm{UAV}}, \tag{4.6}$$

where $\mathrm{PL}_{\mathrm{LoS}}^{\mathrm{UAV}}$ and $\mathrm{PL}_{\mathrm{NLoS}}^{\mathrm{UAV}}$ are excessive path losses introduced for LoS and NLoS sub-6 GHz UAV communication [98] and FSPL is the free space path loss and is given by

$$\mathrm{FSPL} = 20 \times \log\left(\frac{4\pi f_c^{\mathrm{UAV}} x}{c}\right), \tag{4.7}$$

where f_c^{UAV} is the carrier frequency of UAV operating on sub-6 GHz band, c is the speed of light and x is the separating distance between the UAV and the user. The path loss model for SC operating at THz frequency band similar to [61] can be expressed as

$$\mathrm{PL}_{\mathrm{SC}} = \mathrm{PL}(f,d)_{spread}[dB] + \mathrm{PL}(f,d)_{absorption}[dB], \tag{4.8}$$

where $\mathrm{PL}(f,d)_{spread}$ is the spreading loss due to the expansion of wave as it travels through the medium, and is given by

$$\mathrm{PL}(f,d)_{spread}[dB] = 20 \times \log\left(\frac{4\pi f d}{c}\right), \tag{4.9}$$

where d is the distance between the SBS and user, f is the carrier frequency of SC operating on THz band and c is the speed of light. $\mathrm{PL}(f,d)_{absorption}$ is the attenuation in the EM wave of frequency f due to molecular absorption while traveling a distance d. $\mathrm{PL}(f,d)_{absorption}$ is related to transmittance of a medium, τ, given by

$$\mathrm{PL}(f,d)_{absorption}[dB] = \frac{1}{\tau(f,d)} = \exp^{-k(f)d}, \tag{4.10}$$

where $k(f)$ is the frequency-dependent molecular absorption coefficient [128]. $k(f)$ can be calculated by using radiative transfer theory and the information provided by the high resolution transmission molecular absorption (HITRAN) database [129]. The received power of a user associated with tier j can be computed as

$$P_{r,j}[dB] = P_{t,j} + G(\phi_j) + \mu_j - \mathrm{PL}_j : \quad j \in \{MBS, UAV, SC\}, \tag{4.11}$$

where, μ_j is the multi-path fading and $G(\phi_j)$ is the directional antenna gain. The

directional antenna gain, $G(\phi_j)$, is given by

$$G\left(\phi_j\right)[dB] = \begin{cases} 0 & j \in MBS \\ \frac{Y}{\omega_h \times \omega_v} = \frac{Y}{\omega^2} & j \in \{UAV, SC\} \end{cases}, \tag{4.12}$$

where Y is an aperture dependent factor, and ω_h and ω_v are the horizontal and vertical beamwidths, respectively. It is assumed that the horizontal and vertical beamwidths are identical such that ω_h=ω_v= ω. The multi-path fading co-efficient, μ_j, can be given as

$$\mu_j[dB] = \begin{cases} 0 & j \in MBS \\ \mu_q & j \in \{UAV, SC\}\ q \in \{\text{LoS}, NLoS\} \end{cases} \tag{4.13}$$

The received power of each user associated with MBS tier can be given as

$$P_{r,\text{MBS}}\left[\text{dB}\right] = P_{t,\text{MBS}} - \text{PL}_{\text{MBS}}, \tag{4.14}$$

where $P_{r,\text{MBS}}$ is the received power and $P_{t,\text{MBS}}$ is the transmitted power. The maximum biased average received power with tier j is given by

$$P_{r,j}[dB] = P_{t,j} + G(\phi_j) + \mu_j - \text{PL}_j + \theta_j : j \in \{MBS, UAV, SC\}, \tag{4.15}$$

where $P_{r,j}$ is the received power from j^{th} tier, $P_{t,j}$ is the transmission power of tier j, PL_j is the path loss from tier j and θ_j is the bias factor for the tier j.

4.2 Performance Analysis

Assuming no power control, the users connected to the MBS operating at sub-6 GHz band will experience interference from the UAVs belonging to the tier 3 operating at sub-6 GHz band. Then signal-to-interference plus noise ratio (SINR) of a user u connected with the serving MBS b_0 of tier M is given as

$$\text{SINR}_{u,MBS} = \frac{P_{r,MBS}}{\sum_{i \in \{MBS/b_0 \cup UAV\}} P_i + \sigma^2}, \tag{4.16}$$

where P_i is the sum of interference from all the neighboring UAVs operating at sub-6 GHz band and σ^2 is the noise power spectral density. The achievable data rate of each user connected with MBS tier in the downlink transmission is given by

$$R_{u,MBS} = \frac{\alpha_{MBS} \times B_{MBS}}{U_{MBS}} \times \log_2\left(1 + \text{SINR}_{u,MBS}\right), \tag{4.17}$$

where B_{MBS} is the total bandwidth available to the MBS tier to serve the users and U_{MBS} is the total number of users associated to the MBS tier.

Similarly, the users connected to a UAV will get interference from other UAVs and MBS operating at sub-6 GHz band. The SINR will be computed as

$$\text{SINR}_{u,UAV} = \frac{P_{r,UAV}}{\sum_{i \in \{MBS \cup UAV/u_0\}} P_i + \sigma^2}, \tag{4.18}$$

where σ^2 is the noise power spectral density. The achievable data rate for each

user will be

$$R_{u,UAV} = \frac{\alpha_{UAV} \times B_{UAV}}{U_{UAV}} \times \log_2\left(1 + \text{SINR}_{u,UAV}\right), \tag{4.19}$$

where B_{UAV} is the bandwidth available to the UAV operating at sub-6 GHz frequency band and U_{UAV} is the number of users connected to the UAV operating at sub-6 GHz frequency band. Similarly, the users connected to *SC* will get only interference from other *SCs*. The SINR will be computed as

$$\text{SINR}_{u,SC} = \frac{P_{r,SC}}{\sum_{i \in SC/s_0} P_j + \sigma^2_{THz}}, \tag{4.20}$$

where σ^2_{THz} is the noise power spectral density at THz frequency band. The achievable data rate for each user will be

$$R_{u,SC} = \frac{\alpha_{SC} \times B_{SC}}{U_{SC}} \times \log_2\left(1 + \text{SINR}_{u,SC}\right), \tag{4.21}$$

where B_{SC} is the bandwidth available to the SBS operating at THz frequency band and U_{SC} is the number of users connected to the SBS operating at THz frequency band. The achievable rate of the users connected to UAVs and THz SCs without their own backhual capability is restricted by the available backhaul capacity of the selected BS of any tier for the wireless backhaul and is given by

$$R^{\text{effective}}_{u,j} = \min\left(R_{u,j}, R^{\text{BH}}_{u,w}\right), j \in \{UAV, SC\}\ w \in \mathbf{W}, \tag{4.22}$$

where $R^{\text{BH}}_{u,w}$ is the achievable rate of user u in the backhaul link with the selected BS belonging to $\mathbf{W}$ having its own backhaul capability. The SINR coverage prob-

ability at a given threshold τ_j is given by

$$P_{cov,j}\left(\tau_j\right) = P\left(SINR_{u,j} > \tau_j\right) \tag{4.23}$$

Similarly, the rate coverage probability for a given threshold, γ_j, is given by

$$P_{\text{Rate},j}(\gamma_j) = P(R_{u,j}^{\text{effective}} > \gamma_j) = P\left(\text{SINR}_{u,j} > 2^{\frac{\gamma_j \times U_j}{\alpha_J \times B_j}} - 1\right) \tag{4.24}$$

The total coverage probability, $P_{cov}(\tau)$, using the total law of probability can be computed by

$$P_{cov}(\tau) = \sum_{j \in \mathbf{J}} A_j \times P_{cov,j}\left(\tau_j\right), \tag{4.25}$$

where $\mathbf{J} = \{MBS, SC, UAV\}$, $P_{cov,j}\left(\tau_j\right)$ is the coverage probability of tier j for the given SINR threshold τ_j and A_j is the association probability of tier j. Similarly, the total rate coverage probability $P_{Rate}(\gamma)$ using the total law of probability can be computed by

$$P_{\text{effective rate}}(\gamma) = \sum_{j \in \mathbf{J}} A_j \times P_{Rate,j}\left(\gamma_j\right), \tag{4.26}$$

where $P_{Rate,j}\left(\gamma_j\right)$ is the rate coverage probability of tier j for the given rate threshold γ_j.

Table 4.1: Simulation Parameters

Parameter	Value	Parameter	Value
$f_c^{\text{MBS}}, f_c^{\text{UAV}}$	2.4 GHz	NF	9 dB
B_{MBS}, B_{UAV}	20 MHz	K	200
$P_{t,MBS}$	40 dBm	β	3
$P_{t,UAV}$	30 dBm	h_{UAV}	30 m
b	0.11	a	9
μ_{LoS},μ_{NLoS}	5, 1	f_c^{THF}	0.3 THz
$P_{t,SC}$	20 dBm	k(f)	.0033 m^{-1}
$Area$	250000 m^2	B_{SC}	10 GHz

4.3 Performance Evaluation

The proposed multi-tier HetNet framework is evaluated by performing in-detail simulations in MATLAB. The results demonstrate the effectiveness of offloading the users from the traditional cellular infrastructure to small cells operating on THz bands and the UAVs operating at sub-6 GHz. Moreover, the Monte Carlo simulations have been carried out to further validate the simulation results. In this simulation setup, we have assumed K number of users which are generated uniformly and are deployed randomly in an area of 500 $\times$ 500 m^2. The number of users can vary, we have assumed a random number $K = 200$ for our simulation setup. The downlink transmission power for each tier, i.e. MBS, UAVs and THz cells, are denoted by $P_{t,MBS}$, $P_{t,UAV}$ and $P_{t,SC}$, respectively. The operating frequency f_c^{MBS} of MBS and the UAVs f_c^{UAV} is 2.4 GHz (sub-6 GHz frequency band), while THz-enabled cells are operating at f_c^{THF} = 0.3 THz frequency. The bandwidth of each tier is represented as B_{MBS} and B_{UAV} for sub-6 GHz operations, whereas, B_{SC} is used to support THz-enabled users. A constant path loss exponent β = 3 is assumed for all tiers. Moreover, it is assumed that the UAVs are located at

a height of h_{UAV} = 30 m with respect to a perpendicular distance from the ground plane. Furthermore, the detailed simulation parameters are listed in Table 5.2.

4.3.1 Association Probabilities for different Bias values in a HetNet

Fig. 4.2 shows the association of users to each tier in a HetNet for different bias, θ_{SC}, values. The bias values are important to compensate for the high propagation losses associated with THz frequencies and to offload users from the MBS-tier to THz-tier. We have considered the bias value for UAVs, to offload the users from MBS to different UAVs-enabled cells. In Fig. 5.2 the bias value of UAVs is assumed to be 5 dB. The bias value of 5 dB is assumed for UAVs due to its low transmit power 1W as compared to MBS transmit power 10W to offload some users from MBS to UAVs. It can be seen in Fig. 5.2, that by keeping the value of θ_{UAV} fixed and increasing the value of θ_{SC}, more users start to offload from the MBS to THz-tier. This type of user-association helps to fulfill the demands of users requiring a very high data rate to meet their QoS needs.

If we increase the number of users in the given area, user associates to the BS or UAV of a particular tier which provides maximum biased received power. If we increase the bias power of UAV from 5 dB to some higher value, it would follow the same trend as of SBS association curve in Fig. 5.2. More biased power for UAV means more number of users will now get associated with UAVs and we will see an increase in the association probability for UAVs.

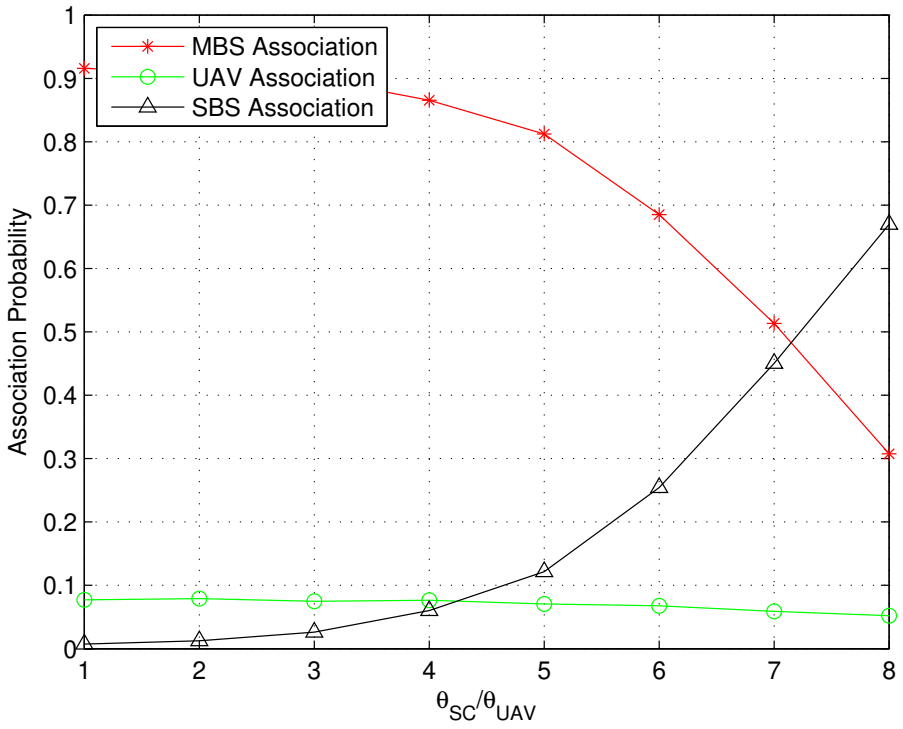

Figure 4.2: Association probability versus varying θ_{SC} with $\theta_{UAV} = 5$ dB, $\theta_{MBS} = 0$ dB, $\lambda_{MBS} = 4 \times 10^{-6}$ BS$/m^2$, $\lambda_{SC} = 100 \times \lambda_{MBS}$ BS$/m^2$, $\lambda_{UAV} = 3 \times \lambda_{MBS}$ BS$/m^2$ and $\tau_{\text{MBS}} = \tau_{\text{SC}} = \tau_{\text{UAV}} = 0$ dB.

4.3.2 Coverage probability for varying THz BSs density in a HetNet

Fig. 4.3 depicts the rate coverage probability of the total users in the network by varying the density of THz BSs, i.e., by increasing the number of THz-enabled cells in the network. By increasing the number of THz-enabled SBSs in the given area, the number of users associated with SBSs increases. In Fig. 4.3, it can be seen that by increasing the number of THz-enabled SBSs from 40 to 130, the effective rate coverage probability is increased by 22 % from 0.15 to 0.37 for a threshold of 100 Mbps. This increase is due to the fact that as we increase the

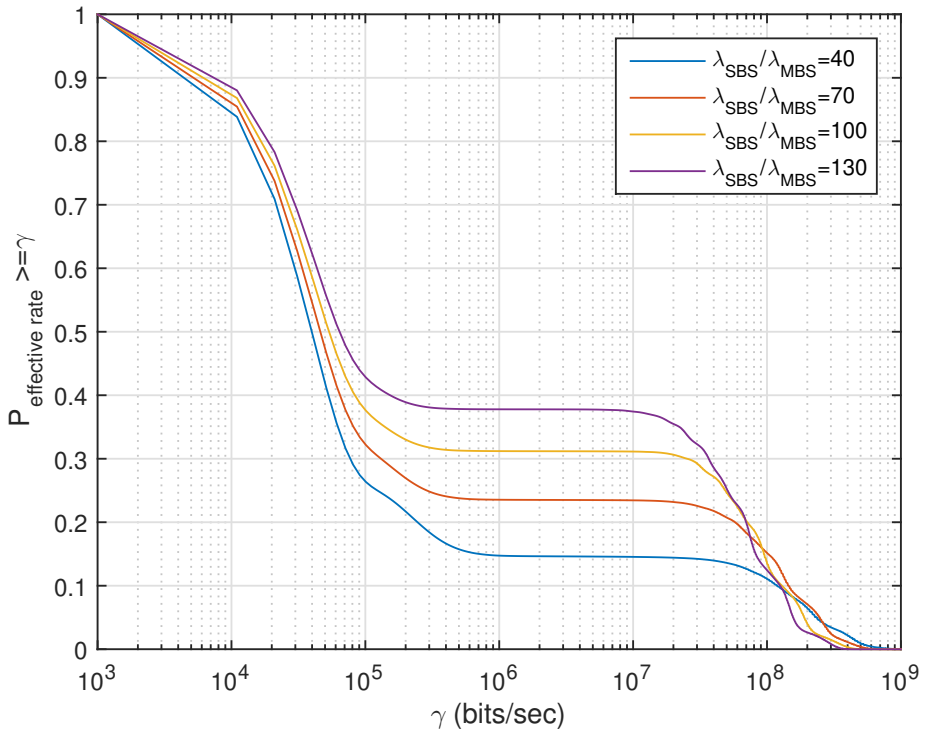

Figure 4.3: Effective rate coverage probability versus rate threshold γ for varying density of THz-enabled SBSs with $\lambda_{MBS} = 4 \times 10^{-6}$ BS$/m^2$, $\lambda_{UAV} = 3 \times \lambda_{MBS}$ BS$/m^2$, $\theta_{SC} = 30$ dB, $\theta_{MBS} = 0$ dB, $\theta_{UAV} = 6$ dB and $\tau_{\text{MBS}} = \tau_{\text{SC}} = \tau_{\text{UAV}} = 0$ dB.

number of THz SBSs more number of users will be offloaded from sub-6 GHz BSs and associate with THz-enabled SBSs. This increase in the effective rate coverage probability is due to the large bandwidth available at the THz frequencies.

4.3.3 Rate Coverage Probability versus Bandwidth Proportion in Access and Backhaul Links

The variation on rate coverage probability for each user, by changing the proportion of bandwidth of each link, i.e., the bandwidth reserve by each BS for its access and backhaul operation is shown in Fig. 4.4. In Fig. 4.4, the tuning pa-

rameter α is assumed to be the same for all the tiers. It has been seen that users will experience high data rates when the BSs reserve equal proportion (α=0.5) of its allotted bandwidth to access and backhaul links. Assigning an unequal portion of bandwidth to access and backhaul links results in a reduction in data rates for each user.

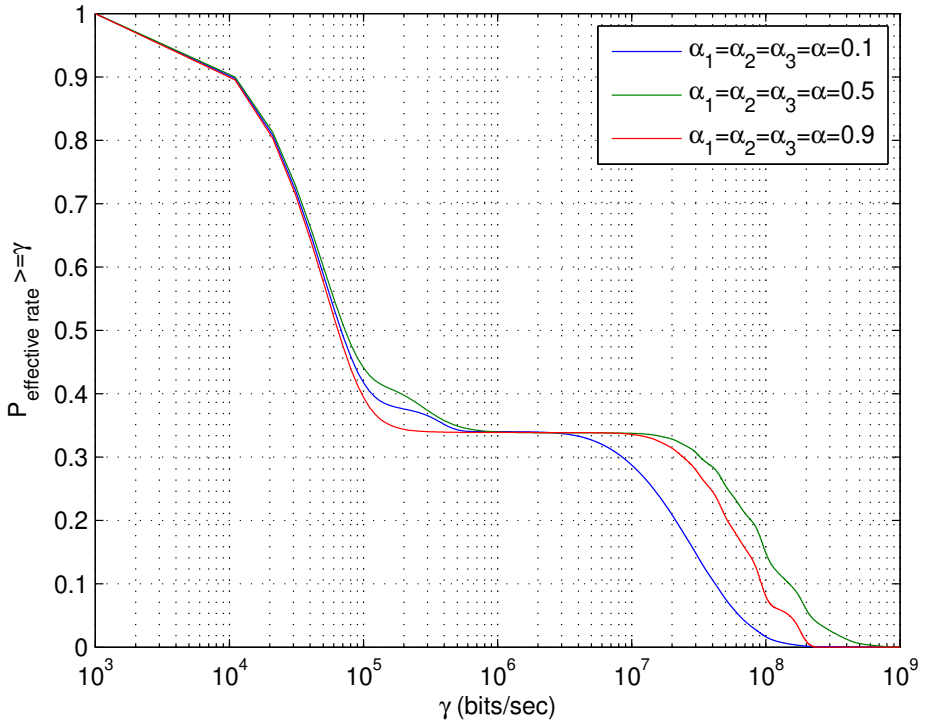

Figure 4.4: Effective rate coverage probability versus rate threshold γ for varying α with $\lambda_{MBS} = 4 \times 10^{-6}$ BS$/m^2$, $\lambda_{SC} = 100 \times \lambda_{MBS}$ BS$/m^2$, $\lambda_{UAV} = 3 \times \lambda_{MBS}$ BS$/m^2$, $\theta_{SC} = 30$ dB, $\theta_{MBS} = 0$ dB, $\theta_{UAV} = 6$ dB and $\tau_{\mathrm{MBS}} = \tau_{\mathrm{SC}} = \tau_{\mathrm{UAV}} = 0$ dB.

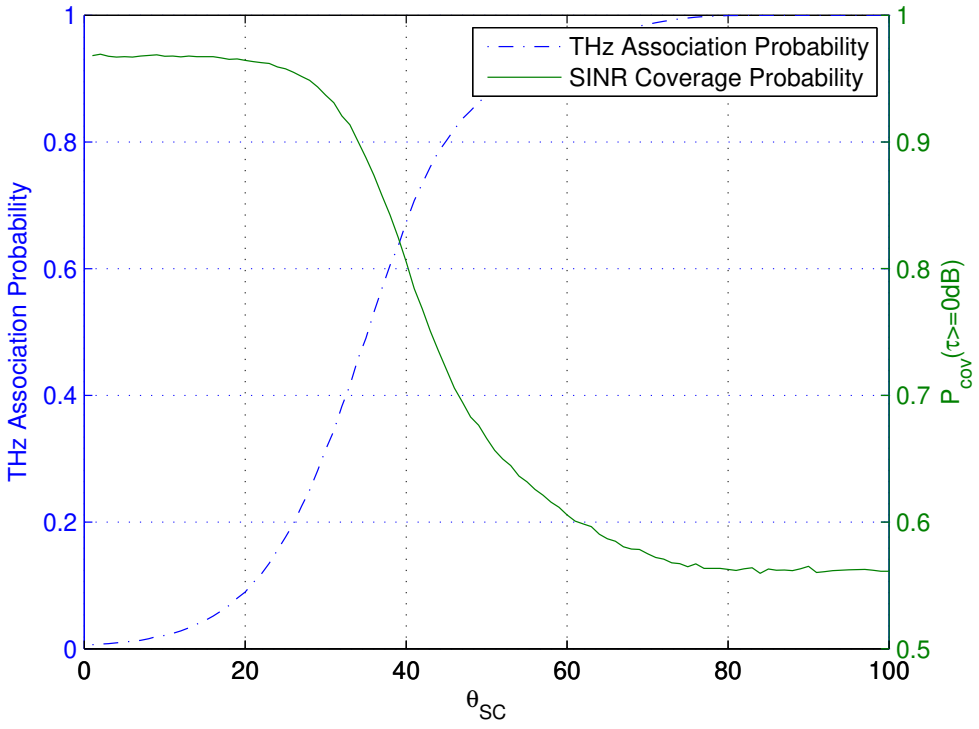

Figure 4.5: Trend of user association with THz cells and SINR coverage probability versus varying θ_{SC} with $\lambda_{MBS} = 4 \times 10^{-6}$ BS$/m^2$, $\lambda_{SC} = 100 \times \lambda_{MBS}$ BS$/m^2$, $\lambda_{UAV} = 3 \times \lambda_{MBS}$ BS$/m^2$, $\theta_{MBS} = 0$ dB, $\theta_{UAV} = 6$ dB and $\tau_{\text{MBS}} = \tau_{\text{SC}} = \tau_{\text{UAV}} = 0$ dB.

4.3.4 User Association with THz cells and SINR Coverage Probability versus varying Bias Values

Fig. 4.5 shows the variation of the results related to the associated probability of users to THz cells and the SINR coverage probability w.r.t varying the THz bias value from 0 dB to 100 dB. The SINR coverage threshold τ is set to be 0 dB, and the SINR performance is depicted for different THz biasing values. It is observed that the best performance of SINR is achieved without biasing the THz cells. As we increase the bias value, the SINR starts degrading. This is due to the presence

of high propagation losses at THz frequencies and as more users get associated with THz cells, it results in the overall degradation of total SINR. As THz bias factor, θ_{SC} is increased from 0 to 40 dB having τ = 0 dB, the SINR coverage probability drops from 0.92 to 0.62.

4.3.5 SINR Coverage and Effective Rate Probabilities versus different SINR threshold values

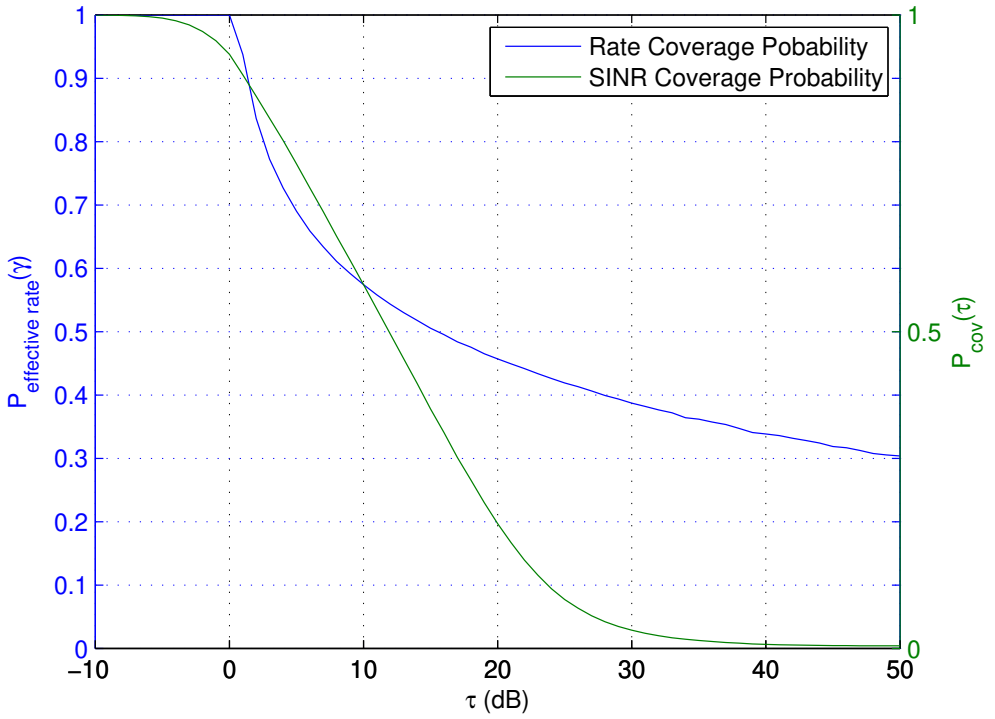

Figure 4.6: Impact of SINR threshold on coverage probability and effective rate coverage probability with $\lambda_{MBS} = 4 \times 10^{-6}$ BS$/m^2$, $\lambda_{UAV} = 3 \times \lambda_{MBS}$ BS$/m^2$, $\theta_{SC} = 30$ dB, $\theta_{MBS} = 0$ dB, $\theta_{UAV} = 6$ dB and $\gamma = 1$ Kbps.

To further justify the performance improvement in the SINR and rate coverage probability of the users, we have shown the variation on SINR coverage and

effective rate probabilities against the different SINR threshold values in Fig. 4.6. Rate coverage probability is analyzed for a threshold of γ = 1 Kbps. For this simulation result, we have fixed the values of θ_{MBS} = 0 dB, θ_{UAV} = 6 dB, and θ_{SC} = 30 dB, respectively. It can be seen that the rate coverage probability drops as the SINR threshold is increased. This is due to the fact that the number of users in coverage decreases with the increasing threshold. It can also be noted that as the SINR threshold is varied from 0 to 20 dB, the SINR coverage probability of HetNet drops down to 20%.

4.4 Conclusions

In this chapter, a Heterogeneous Network consisting of sub-6 GHz frequency bands enabled MBS and UAVs and small cells operating at THz frequencies is considered. It has been observed from the simulation results that sub-6 GHz BSs outperforms TSCs in providing better SINR coverage, whereas, THz cells provide users with very high data rates hence help in fulfilling high Quality-of-Service requirements. Effect on rate coverage probabilities have also been observed by changing the proportion of bandwidths in access and backhaul links. Simulation results also show that use of HetNet provides better coverage to the users than the traditional networks by making use of UAVs mobility and fast deployment to the cell edges. Also mmWave and THz large bandwidth provide very high data rates that are not achievable by traditional sub-6 GHz networks.

Chapter 5

Coverage Analysis of Heterogeneous Network

Heterogeneous networks emerge as a viable solution to the problems such as coverage holes, overly crowded areas and the coverage for end users located at the boundary of the coverage area. Placement of small cells operating at mmWave and THz frequencies can greatly improve the rate coverage probability of the users. Induction of UAVs in the HetNet make provision for deployments in crowded areas such as sports matches and political gatherings. UAVs provide better coverage due to its ability to provide Line of Sight links to the users.

This chapter presents an extensive analytical framework based on tools from stochastic analysis for coverage and rate analysis in a multi-tier HetNet comprising of four tiers. Macro base station (MBS) operating on sub-6 GHz constitute tier 1, small cells operating on mmWave frequency represents tier 2,THz enabled small cells make up the tier 3 and UAVs operating at mmWave frequencies represents tier 4. [130].

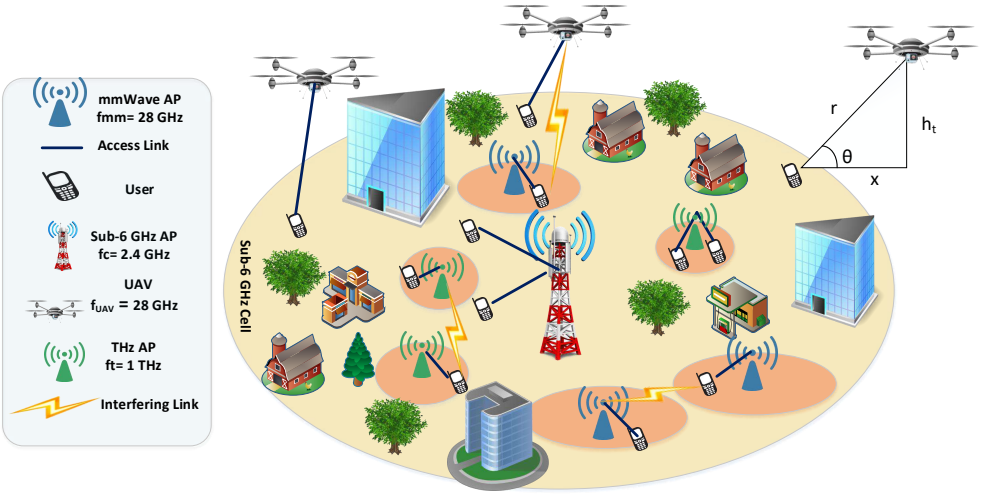

Figure 5.1: A graphical snapshot of integrated aerial and terrestrial heterogeneous network consisting of MBS operating at sub-6 GHz band with density $\lambda_1 = 4 \times 10^{-6}$ BS$/m^2$, mmWave-enabled access points with density $\lambda_2 = 3 \times \lambda_1$ BS$/m^2$ and THz-enabled access points with density $\lambda_3 = 3 \times \lambda_1$ BS$/m^2$ supported by aerial base stations with density $\lambda_4 = 3 \times \lambda_1$ BS$/m^2$ in area with cellular radius = 500 meters.

5.1 System Model

We consider a multi-tier HetNet as shown in Fig. 1. The tier 1 consists of sub-6 GHz MBSs, tier 2 is composed of mmWave small cells (MSC), tier 3 comprises of THz small cells (TSC) and tier 4 constitutes mmWave UAVs. Independent homogeneous Poisson point processes (HPPP), ϕ_i, are used to model BS locations having densities λ_i where $i \in \{1,2,3,4\}$ for MBS, MSC, TSC and UAV, respectively. It is assumed that all the BSs of a particular tier have the same transmission power. The user locations also follow an independent homogeneous PPP, ϕ_u, with density λ_u. Each user measures the channel quality and associates with the BS providing maximum biased average received power. The envelope of the fading,

$|h|$, between a transmitter and a receiver, follows a Nakagami fading model and its probability density function (PDF) is as follows

$$|h| \sim f_{|h|}(l, \Omega_w) \triangleq \frac{\Omega_w^{\Omega_w} l^{\Omega_w - 1} \exp\{-\Omega_w l\}}{\gamma(\Omega_w)}, \forall l > 0, \tag{5.1}$$

where Ω_w is the Nakagami fading parameter wherein $w \in \{l_m, n_m\}$ and $\gamma(.)$ is the gamma function. Ω_{l_m} and Ω_{n_m} are Nakagami fading parameters, where LoS and NLoS propagation environments are represented by l_m and n_m, respectively. The Nakagami parameter for each environment is differently characterized. The channel for sub-6 GHz frequencies is assumed to be Rayleigh fading, i.e., Nakagami fading with $\Omega_w = 1$.

In our work, the maximum biased received power is considered for user association with a BS. The association scheme determines the tier k for a typical user such that

$$k = \arg \max_{i \in \{1,2,3,4\}} \left(\overline{P}_i \psi_i G_i x^{-\beta_i} \right), \tag{5.2}$$

where $\overline{P}_i$ is the transmission power of tier i, ψ_i is the bias value of i^{th} tier, G_i denotes the antenna gains for tier i, x represents the distance between the typical user and the BS of tier i, β_i is the path loss exponent of tier i, $f_{c,i}$ is the carrier frequency of that particular tier and c is the speed of light. We now discuss the system model of each tier.

5.1.1 Sub-6 GHz MBS tier

The received power at a typical user in tier 1 (i.e. MBS) is given as

$$P_{r,\mathrm{MBS}}\left[dB\right] = \tilde{P}_1 - PL_{\mathrm{MBS}}, \tag{5.3}$$

where $\tilde{P}_1$ is the biased transmitted power and PL_{MBS} is the path loss of tier 1. PL_{MBS} can be evaluated as

$$PL_{\mathrm{MBS}} = 20\log\left(\frac{4\pi f_{c,1}}{c}\right) + 10\beta_1\log(x), \tag{5.4}$$

where $f_{c,1}$ represents the carrier frequency, x denotes the distance between the transmitter and the receiver, and β_1 is the path loss exponent. The signal-to-interference plus noise ratio (SINR) experienced by a typical user is given as

$$\mathrm{SINR}_{\mathrm{MBS}} = \frac{P_{r,\mathrm{MBS}}}{\sigma_1^2 + I_1}, \tag{5.5}$$

where σ_1^2 denotes the power spectral density of the noise and $I_1 = \sum_{k\in\phi_1/\{a_o\}} \tilde{P}_1 h_k x_k^{-\beta_1}$ is the cumulative interference from other BSs in tier 1.

5.1.2 mmWave Small Cell tier

The mmWave small cells are distributed using a PPP and because of the blockages in the mmWave band, this distribution can be further divided into two independent non-homogeneous PPPs, $\phi_{mm,L}$ and $\phi_{mm,N}$ for LoS and NLoS mmWave small cells, respectively, by using the independent thinning theorem. For analytical tractability, a typical user is assumed to be located at origin O. The user is

considered in LoS to MSC BS located at T if there is no blockage in the path OT. $\phi_{mm,L}$ and $\phi_{mm,N}$ have the densities $\mathfrak{P}_{LoS}(x)\lambda_2$ and $(1-\mathfrak{P}_{LoS}(x))\lambda_2$, where $\mathfrak{P}_{LoS}(x)$ is the LoS probability function. The function $\mathfrak{P}_{LoS}(x)$ can be evaluated using blockage models from stochastic geometry or from field measurements and is given by $e^{-\varphi x}$ where φ is the environment-dependent variable and x is the distance between transmitter and the receiver.

The MSC tier incorporates directional beamforming to compensate for the path loss at mmWave frequencies. For the MSC tier, the SINR experienced by a typical user connected to serving MSC b_o is given by

$$\text{SINR}_{\text{MSC}} = \frac{\overbrace{\overline{P}_2 \psi_2}^{\tilde{P}_2} G_r^{mm} G_t^{mm} h_x x^{-\beta_2}}{\sum_{i\in(l,n)} \sum_{j\in\{\phi_{mm}/b_o \cup \phi_{UAV}\}} \tilde{P}_2 G_V h_j x_j^{-\beta_{2i}} + \sigma_2^2}, \tag{5.6}$$

where $\overline{P}_2$ represents the transmit power of MSC BS, ψ_2 is the bias factor, $\tilde{P}_2$ is the biased transmit power, G_r^{mm} and G_t^{mm} are the receiver and transmitter antennas main lobe gains, respectively, h_x is the Nakagami fading, x denotes the distance between the user and the MSC, β_2 is the path loss exponent, l and n represents the LoS and NLoS interfering links, ϕ_{mm} and ϕ_{UAV} represents the PPP distributions for mmWave small cells and UAVs and σ_2^2 is the noise power spectral density. The directivity gain of the interfering antenna is given by G_V^{mm}. Both BSs and users are assumed to be in perfect alignment so the desired link directivity gain is

given by $G_r^{mm}G_t^{mm}$. The directivity gain, G_V^{mm}, where $V \in \{1,2,3,4\}$ is given as,

$$G_V^{mm} = \begin{cases} G_1 = G_r^{mm}G_t^{mm}, & \text{with prob.} \dfrac{\Theta_r\Theta_t}{4\pi^2} \\ G_2 = G_r^{mm}g_t^{mm}, & \text{with prob.} \dfrac{\Theta_r(2\pi-\Theta_t)}{4\pi^2} \\ G_3 = g_r^{mm}G_t^{mm}, & \text{with prob.} \dfrac{(2\pi-\Theta_r)\Theta_t}{4\pi^2} \\ G_4 = g_r^{mm}g_t^{mm}, & \text{with prob.} \dfrac{(2\pi-\Theta_r)(2\pi-\Theta_t)}{4\pi^2} \end{cases}, \tag{5.7}$$

where g_t^{mm} and g_r^{mm} are side lobe gains for transmitter and receiver, and the half power beamwidths of transmitter and receiver are given by Θ_t and Θ_r.

5.1.3 THz Small Cell tier

Because of dense deployments and high molecular absorption losses, the LoS transmissions become dominant over NLoS transmissions. The channel power for the LoS communication is modeled between users and THz small cells as

$$l(x) = exp(-k(f_{c,3})x)x^{-\beta_3}, \tag{5.8}$$

where x denotes the distance, $f_{c,3}$ represents the THz frequency and $k(f_{c,3})$ is the molecular absorption coefficient dependent on frequency [129]. The directional transmitter and receiver antenna gains $G_t^T(\Theta)$ and $G_r^T(\Theta)$ are modeled as

$$G_y^T = \begin{cases} G_y^{T(max)}, & |\Theta| \leq s_y \\ G_y^{T(min)}, & |\Theta| > s_y \end{cases}, \tag{5.9}$$

where y $\in \{t, r\}$, Θ represents the beamwidth angle, s_y is the main lobe beamwidth, $G_y^{T(max)}$ and $G_y^{T(min)}$ represents the main lobe and side lobe beamforming gains, respectively.

The SINR of a user in tier 3 can be computed as,

$$\text{SINR}_\text{T} = \frac{\overbrace{\overline{P}_3 \psi_3}^{\tilde{P}_3} G_t^{T(max)}(\Theta) G_r^{T(max)}(\Theta) l(x)}{\sigma_3^2 + I_3}, \tag{5.10}$$

where $I_3 = \sum_{i \in \phi_T / c_o} \tilde{P}_3 G_y^T l(x_i)$ is the cumulative interference from other TSCs, x_i represents the distance, $\overline{P}_3$ denotes the transmit power of the THz BS, ψ_3 is the bias factor and σ_3^2 is the thermal noise.

5.1.4 mmWave UAV tier

UAVs are distributed in the considered region of interest according to a PPP, ϕ_{UAV}, with density λ_4. λ_4 is divided into two independent PPPs with densities $\overline{\lambda_4}$ and $\widetilde{\lambda_4}$. $\overline{\lambda_4}$ represents the proportion of UAVs operating on mmWave band denoted by $\alpha \times \lambda_4$ whereas $\widetilde{\lambda_4}$ represents the proportion of UAVs operating on sub-6 GHz band denoted by $(1-\alpha) \times \lambda_4$. Because of the blockage effect in the mmWave band, the UAV network can be further divided into two independent PPPs. One non-homogeneous PPP, ϕ_L, represents the LoS mmWave UAVs and has a density of $\alpha \times \lambda_4 \times \mathcal{P}_{LoS}(x)$. Similarly, other non-homogeneous PPP, ϕ_N, represents the NLoS mmWave UAVs with density $\alpha \times \lambda_4 \times (1 - \mathcal{P}_{LoS}(x))$. A geometric model given in [95] is used for the derivation of LoS probability, $\mathcal{P}_{LoS}$, and is given as

$$\mathcal{P}_{LoS} = \frac{1}{1 + a_u \exp\left[-b_u \left(\Lambda_{UAV} - a_u\right)\right]}, \tag{5.11}$$

where a_u and b_u are environment dependent parameters and Λ_{UAV} is the elevation angle. Λ_{UAV} is given by

$$\Lambda_{UAV} = \arctan\left(\frac{h_t}{\sqrt{r^2 - h_t^2}}\right), \tag{5.12}$$

where h_t denotes the height of the UAV, r represents the 3D distance and $\sqrt{r^2 - h_t^2}$ represents the horizontal distance between UAV and a user. The NLoS probability is given by

$$\mathcal{P}_{NLoS} = 1 - \mathcal{P}_{LoS}, \tag{5.13}$$

Because of the existence of two links, LoS and NLoS, between the user and the UAV due to blockages, two different path loss functions for LoS and NLoS links exist and are given as,

$$PL(r) = \begin{cases} PL^{L}(r) = C_L r^{-\beta_L} \\ PL^{NL}(r) = C_N r^{-\beta_N} \end{cases}, \tag{5.14}$$

where C_L and C_N are the intercepts for the LoS and NLoS formulas, β_L and β_N are the LoS and NLoS path loss exponents. The values of β_L, β_N, C_L and C_N are found using field tests [121, 131]. The antenna gain for the UAV mmWave

network, G_e^{uav}, where $e \in \{1,2,3,4\}$ is given as,

$$G_e^{uav} = \begin{cases} G_1 = G_r^{uav} G_t^{uav}, & \text{with prob.} \dfrac{\Theta_r \Theta_{uav}}{4\pi^2} \\ G_2 = G_r^{uav} g_t^{uav}, & \text{with prob.} \dfrac{\Theta_r \left(2\pi - \Theta_{uav}\right)}{4\pi^2} \\ G_3 = g_r^{uav} G_t^{uav}, & \text{with prob.} \dfrac{\left(2\pi - \Theta_r\right) \Theta_{uav}}{4\pi^2} \\ G_4 = g_r^{uav} g_t^{uav}, & \text{with prob.} \dfrac{\left(2\pi - \Theta_r\right) \left(2\pi - \Theta_{uav}\right)}{4\pi^2} \end{cases}, \tag{5.15}$$

where G_t^{uav} , G_r^{uav} and g_t^{uav}, g_r^{uav} are main lobe gains and side lobe gains for transmitter and receiver, and the half power beamwidths of transmitter and receiver are given by Θ_{uav} and Θ_r.

Considering now the user associates with LoS and NLoS UAV u_o at a distance r, then the SINR can be given as,

$$\text{SINR}_{UAV} = \frac{\overbrace{\overline{P}_4 \psi_4}^{\tilde{P}_4} r^{-\beta_4} h_r G_r^{uav} G_t^{uav}}{I_4 + \sigma_4^2} \tag{5.16}$$

where $\overline{P}_4$ is the UAV transmit power, h is the Nakagami fading, G_e^{uav} is the antenna gain, ψ_4 is the bias factor, $I_4 = \sum_{i \in (l,n)} \sum_{j \in \{\phi_{UAV}/u_o \cup \phi_{mm}\}} \tilde{P}_4 G_e^{uav} h_j r_j^{-\beta_{4i}}$ is the aggregate interference power from other UAVS and mmWave small cells, and σ_4^2 is the noise power spectral density.

5.2 Performance Evaluation

In this section, we derive the association and coverage probabilities of a typical user, assumed at origin, which is connected to one of the HetNet tiers. We start with the following lemma.

Table 5.1: List of Symbols

$\overline{P_i}$	Transmit power of tier i
$\tilde{P_i}$	Biased transmit power of tier i
ψ_i	Bias value of tier
β	Path loss exponent
$f_{c,i}$	Carrier frequency of tier i
$\Omega_{l_m}, \Omega_{n_m}$	Nakagami fading parameters for LoS and NLoS propagation environments
P_r	Received Power
G_r, G_t	Main lobe antenna gains for receiver and transmitter
g_r, g_t	Side lobe antenna gains for receiver and transmitter
a_u, b_u	Environment dependent parameters
λ_i	BS density of tier i
ϕ_{mm}, ϕ_{UAV}	PPP distribution of mmWave small cells and UAVs
x	Distance between the transmitter and receiver
Θ_r, Θ_t	Receiver and transmitter half power beamwidths
$\mathfrak{P}_{LoS}(x)$	Probability of line of sight for mmWave small cells
$\mathcal{P}_{LoS}$	Probability of line of sight function for UAVs
Λ_{UAV}	Elevation angle of UAV
h_t	Height of the UAV
r	Distance between the UAV and the user
PL	Path loss function
Γ_i	SINR Threshold of tier i
δ_i	Association probability of tier i
$f_{X_i}(x)$	PDF of the distance between the typical user and BS
$P_c^1(\Gamma_1, x)$	Conditional coverage probability for a user and the serving BS for distance x
$E_{v,i}(\Gamma, x)$	Interference terms from LoS(NLOS) mmWave small cells
$H_{v,i}(\Gamma, r)$	Interference terms from LoS(NLOS) UAVs
σ_i^2	Noise power spectral density

Lemma 1 *The association probability that a typical user connects with the i^{th} tier*

based on maximum biased received power is given as

$$\begin{aligned}
\delta_i &= \mathbb{E}_{x_i}[\mathbb{P}[P_{r,i} > \max_{n,n\neq i} P_{r,n}]] \\
&= \mathbb{E}_{x_i}[\prod_{n=1,n\neq i}^{4} [\mathbb{P}[P_{r,i} > P_{r,n}]] \\
&\overset{(a)}{=} \mathbb{E}_{x_i}\left[\prod_{n=1,n\neq i}^{4} [\mathbb{P}[x_n > \left(\frac{\widetilde{P}_n G_n x_i^{\beta_i}}{\widetilde{P}_i G_i}\right)^{1/\beta_n}]]\right] \\
&= \int_0^{\infty} \underbrace{\left[\prod_{n=1,n\neq i}^{4} [\mathbb{P}[x_n > \left(\frac{\widetilde{P}_n G_n x_i^{\beta_i}}{\widetilde{P}_i G_i}\right)^{1/\beta_n}]]\right]}_{\kappa} f_{X_i}(x)\, dx,
\end{aligned} \tag{5.17}$$

where (a) is based on downlink user association. The detailed derivation of Lemma 1 is given in Appendix A.

From Lemma 1, we can infer that the typical association of a user to a particular tier depends upon the distance between the user and the BS, transmit power, path loss exponent, and antenna gains of that tier. The user will associate to the BS that provides the maximum biased received power and the association probability to a particular tier can be increased by increasing the transmit power or the bias of that particular tier. This biasness helps in offloading the users to tiers with high available bandwidth.

Now that the user association probability with a particular tier is known, we now revert our attention to finding the coverage probability of a user with that particular tier. Please refer to the following lemma.

Lemma 2 *The SINR coverage probability at the user connecting with MBS is given by*

$$P_c^1(\Gamma_1) = \int_0^\infty P_c^1(\Gamma_1, x) f_{X_1}(x)\, dx, \tag{5.18}$$

where $P_c^1(\Gamma_1, x)$ *denotes the conditional coverage probability for a typical user and the serving MBS for a distance x and* $f_{X_1}(x)$ *is the PDF of the distance between the typical user and MBS and is given as*

$$\begin{aligned} f_{X_1}(x) = \frac{2\pi\lambda_1}{\delta_1} x exp\Bigg(&- \pi\lambda_1 x^2 - 2\pi\lambda_2 \Upsilon(x) \\ &- 2\pi\lambda_3 T(x) - 2\pi\lambda_4 U(x) \Bigg), \end{aligned} \tag{5.19}$$

where δ_1 *is the user association probability with tier 1 and is given as,*

$$\begin{aligned} \delta_1 = 2\pi\lambda_1 \int_0^\infty x exp\Bigg(&- \pi\lambda_1 x^2 - 2\pi\lambda_2 \Upsilon(x) - 2\pi\lambda_3 T(x) \\ &- 2\pi\lambda_4 U(x) \Bigg) dx, \end{aligned} \tag{5.20}$$

The conditional coverage probability $P_c^1(\Gamma_1, x)$*, is given as,*

$$P_c^1(\Gamma_1, x) = exp\left(\frac{-\Gamma_1 x^{\beta_1} \sigma_1^2}{\widetilde{P}_1}\right) \mathbb{E}_{I_1}\left[\mathcal{L}_{I_1}\left(\frac{\Gamma_1 x^{\beta_1}}{\widetilde{P}_1}\right)\right], \tag{5.21}$$

Proof: See Appendix B.

Lemma 3 *The SINR coverage probability of a user connecting with MSC tier is*

given as,

$$P_c^2(\Gamma_2) = \sum_{v\in\{L,N\}} \delta_{2,v} P_c^{2,v}(\Gamma_2), \tag{5.22}$$

where $P_c^{2,L}(\Gamma_2)$ *and* $P_c^{2,N}(\Gamma_2)$ *are the conditional coverage probabilities that a user is connected with MSC in* ϕ_L *and* ϕ_N*, respectively.* $P_c^{2,v}(\Gamma_2)$ *can be computed as,*

$$\begin{aligned} P_c^{2,v}(\Gamma_2) = \sum_{i=1}^{\Omega_w} (-1)^{i+1} \binom{\Omega_w}{i} \int_0^\infty exp\left(\frac{-i\rho_w x^{\beta_v} \Gamma_2 \sigma_2^2}{G_r^{mm} G_t^{mm}} \right. \\ \left. - E_{v,i}(\Gamma_2, x) - H_{v,i}(\Gamma_2, r) \right) f_v(x), dx, \end{aligned} \tag{5.23}$$

where $E_{v,i}(\Gamma_2, x)$ *and* $H_{v,i}(\Gamma_2, r)$ *accounts for the interference terms from LoS(NLoS) mmWave small cells and UAVs,* $\rho_w = \Omega_w (\Omega_w!)^{-1/\Omega_w}, w \in \{l_m, n_m\}$*,* $F(\Omega_w, x) = 1 - \frac{1}{(1+x)^{\Omega_w}}$ *and* $\hat{a}_i = \frac{a_i}{G_r^{mm} G_t^{mm}}$.

$$\begin{aligned} E_{L,i}(\Gamma_2, x) = 2\pi\lambda_2 \sum_{i=1}^{4} p_i \left[\int_x^\infty F\left(\Omega_{l_m}, \frac{i\rho_{l_m} \hat{a}_i \Gamma_2 x^{\beta_L}}{\Omega_{l_m} t^{\beta_L}} \right) \right. \\ t \mathfrak{P}_{LoS}(t)\, dt + \int_{\Xi_L(x)}^\infty F\left(\Omega_{n_m}, \frac{i\rho_{l_m} \hat{a}_i \Gamma_2 x^{\beta_L}}{\Omega_{n_m} t^{\beta_N}} \right) \\ \left. t\left(1 - \mathfrak{P}_{LoS}(t)\right) dt \right], \end{aligned} \tag{5.24}$$

$$E_{N,i}(\Gamma_2,x) = 2\pi\lambda_2 \sum_{i=1}^{4} p_i \left[\int_{\Xi_N(x)}^{\infty} F\left(\Omega_{l_m}, \frac{i\rho_{n_m}\hat{a}_i\Gamma_2 x^{\beta_N}}{\Omega_{l_m} t^{\beta_L}}\right) t\mathfrak{P}_{LoS}(t)\, dt + \int_{x}^{\infty} F\left(\Omega_{n_m}, \frac{i\rho_{n_m}\hat{a}_i\Gamma_2 x^{\beta_N}}{\Omega_{n_m} t^{\beta_N}}\right) t\left(1-\mathfrak{P}_{LoS}(t)\right) dt \right], \tag{5.25}$$

$$H_{L,i}(\Gamma_2,r) = 2\pi\alpha\lambda_4 \sum_{i=1}^{4} p_i \left[\int_{r}^{\infty} F\left(\Omega_{l_m}, \frac{i\rho_{l,m}\hat{a}_i\Gamma_2 x^{\beta_L}}{\Omega_{l_m} t^{\beta_L}}\right) t\mathcal{P}_{LoS}(t)\, dt + \int_{\xi_L(r)}^{\infty} F\left(\Omega_{n_m}, \frac{i\rho_{l,m}\hat{a}_i\Gamma_2 x^{\beta_L}}{\Omega_{n_m} t^{\beta_N}}\right) t\left(1-\mathcal{P}_{LoS}(t)\right) dt \right], \tag{5.26}$$

$$H_{N,i}(\Gamma_2,r) = 2\pi\alpha\lambda_4 \sum_{i=1}^{4} p_i \left[\int_{\xi_N(r)}^{\infty} F\left(\Omega_{l_m}, \frac{i\rho_{n_m}\hat{a}_i\Gamma_2 x^{\beta_N}}{\Omega_{l_m} t^{\beta_L}}\right) t\mathcal{P}_{LoS}(t)\, dt + \int_{r}^{\infty} F\left(\Omega_{n_m}, \frac{i\rho_{n_m}\hat{a}_i\Gamma_2 x^{\beta_N}}{\Omega_{n_m} t^{\beta_N}}\right) t\left(1-\mathcal{P}_{LoS}(t)\right) dt \right], \tag{5.27}$$

Proof: See Appendix C.

Lemma 4 *The SINR coverage probability of a user connecting with TSC tier is*

given as,

$$P_c^3(\Gamma_3) = \sum_{v\in\{L,N\}} \delta_{3,v} P_c^{3,v}(\Gamma_3), \tag{5.28}$$

The conditional probability $P_c^{3,v}(\Gamma_3)$ *can be derived as*

$$\begin{aligned} P_c^{3,v}(\Gamma_3) = \sum_{i=1}^{\Omega_w} (-1)^{i+1} \binom{\Omega_w}{i} \int_0^\infty exp\Bigg(& \frac{-i\rho_w x^{\beta_v} \Gamma_3 \sigma_3^2}{\widetilde{P}_3 exp\left(-k\left(f_{c,3}\right)x\right) G_r^T G_t^T} \\ & - S_{v,i}(\Gamma_3, x) \Bigg) f_{X_3}(x)\, dx, \end{aligned} \tag{5.29}$$

where $f_{X_3}(x)$ *is the PDF of the distance between the typical user and TSC tier.* $S_{v,i}(\Gamma_3, x)$ *in (5.29) accounts for interference terms in TSC tier and can be computed using similar steps followed in Appendix C.*

Proof: Proof follows similar steps introduced in Appendix C.

Lemma 5 *The SINR coverage probability of a user connecting with UAV tier is given as,*

$$P_c^4(\Gamma_4) = \sum_{v\in\{L,N\}} \delta_{4,v} P_c^{4,v}(\Gamma_4), \tag{5.30}$$

where $P_c^{4,L}(\Gamma_4)$ *and* $P_c^{4,N}(\Gamma_4)$ *are the conditional coverage probabilities that a user is connected with UAV tier in* ϕ_L *and* ϕ_N*, respectively.* $P_c^{4,v}(\Gamma_4)$ *can be com-*

puted as

$$P_c^{4,v}(\Gamma_4) = \sum_{i=1}^{\Omega_w} (-1)^{i+1} \binom{\Omega_w}{i} \int_{h_t}^{\infty} exp\left(\frac{-i\rho_w r^{\beta_v} \Gamma_4 \sigma_4^2}{G_r^{uav} G_t^{uav}} - H_{v,i}(\Gamma_4, r) - E_{v,i}(\Gamma_4, x) \right) f_v(r)\, dr, \tag{5.31}$$

where $f_v(r)$ is the PDF of the distance between a user and UAV tier, $\rho_w = \Omega_w (\Omega_w!)^{-1/\Omega_w}, w \in \{l_m, n_m\}$, $H_{v,i}(\Gamma_4, r)$ and $E_{v,i}(\Gamma_4, r)$ accounts for the interference terms from LoS(NLoS) mmWave UAVs and mmWave small cells, where

$$H_{L,i}(\Gamma_4, r) = 2\pi\alpha\lambda_4 \sum_{i=1}^{4} p_i \left[\int_r^{\infty} F\left(\Omega_{l_m}, \frac{i\rho_{l_m} \hat{a}_i \Gamma_4 r^{\beta_L}}{\Omega_{l_m} t^{\beta_L}} \right) t\mathcal{P}_{LoS}(t)\, dt + \int_{\xi_L(r)}^{\infty} F\left(\Omega_{n_m}, \frac{i\rho_{l_m} \hat{a}_i \Gamma_4 r^{\beta_L}}{\Omega_{n_m} t^{\beta_N}} \right) t(1 - \mathcal{P}_{LoS}(t))\, dt \right], \tag{5.32}$$

$$H_{N,i}(\Gamma_4, r) = 2\pi\alpha\lambda_4 \sum_{i=1}^{4} p_i \left[\int_{\xi_N(r)}^{\infty} F\left(\Omega_{l_m}, \frac{i\rho_{n_m} \hat{a}_i \Gamma_4 r^{\beta_N}}{\Omega_{l_m} t^{\beta_L}} \right) t\mathcal{P}_{LoS}(t)\, dt + \int_r^{\infty} F\left(\Omega_{n_m}, \frac{i\rho_{n_m} \hat{a}_i \Gamma_4 r^{\beta_N}}{\Omega_{n_m} t^{\beta_N}} \right) t(1 - \mathcal{P}_{LoS}(t))\, dt \right], \tag{5.33}$$

$$E_{L,i}(\Gamma_4,x) = 2\pi\lambda_2 \sum_{i=1}^{4} p_i \Bigg[\int_x^{\infty} F\left(\Omega_{l_m}, \frac{i\rho_{l_m}\hat{a}_i\Gamma_4 x^{\beta_L}}{\Omega_{l_m} t^{\beta_L}}\right) t\mathfrak{P}_{LoS}(t)\, dt + \int_{\Xi_L(x)}^{\infty} F\left(\Omega_{n_m}, \frac{i\rho_{l_m}\hat{a}_i\Gamma_4 x^{\beta_L}}{\Omega_{n_m} t^{\beta_N}}\right) t(1-\mathfrak{P}_{LoS}(t))\, dt \Bigg], \tag{5.34}$$

$$E_{N,i}(\Gamma_4,x) = 2\pi\lambda_2 \sum_{i=1}^{4} p_i \Bigg[\int_{\Xi_N(x)}^{\infty} F\left(\Omega_{l_m}, \frac{i\rho_{n_m}\hat{a}_i\Gamma_4 x^{\beta_N}}{\Omega_{l_m} t^{\beta_L}}\right) t\mathfrak{P}_{LoS}(t)\, dt + \int_{x}^{\infty} F\left(\Omega_{n_m}, \frac{i\rho_{n_m}\hat{a}_i\Gamma_4 x^{\beta_N}}{\Omega_{n_m} t^{\beta_N}}\right) t(1-\mathfrak{P}_{LoS}(t))\, dt \Bigg], \tag{5.35}$$

Proof: See Appendix D for the proof.

Special Case: By setting $\Omega_{l_m} = \Omega_{n_m} = \rho_{l_m} = \rho_{n_m} = 1$, and taking the density for LoS sub-6 GHz UAVs as $(1-\alpha)\times\lambda_4\times\mathcal{P}_{LoS}(x)$ and for NLoS sub-6 GHz UAVs as $(1-\alpha)\times\lambda_4\times(1-\mathcal{P}_{LoS}(x))$, Eq. (5.31) can be transformed into conditional coverage probability for sub-6 GHz UAVs. The conditional coverage probability for sub-6 GHz UAVs is then given as,

$$P_c^{4,v}(\Gamma_4) = \int_{h_t}^{\infty} exp\left(\frac{-ir^{\beta_v}\Gamma_4\sigma_4^2}{G_r^{uav}G_t^{uav}} - H_{v,i}(\Gamma_4,r)\right) f_v(r)\, dr, \tag{5.36}$$

where $H_{v,i}(\Gamma_4,r)$ is the interference from the LoS and NLoS sub-6 GHz UAVs. From the above-mentioned lemmas, we can see that the SINR coverage probability of a user connecting to a particular tier depends upon the SINR threshold. As

we increase the threshold value, SINR coverage probability tends to decrease as fewer number of users remain in the coverage.

Proposition 1 *The total coverage probability, $P_{c,T}$, for the multi-tier hybrid network is defined as*

$$P_{c,T} = \sum_{i=1}^{4} P_c^i \delta_i, \tag{5.37}$$

where δ_i represents the user association probability for tier i and P_c^i denotes the coverage probability for tier i.

Lemma 6 *The achievable ergodic rate for a user connecting with i^{th} tier is given as,*

$$R_i = \frac{1}{ln2} \int_0^{\infty} \frac{P_c^i(\Gamma_i)}{1+\Gamma_i} d\Gamma_i, \tag{5.38}$$

where P_c^i is the coverage probability of tier i and Γ_i is the SINR threshold of tier i.

Proof: See Appendix E.

From Lemma 6, rate coverage probability can be defined for a given threshold, τ, as

$$P_{rate,i}(\tau) = P(R_i > \tau), \tag{5.39}$$

where τ is the rate coverage probability threshold and is assumed to be same for all tiers.

From Lemma 6, we can see that rate coverage probability depends upon the rate threshold. A higher threshold value implies that fewer of users will satisfy

the higher data rate requirements. The higher data rate requirements can be met if the users are connected to mmWave or THz frequency tiers because of the higher available bandwidth.

Proposition 2 *The total rate coverage probability, P_{rate}, for the HetNet is defined as*

$$P_{rate}(\tau) = \sum_{i=1}^{4} P_{rate,i}\delta_i, \tag{5.40}$$

where δ_i is the association probability of tier i and $P_{rate,i}$ is the rate coverage probability of the tier i.

5.3 Performance Evaluation and Discussion

In this section, we present the simulation results for the proposed hybrid HetNet. In our simulation setup, we assume the MBS density to be $\lambda_1 = \frac{3}{500^2 \times \pi}$. The downlink transmission powers are assumed to be 40 Watts for MBS and 1 Watt for other tiers. The transmission frequency $f_{c,1}$ is set to be 2.4 GHz, $f_{c,3}$ is taken as 1 THz, $f_{c,2}$ and $f_{c,4}$ are taken as 28 GHz. Furthermore, Table 5.2 lists the detailed parameters used for simulation setup. The results are averaged over 10^5 Monte Carlo iterations.

5.3.1 User Association Probability for different TSC densities

Fig. 5.2 depicts the probability of user association to each tier versus different TSC densities. It can be seen in Fig. 5.2, that if we increase the TSC density, user association probability increases as more users start to associate with the TSC.

Table 5.2: Simulation Parameters

Parameter	**Value**	**Parameter**	**Value**
$f_{c,2}, f_{c,4}$	28 GHz	B_{MSC}, B_{UAV}	100 MHz
$f_{c,1}$	2.4 GHz	B_{MBS}, B_{TSC}	20 MHz, 1 GHz
$f_{c,3}$	1 THz	f_c(sub-6 GHz $UAVs$)	2.6 GHz
$g_r^{mm}, g_r^{uav}, g_r^T$	-10 dB	$g_t^{mm}, g_t^{uav}, g_t^T$	0 dB
β_1	4	β_L, β_N	2, 4
$\overline{P_1}$	40 W	$\overline{P_2}, \overline{P_3}, \overline{P_4}$	1 W
G_r^T, G_t^T	25 dB	$G_r^{mm}, G_t^{mm}, G_r^{uav}, G_r^{uav}$	10 dB
a_u, b_u	9, 0.11	$k(f)$	.05 m^{-1}
h_t	50 m	Θ_r, Θ_t	$90^o, 30^o$

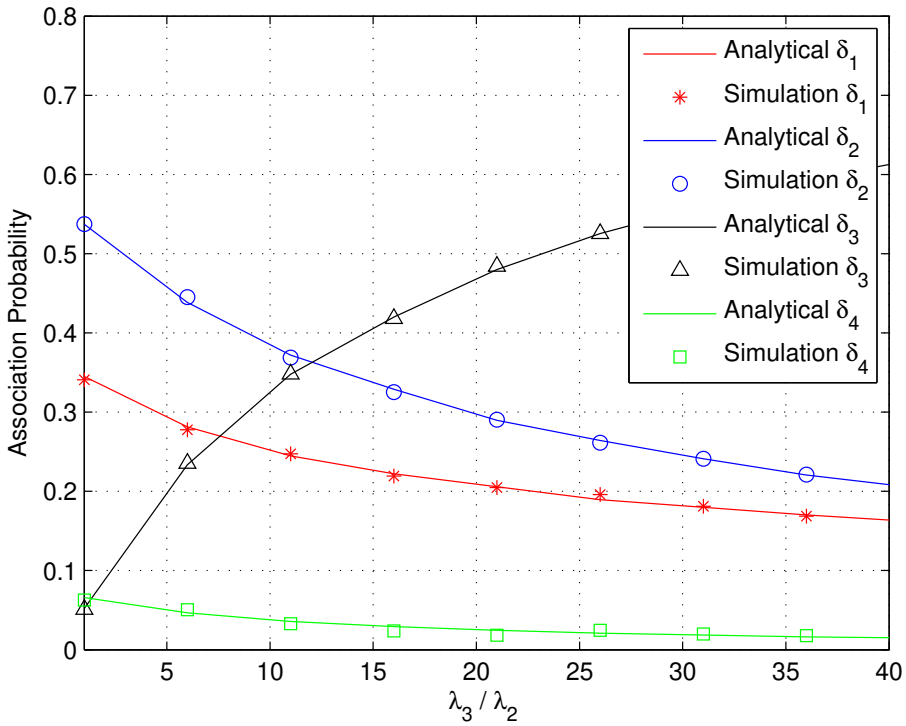

Figure 5.2: Association probability vs. varying λ_3 with $\lambda_1 = 4 \times 10^{-6}$ BS$/m^2$, $\lambda_2 = 3 \times \lambda_1$, BS$/m^2$, $\lambda_4 = 3 \times \lambda_1$ BS$/m^2$ and $\psi_1 = \psi_2 = 0$ dB, $\psi_3 = \psi_4 = 5$ dB.

In Fig. 5.2 by increasing the ratio of densities from 5 to 25, the user association probability with THz cells increase by 32% from 0.2 to 0.52. This offloading of

users from other tiers to TSC, results in a decrease in the association probabilities of other tiers. For the same increase in density ratio, 18% of users are offloaded from mmWave tier. So there is a tradeoff between having better SINR coverage at lower frequencies than having a better rate coverage at higher frequencies. This increased association to TSC helps to fulfill the user' demand of very high data rates. It can also be seen in Fig. 5.2 that analytical results are in compliance with the simulation results.

5.3.2 User Association Probabilities for different bias values for UAV tier

Fig. 5.3 demonstrates the user association probabilities versus the ratio of bias values for UAV tier w.r.t. TSC tier. This biasness is necessary in order to overcome the high propagation losses encountered by UAVs at mmWave frequencies and also assists in offloading the users from the sub-6 GHz BSs to mmWave UAVs. In Fig. 5.3, the ψ_3 is fixed to be 5 dB. We can see an increasing trend in the user association probability with UAV tier for an increased ψ_4 w.r.t. ψ_3. For example, if we increase the ratio from 0 dB to 30 dB, there is an increase of about 35% in user association with the UAV. This increased association of users with UAV results in a lower association of users with other tiers. For the same increase in the ratio, we can see a decline in user association with MSC, MBS, and TSC by 20%, 11%, and 5%, respectively.

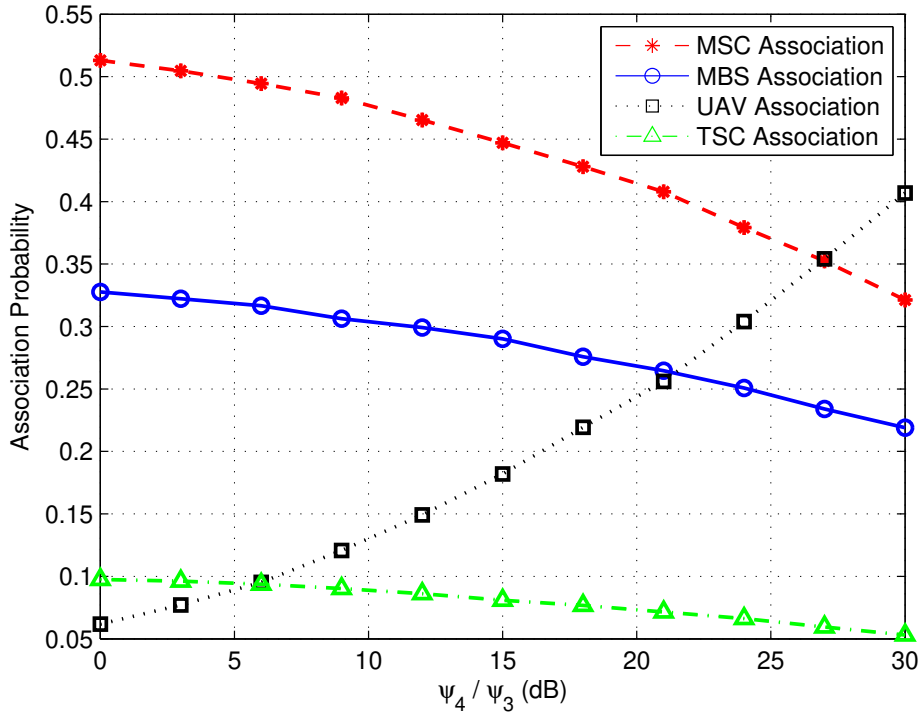

Figure 5.3: User association probability vs. varying ψ_4 with $\lambda_1 = 4 \times 10^{-6}$ BS/m^2, $\lambda_2 = 3 \times \lambda_1$ BS/m^2, $\lambda_3 = 2 \times \lambda_2$ BS/m^2, $\lambda_4 = 3 \times \lambda_1$ BS/m^2, $\psi_3 = 5$ dB, $\psi_1 = \psi_2 = 0$ dB.

5.3.3 SINR coverage probability for various bias values for UAV tier

Fig. 5.4 depicts the SINR coverage probability of HetNet versus the ratio of bias values for UAV tier w.r.t. TSC tier for various SINR threshold values. It can be seen in Fig. 5.4 that with an increase in biasness, more users start to associate with mmWave UAVs. This results in a decrease in the SINR coverage probability of HetNet because of the high propagation losses experienced by users at mmWave frequencies. In Fig. 5.4, it can be seen that for an increase of ratio from 0 dB to 30 dB for an SINR threshold of -10 dB, the number of users in coverage reduces

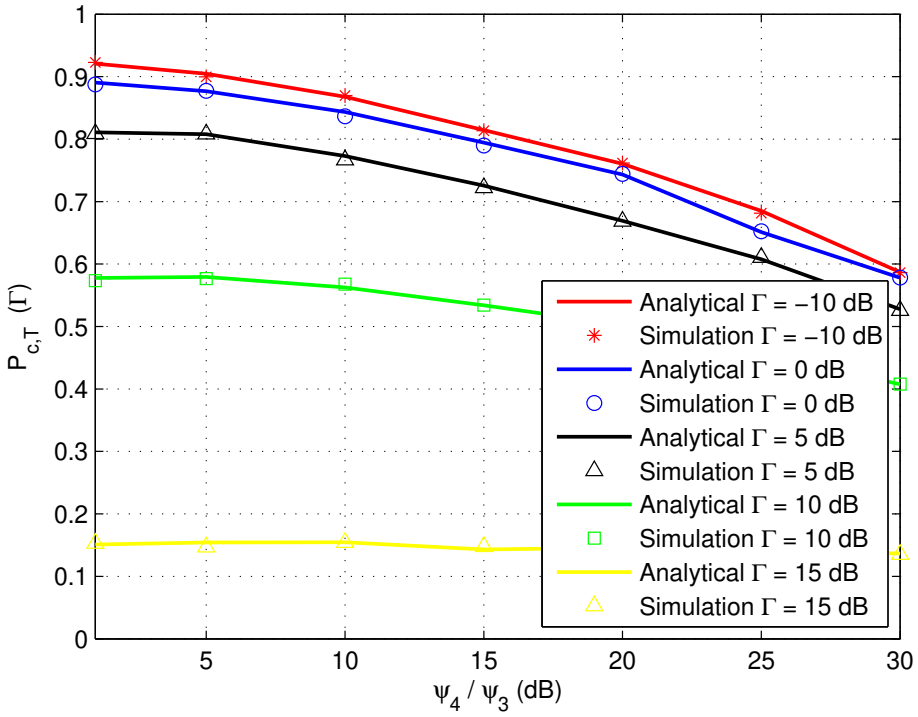

Figure 5.4: SINR coverage probability vs. varying ψ_4 with $\lambda_1 = 4 \times 10^{-6}$ BS$/m^2$, $\lambda_2 = 10 \times \lambda_1$ BS$/m^2$, $\lambda_3 = 3 \times \lambda_2$ BS$/m^2$, $\lambda_4 = 10 \times \lambda_1$ BS$/m^2$, $\psi_1 = \psi_2 = 0$ dB, $\psi_3 = 30$ dB and $\Gamma_1 = \Gamma_2 = \Gamma_3 = \Gamma_4 = \Gamma = 0$ dB.

by 34% from 0.92 to 0.58. This figure also shows the impact of various SINR thresholds on the coverage probability of HetNet. In Fig. 5.4, we can see that by increasing the SINR threshold from -10 dB to 15 dB, the number of users in coverage reduces from 85% to 15% for a biased ratio of 10 dB.

5.3.4 UAV association probability and SINR coverage probability of HetNet versus transmit power of UAVs

Fig. 5.5 depicts the UAV association probability and SINR coverage probability of HetNet versus transmit power of UAVs. It can be seen in Fig. 5.5 that when the

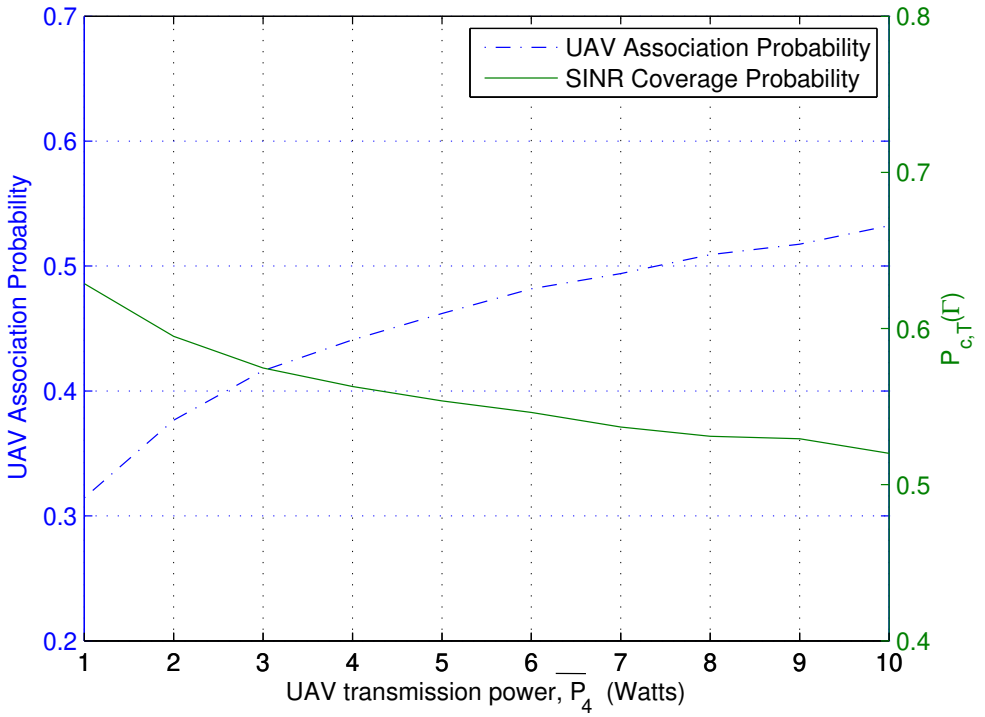

Figure 5.5: Impact of UAV transmit power on user association with UAVs and SINR coverage probability with $\lambda_1 = 4 \times 10^{-6}$ BS$/m^2$, $\lambda_2 = 10 \times \lambda_1$ BS$/m^2$, $\lambda_3 = 3 \times \lambda_2$ BS$/m^2$, $\lambda_4 = 10 \times \lambda_1$ BS$/m^2$, $\psi_1 = \psi_2 = 0$ dB, $\psi_3 = 30$ dB, $\psi_4 = 10$ dB and $\Gamma_1 = \Gamma_2 = \Gamma_3 = \Gamma_4 = \Gamma = 0$ dB.

transmit power is increased from 1 Watt to 10 Watts more user starts to associate with UAVs. As UAVs are operating on mmWave frequencies, any user associated with UAV will face high propagation losses as opposed to the users associated with sub-6 GHz frequency band. This increased association of users with mmWave UAVs results in a decreased SINR coverage probability of HetNet. If we increase the transmit power of UAVs from 1 Watt to 10 Watts, we can a see 13% decline in the number of users in SINR coverage. In Fig. 5.5 we also have seen an increase in user association with an increase in transmit power. This increase means more users will now experience high data rates available at mmWave frequencies.

5.3.5 Variation in rate coverage probability versus different rate threshold values for different TSC densities

Fig. 5.6 shows the variation in rate coverage probability versus different rate threshold values τ for different densities of THz cells. The values of τ have been taken from 1 Mbps to 1 Gbps. It is shown that if we increase the rate thresholds lesser number of users remains in the coverage. In Fig. 5.6 we can see that for the same density of MSC BSs and TSC BSs, around 75% of the users are getting data rates around 100 Mbps and 12% of the users receive data rates up to 1 Gbps. Fig. 5.6 also depicts the effects of increasing the TSC density on the achievable data

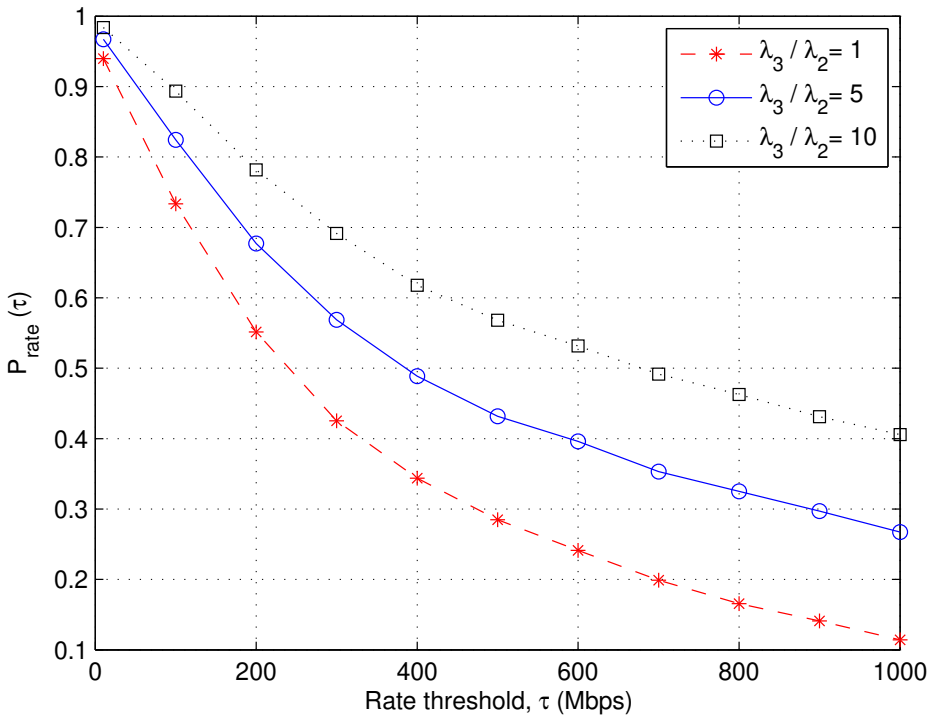

Figure 5.6: Rate coverage probability vs. rate thresholds τ for different τ with $\lambda_1 = 4 \times 10^{-6}$ BS$/m^2$, $\lambda_2 = 2 \times \lambda_1$ BS$/m^2$, $\lambda_4 = 2 \times \lambda_1$ BS$/m^2$, $\psi_1 = \psi_2 = 0$ dB, $\psi_3 = 20$ dB, $\psi_4 = 20$ dB .

rates. An increase in TSC density means more users are now associated with THz small cells which result in higher achievable data rates. In Fig. 5.6, it is shown that if we increase the TSC density from 1 to 10, 90% of the users are getting the data rates up to 100 Mbps.

5.3.6 Rate Coverage Probability for different thresholds for various THz bandwidths

Fig. 5.7 depicts the variations in rate coverage probability curves versus rate thresholds for various TSC bandwidth settings. The density of the THz BSs is assumed to be fixed. From Fig. 5.7 we can see a similar decline in rate coverage probability as we observed in Fig. 5.6. As we increase the rate threshold, fewer users are able to satisfy higher threshold values which result in decreased coverage probability. In Fig. 5.7, it is shown that if we increase the threshold from 200 Mbps to 800 Mbps for 0.5 GHz TSC bandwidth, the rate coverage probability decreases by 38%. Fig. 5.7 also depicts the effect of an increased bandwidth on coverage probability at THz frequencies. In Fig. 5.7 we can see that for a fixed TSC density if we increase the bandwidth from 0.5 GHz to 1 GHz more users start to experience higher data rates. For a rate threshold of 600 Mbps, if we increase the bandwidth of TSC from 0.5 GHz to 1 GHz, 4% more users will come into coverage. An increase in bandwidth allows more users to experience high data rates as the capacity increases with an increase in available bandwidth.

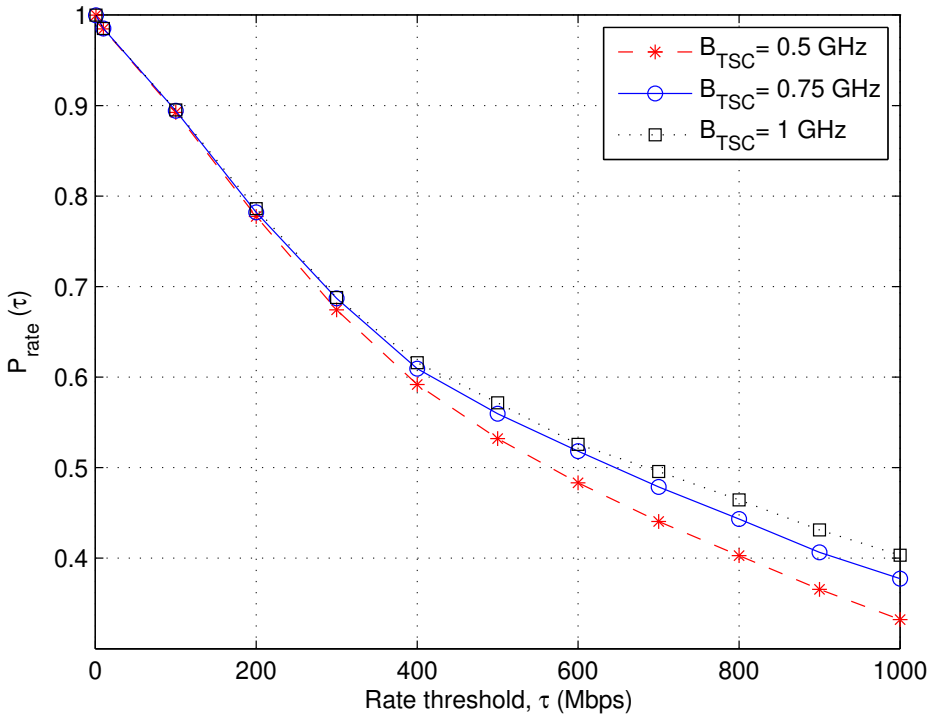

Figure 5.7: Rate coverage probability vs. rate thresholds τ for various THz Bandwidths with $\lambda_1 = 4 \times 10^{-6}$ BS$/m^2$, $\lambda_2 = 2 \times \lambda_1$ BS$/m^2$, $\lambda_3 = 5 \times \lambda_2$ BS$/m^2$, $\lambda_4 = 2 \times \lambda_1$ BS$/m^2$, $\psi_1 = \psi_2 = 0$ dB, $\psi_3 = 20$ dB, $\psi_4 = 20$ dB .

5.3.7 SINR coverage probability versus proportion of sub-6 GHz UAVs to mmWave-enabled UAVs in the HetNet for various SINR threshold values

Fig. 5.8 depicts the SINR coverage probability versus proportion of sub-6 GHz UAVs to mmWave-enabled UAVs in the HetNet for various SINR threshold values. In Fig. 5.8, $(1-\alpha)$ represents the proportion of UAVs operating on sub-6 GHz frequency in the HetNet. Sub-6 GHz UAVs are assumed to operate at 2.6 GHz frequency. It is also assumed that the sub-6 GHz UAVs use directional antennas with an antenna gain of 10 dB. From Fig. 5.8 we can see that if we increase

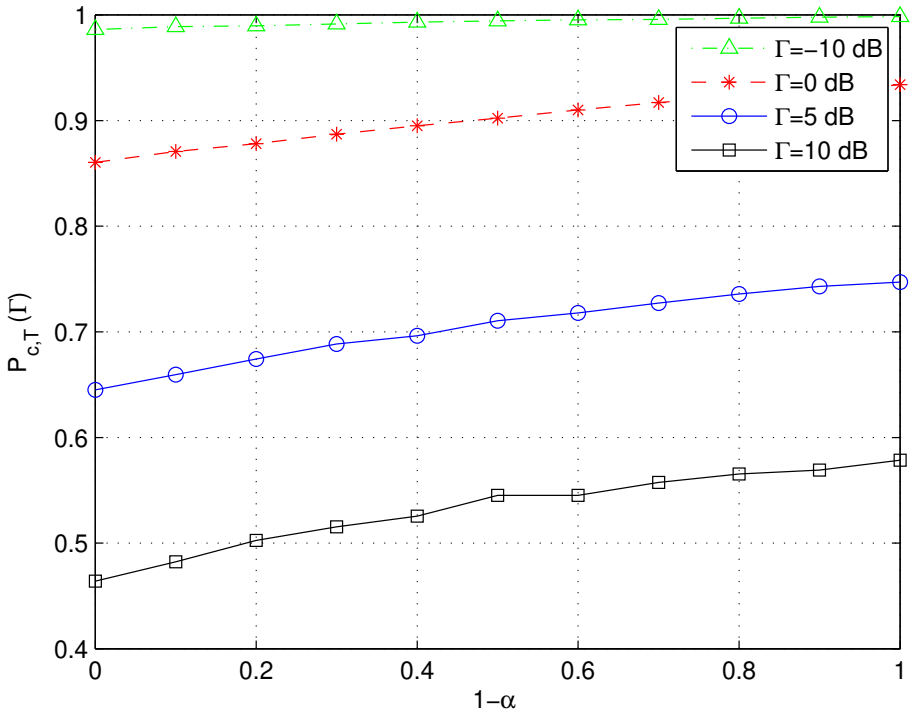

Figure 5.8: Impact of proportion of sub-6GHz UAVs to mmWave-enabled UAVs, $(1-\alpha)$ on SINR coverage probability with $\lambda_1 = 4 \times 10^{-6}$ BS$/m^2$, $\lambda_2 = 10 \times \lambda_1$ BS$/m^2$, $\lambda_3 = 1 \times \lambda_2$ BS$/m^2$, $\lambda_4 = 10 \times \lambda_1$ BS$/m^2$, $\psi_1 = \psi_2 = 0$ dB, $\psi_3 = 20$ dB, $\psi_4 = 10$ dB.

the proportion of sub-6 GHz UAVs by 0% to 100% by varying the value of tuning parameter $1-\alpha$ from 0 (all mmWave UAVs) to 1 (all sub-6 GHz UAVs), there is an increase in the SINR coverage probability. This increase is due to fact that there are fewer propagation losses at sub-6 GHz frequencies than the mmWave frequencies. In Fig. 5.8, for an the SINR threshold of 10 dB, an increase of 16% in SINR coverage probability is observed when sub-6 GHz UAVs are increased from 0% to 100% in the HetNet. Fig. 5.8 also shows the effect of increasing SINR threshold from -10 dB to 10 dB on SINR coverage probability. It can be seen from Fig. 5.8 that an increase in the SINR threshold results in fewer users

being in coverage. For example, if we have 60% sub-6 GHz UAVs in the HetNet, 90% of users are in coverage for an SINR threshold of 0 dB. If we increase the SINR threshold for the same proportion of sub-6 GHz UAVs, there is a decrease of about 40% users in coverage.

5.3.8 User association probability versus proportion of sub-6 GHz UAVs to mmWave-enabled UAVs

Fig. 5.9 shows the effect of user association probability versus proportion of sub-6 GHz UAVs to mmWave-enabled UAVs in the HetNet. From Fig. 5.9, it is observed that for an increase in sub-6 GHz UAVs in the HetNet, there is an increase in the user association with sub-6 GHz UAVs. If we increase sub-6 GHz UAVs in the HetNet from 0% to 50%, we can see that 10% more users are now associated with sub-6 GHz UAVs. As we increase the proportion of sub-6 GHz UAVs in HetNet, users associated with mmWave UAVs start to decrease. It can be concluded from Fig. 5.8 and Fig. 5.9 that an increase in the number of sub-6 GHz UAVs in the HetNet results in more users connecting with sub-6 GHz UAVs and a better SINR coverage for users associated with sub-6 GHz UAVs than users connected with mmWave UAVs.

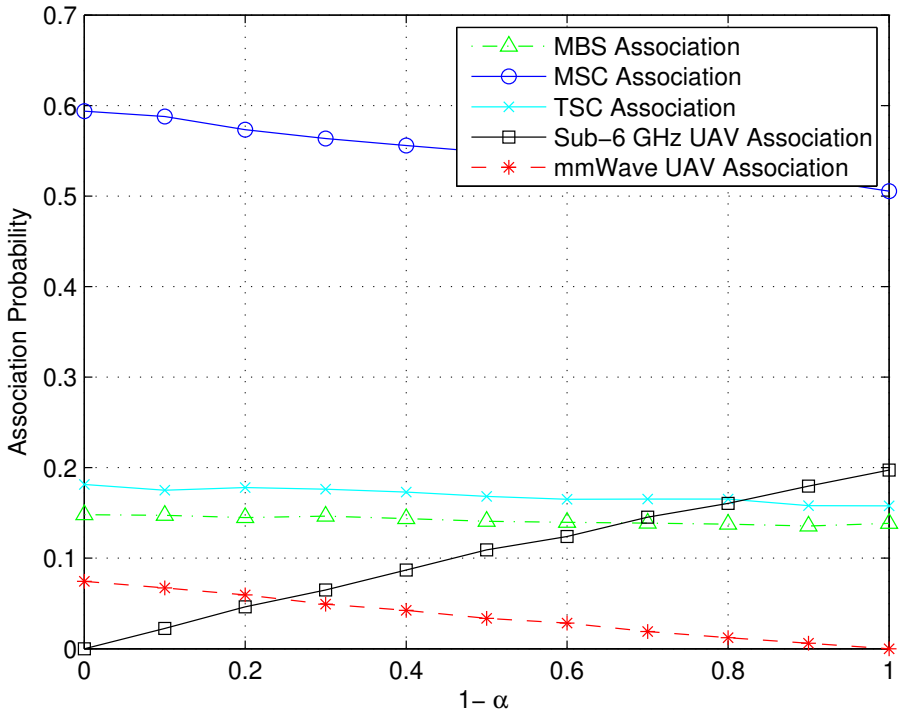

Figure 5.9: Impact of proportion of sub-6GHz UAVs to mmWave-enabled UAVs, $(1-\alpha)$ on Association probability with $\lambda_1 = 4 \times 10^{-6}$ BS$/m^2$, $\lambda_2 = 10 \times \lambda_1$ BS$/m^2$, $\lambda_3 = 1 \times \lambda_2$ BS$/m^2$, $\lambda_4 = 10 \times \lambda_1$ BS$/m^2$, $\psi_1 = \psi_2 = 0$ dB, $\psi_3 = 20$ dB, $\psi_4 = 10$ dB.

5.3.9 Rate coverage probability versus proportion of sub-6 GHz UAVs to mmWave-enabled UAVs for different data rate thresholds

The trend of rate coverage probability versus proportion of sub-6 GHz UAVs to mmWave-enabled UAVs for different data rate thresholds is shown in Fig. 5.10. It can be observed from Fig. 5.10, that an increase in the sub-6 GHz UAVs in the HetNet results in a lesser rate coverage probability. This decrease is due to the availability of lesser bandwidth at sub-6 GHz UAVs. For a rate threshold of

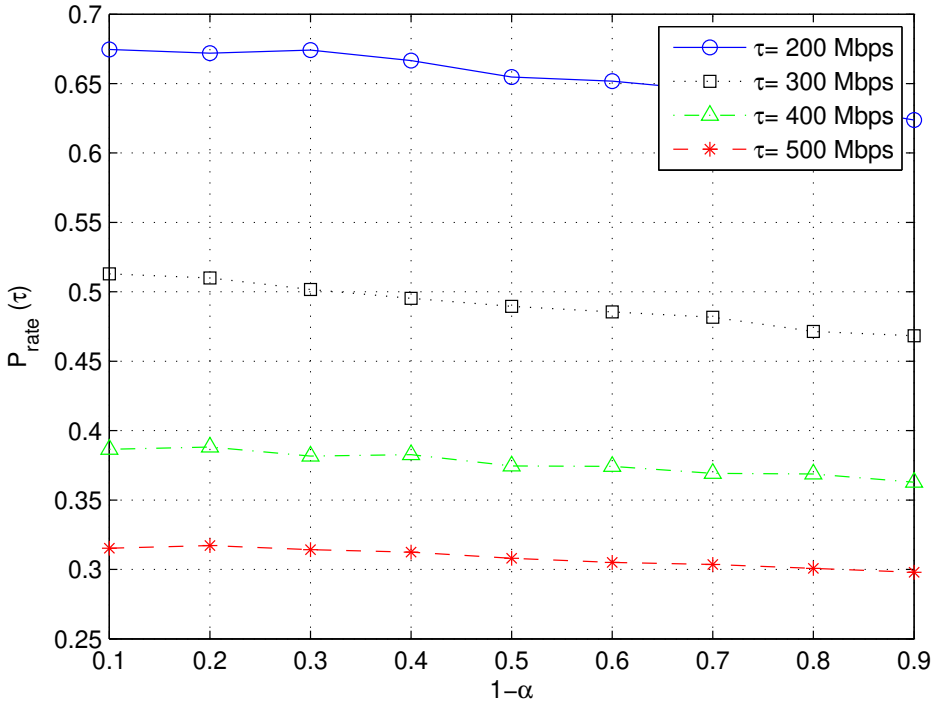

Figure 5.10: Rate coverage probability vs. proportion of sub-6GHz UAVs to mmWave-enabled UAVs, $1-\alpha$ with $\lambda_1 = 4\times10^{-6}$ BS$/m^2$, $\lambda_2 = 10\times\lambda_1$ BS$/m^2$, $\lambda_3 = 1\times\lambda_2$ BS$/m^2$, $\lambda_4 = 10\times\lambda_1$ BS$/m^2$, $\psi_1 = \psi_2 = 0$ dB, $\psi_3 = 20$ dB, $\psi_4 = 10$ dB .

300 Mbps, we can see a decline of around 5% in rate coverage probability for an increase in the proportion of sub-6 GHz UAVs in the HetNet by 80% by adjusting the tuning paramter, $1-\alpha$, from 0.1 to 0.9. Fig. 5.10 also depicts the effect of various rate thresholds on rate coverage probability. By increasing the rate thresholds from 200 Mbps to 500 Mbps, we can see the number of users attaining higher data rates decreases significantly. For an equal number of sub-6 GHz and mmWave UAVs in the HetNet ($1-\alpha = 0.5$), the rate coverage probability drops by around 34% if we increase the rate threshold τ from 200 Mbps to 500 Mbps. It can be concluded that an increase in sub-6 GHz UAVs in the HetNet results in

a better SINR coverage probability on the expense of lower achievable data rates while mmWave UAVs provide better rate coverage probability on the expense of lower SINR coverage probability.

5.4 Conclusions

In this chapter, a multi-tier HetNet is considered comprising of sub-6 GHz, mmWave and THz-enabled terrestrial BSs and mmWave frequencies enabled UAVs. An analytical model is derived for its coverage analysis. Extensive Monte Carlo Simulations has been performed to highlight the impacts of biasness, transmit power, different base station densities and available bandwidths on user association, SINR and rate coverage probabilities. It has been observed that increasing the biasness of different tiers and increasing the mmWave and THz-enabled cell densities result in high data rates availability for the users. A lower SINR coverage probability has been observed while offloading the users from sub-6 GHz to mmWave and THz frequencies. This is due to high propagation losses at high frequencies. On the other hand, the availability of high bandwidths at the mmWave and THz frequencies significantly improve high data rate transmission and provide high data rates to users.

From the results in this chapter, we have seen that if we increase the density of THz SBSs in the HetNet, we observed an increase in the user association probability with THz SBSs and decrease in association probabilities with other tiers of the HetNet. It has also been depicted that if we increase the bias value of the mmWave UAV tier, more number of users offload from other tiers to UAV tier. In this case, SINR coverage probability of the HetNet also decreases because of

the high propagation losses experienced by users at mmWave frequencies. Increasing the transmit power of UAVs also results in an increase in the association of users with UAV tier. It has also been seen that increasing the density of THz SBSs results in a better rate coverage probability of the HetNet because of high available bandwidth at THz frequencies. Rate coverage probability at different thresholds have also been depicted. It has been observed that an increase in the rate threshold results in a decline in the rate coverage probability as fewer users are able to satisfy higher threshold values. The effect of increasing THz bandwidths has been also observed. It has been shown that an increased bandwidth results in a higher rate coverage probability for the users. A special case has also been discussed in the results in which the effect of proportion of sub-6 GHz UAVs to mmWave-enabled UAVs has been seen on the association, SINR and rate coverage probabilities. It has been observed by increasing the proportion of sub-6 GHz from 0% (all mmWave UAVs) to 100% (all sub-6 GHz UAVs), association probability of sub-6 GHz UAVs increases which results in an improved SINR coverage probability because of less propagation losses at sub-6 GHz frequencies. Rate coverage probability of the HetNet decreases in this case due to less bandwidth available at sub-6 GHz frequencies.

Chapter 6

Conclusion and Future Directions

6.1 Conclusion

A fusion of various technologies in HetNets is indispensable to meet the QoS requirements of high data rate applications. To meet such a requirement, the bandwidth is considered as a challenging factor. Although, the sub-6 GHz-based network coverage is currently being used for initial 5G stages to provide high data rates to the users, it is perceived that with an ever-growing number of wireless users, the sub-6 GHz bandwidth will not be sufficient. Standalone THz-enabled networks are considered as one of the key solutions due to the availability of huge bandwidth, yet the high propagation losses at THz frequencies will limit the network coverage.

In this research, we considered a multi-tier HetNet composed of mmWave and THz-enabled aerial and terrestrial BSs and derived an analytical model for its coverage analysis. A tractable approach was developed to derive the SINR coverage probability for each tier using stochastic geometry tools. The results high-

lighted the impacts of different base station densities, biasness, transmit powers, and available bandwidths on user association, SINR, and rate coverage probabilities. We have shown that increasing the mmWave and THz-enabled cell densities and increasing the bias factors of these tiers result in meeting the QoS requirements of high data rates for the users. It has also been found that offloading the users from sub-6 GHz to mmWave and THz frequencies will result in a lower SINR coverage probability due to high propagation losses at high frequencies but the high available bandwidths at these frequencies significantly counter this loss by providing very high data rates to users.

In this research, we have also proposed a HetNet consisting of MBS and UAVs operating at sub-6 GHz frequency bands and small cells operating at THz frequencies with wireless backhaul capabilities. The effect on coverage and rate probabilities have been observed for different parameters such as different THz BS densities, different bandwidth proportion in Access and Backhaul links and different bias values. It has been observed that sub-6 GHz BSs provide better SINR coverage, whereas, THz cells accommodate users having high data rate demands. Simulation results show that the users connected to THz cells get a significant improvement in data rates as compared to users associated with sub-6 GHz tier.

6.2 Future Directions

In the future, the study can be extended to optimize different network parameters, i.e., number of BSs, UAV heights and transmit powers to meet various QoS requirements. Moreover, we can exploit the effect of beamforming, particularly in THz tier, to study rate and coverage performance in the HetNet. UAVs face

challenges with respect to their flight time and energy consumption. This work can be extended to study the effects of flight time and energy consumption on the coverage and rate performance in a HetNet. Similarly, massive MIMO can also be incorporated at the MBS and the effects of increased antenna density on coverage and rate performance can be analyzed. Physical layer security can also be incorporated to see its effect on the legitimate user SINR and rate coverage probabilities. The effect of having IoTs and D2D devices in the HetNet on coverage probabilities can also be investigated in the future. Resource allocation can also be incorporated in the HetNet to analyze its effect on coverage probabilities.

Appendices

Appendix A

DERIVATION OF LEMMA 1

The 2-D PPP null probability can be used to evaluate the probability $\mathbb{P}\left[R_n > \left(\frac{\widetilde{P}_n G_n x_i^{\beta_i}}{\widetilde{P}_i G_i}\right)^{1/\beta_n}\right]$.

κ in (5.17) can be evaluated as follows,

$$\begin{aligned}
\kappa &= \prod_{n=1, n\neq i}^{4} \mathbb{P}[\text{No BS closer than } \left(\frac{\widetilde{P}_n G_n x^{\beta_i}}{\widetilde{P}_i G_i}\right)^{1/\beta_n} \text{ in } n^{th} \text{ tier}] \\
&= exp\left\{-\pi\lambda_1 \left(\frac{\widetilde{P}_1 x^{\beta_i}}{\widetilde{P}_i}\right)^{2/\beta_1}\right\} + exp\{-2\pi\lambda_2 \Upsilon(x)\} \\
&+ exp\{-2\pi\lambda_3 T(x)\} + exp\{-2\pi\lambda_4 U(x)\}, \\
f_{X_i}(x) &= 2\pi\lambda_i x exp\{-\pi\lambda_i x^2\},
\end{aligned} \tag{A.1}$$

For the MSC tier, the association of a typical user is based on link length as the transmit power is assumed to be same for all links in the mmWave tier.

For MSC we assume that the tiers of LoS and NLoS BSs are independent, so

$$\begin{aligned} S_x &= \mathbb{P}[P_{r,i} > P_{r,2}] \\ &= \mathbb{P}[P_{r,i} > \widetilde{P}_2 G x^{-\beta_L}]\mathbb{P}[P_{r,i} > \widetilde{P}_2 G x^{-\beta_N}] \\ &= \mathbb{P}\left[x > \left(\frac{\widetilde{P}_2 G}{\widetilde{P}_i}\right)^{\frac{1}{\beta_L}} x^{\frac{\beta_i}{\beta_L}}\right]\mathbb{P}\left[x > \left(\frac{\widetilde{P}_2 G}{\widetilde{P}_i}\right)^{\frac{1}{\beta_N}} x^{\frac{\beta_i}{\beta_N}}\right] \\ &\quad -2\pi\lambda_2 \underbrace{\left(\int_0^{\Xi_N(x)} t\mathfrak{P}_{LoS}(t)\,dt + \int_0^{\Xi_L(x)} t\left(1-\mathfrak{P}_{LoS}(t)\right)\right)}_{\Upsilon(x)} dt \\ &\overset{(a)}{=} e \end{aligned}, \tag{A.2}$$

where $\Xi_N(x) = \left(\frac{\widetilde{P}_2 G}{\widetilde{P}_i}\right)^{\frac{1}{\beta_L}} x^{\frac{\beta_i}{\beta_L}}$ and $\Xi_L(x) = \left(\frac{\widetilde{P}_2 G}{\widetilde{P}_i}\right)^{\frac{1}{\beta_N}} x^{\frac{\beta_i}{\beta_N}}$
and (a) is derived from the null probability and $\mathfrak{P}_{LoS}(t)$ is the function of the LoS probability.

For the UAV mmWave tier,

$$\begin{aligned} W_r &= \mathbb{P}[P_{r,i} > P_{r,4}] \\ &= \mathbb{P}[P_{r,i} > \widetilde{P}_4 G r^{-\beta_L}]\mathbb{P}[P_{r,i} > \widetilde{P}_4 G r^{-\beta_N}] \\ &= \mathbb{P}\left[r > \left(\frac{\widetilde{P}_4 G}{\widetilde{P}_i}\right)^{\frac{1}{\beta_L}} x^{\frac{\beta_i}{\beta_L}}\right]\mathbb{P}\left[r > \left(\frac{\widetilde{P}_4 G}{\widetilde{P}_i}\right)^{\frac{1}{\beta_N}} x^{\frac{\beta_i}{\beta_N}}\right] \\ &\quad -2\pi\alpha\lambda_4 \underbrace{\left(\int_0^{\xi_N(r)} t\mathcal{P}_{LoS}(t)\,dt + \int_0^{\xi_L(r)} t\left(1-\mathcal{P}_{LoS}(t)\right)\right)}_{U(x)} dt \\ &= e \end{aligned}, \tag{A.3}$$

where $\xi_N(r) = \left(\frac{\widetilde{P}_4 G}{\widetilde{P}_i}\right)^{\frac{1}{\beta_L}} x^{\frac{\beta_i}{\beta_L}}$ and $\xi_L(r) = \left(\frac{\widetilde{P}_4 G}{\widetilde{P}_i}\right)^{\frac{1}{\beta_N}} x^{\frac{\beta_i}{\beta_N}}$
where $r = \sqrt{x^2 + h_t^2}$ and $\mathcal{P}_{LoS}(t)$ is the LoS probability function.

The probability that a user associates with THz BS can be evaluated as follows

$$
\begin{aligned}
&Y_x = \mathbb{P}[P_{r,i} > P_{r,3}] \\
&= \mathbb{P}[P_{r,i} > \widetilde{P}_3 exp\left(-k\left(f_{c,3}\right)x\right)x^{-\beta_L}] \\
&\mathbb{P}[P_{r,i} > \widetilde{P}_3 exp\left(-k\left(f_{c,3}\right)x\right)x^{-\beta_N}] \\
&= \mathbb{P}\left[x > \left(\frac{\widetilde{P}_3 exp\left(-k\left(f_{c,3}\right)x\right)}{\widetilde{P}_i}\right)^{\frac{1}{\beta_3}} x^{\frac{\beta_i}{\beta_3}}\right] \\
&\mathbb{P}\left[x > \left(\frac{\widetilde{P}_3 exp\left(-k\left(f_{c,3}\right)x\right)}{\widetilde{P}_i}\right)^{\frac{1}{\beta_N}} x^{\frac{\beta_i}{\beta_N}}\right] \\
&= e^{-2\pi\lambda_3 \underbrace{\left(\int_0^{\Delta_N(x)} t\mathfrak{P}_{LoS}\left(t\right)dt + \int_0^{\Delta_L(x)} t\left(1-\mathfrak{P}_{LoS}\left(t\right)\right)\right)}_{T(x)} dt},
\end{aligned}
\tag{A.4}
$$

where $\Delta_N\left(x\right) = \left(\frac{\widetilde{P}_3 exp\left(-k\left(f_{c,3}\right)x\right)G}{\widetilde{P}_i}\right)^{\frac{1}{\beta_L}} x^{\frac{\beta_i}{\beta_L}}$ and

$\Delta_L\left(x\right) = \left(\frac{\widetilde{P}_3 exp\left(-k\left(f_{c,3}\right)x\right)G}{\widetilde{P}_i}\right)^{\frac{1}{\beta_N}} x^{\frac{\beta_i}{\beta_N}}$

where $\mathfrak{P}_{LoS}(t)$ is the LoS probability function.

Appendix B

DERIVATION OF LEMMA 2

The conditional coverage probability, $P_c^1(\Gamma_1, x)$, can be evaluated as,

$$\begin{aligned} P_C^1(\Gamma_1, x) &= Pr\left(\frac{\widetilde{P_1} h_M x^{-\beta_1}}{\sigma_1^2 + I_1} > \Gamma_1\right) \\ &= Pr\left(h_M > \frac{\Gamma_1 x^{\beta_1}\left(\sigma_1^2 + I_1\right)}{\widetilde{P_1}}\right) \\ &\overset{(a)}{=} exp\left(\frac{-\Gamma_1 x^{\beta_1}\sigma_1^2}{\widetilde{P_1}}\right)\mathbb{E}_{I_1}\left[exp\left(\frac{-\Gamma_1 x^{\beta_1} I_1}{\widetilde{P_1}}\right)\right] \\ &= exp\left(\frac{-\Gamma_1 x^{\beta_1}\sigma_1^2}{\widetilde{P_1}}\right)\mathbb{E}_{I_1}\left[\mathcal{L}_{I_1}\left(\frac{\Gamma_1 x^{\beta_1}}{\widetilde{P_1}}\right)\right], \end{aligned} \tag{B.1}$$

where (a) follows from the exponential distribution of h_M. By substituting $P_c^1(\Gamma_1, x)$ and $f_{X_1}(x)$ into (5.18), we can compute the SINR coverage probability.

Appendix C

DERIVATION OF LEMMA 3

The conditional coverage probability that a user is associated with BS in ϕ_v where $v \in \{L,N\}$, can be found as

$$P_c^{2,v} = \delta_{2,v} \int_0^\infty \mathbb{P}\left[\frac{\widetilde{P}_2 G_r^{mm} G_t^{mm} h_{o,mm} x^{-\beta_v}}{\sigma^2 + I_L + I_N + I_{L_U} + I_{N_U}} > \Gamma_2\right] f_v(x)\, dx, \tag{C.1}$$

where I_L and I_N are the LoS and NLoS interferences from MSCs and I_{LU} and I_{NU} are the LoS and NLoS interferences from UAVs. The LoS and NLoS link probabilities of the user are given as,

$$\begin{aligned}\delta_{2,L} = 2\pi\lambda_2 \int_0^\infty x \mathfrak{P}_{LoS}(x)\, exp\Bigg(&-2\pi\lambda_2 Z(x) - A(x) - B(x) \\ &- C(x)\Bigg) dx,\end{aligned} \tag{C.2}$$

where

$$Z(x) = \int_0^x t\mathfrak{P}_{LoS}(t)\, dt + \int_0^{x^{\beta_L/\beta_N}} t\left(1 - \mathfrak{P}_{LoS}(t)\right) dt, \tag{C.3}$$

$$A(x) = \pi\lambda_1 \left(\frac{\widetilde{P}_1 x^{\beta_L}}{\widetilde{P}_2} \right)^{2/\beta_1}, \tag{C.4}$$

$$B(x) = 2\pi\lambda_3 T(x), \tag{C.5}$$

$$C(x) = 2\pi\alpha\lambda_4 U(x), \tag{C.6}$$

and

$$\begin{aligned}\delta_{2,N} = 2\pi\lambda_2 \int_0^{\infty} x\mathfrak{P}_{LoS}(x)\, exp\Big(&- 2\pi\lambda_2 Z_N(x) - A_N(x) - B_N(x) \\ &- C_N(x) \Big)\, dx,\end{aligned} \tag{C.7}$$

where

$$Z_N(x) = \int_0^x t\,(1-\mathfrak{P}_{LoS}(t))\, dt + \int_0^{x^{\beta_N/\beta_L}} t\mathfrak{P}_{LoS}(t)\, dt, \tag{C.8}$$

$$A_N(x) = \pi\lambda_1 \left(\frac{\widetilde{P}_1 x^{\beta_N}}{\widetilde{P}_2} \right)^{2/\beta_1}, \tag{C.9}$$

$$B_N(x) = 2\pi\lambda_3 T(x), \tag{C.10}$$

$$C_N(x) = 2\pi\alpha\lambda_4 U(x), \tag{C.11}$$

The PDF of the distance to the LoS BS, given that user is associated with LoS

small cell BS is given by,

$$f_L^{\wedge}(x) = \left(2\pi\lambda_2 x\mathfrak{P}_{LoS}(x)\, exp\left(-2\pi\lambda_2\int_0^x(\mathfrak{P}_{LoS}(t))\,t\,dt\right)\right.$$
$$\left. exp\left(-2\pi\lambda_2\int_0^{\Xi_L(x)}(1-\mathfrak{P}_{LoS}(t))\,t\,dt\right)\right)/\delta_{2,L}, \tag{C.12}$$

where $\mathfrak{P}_{LoS}(x)$ represents the LoS probability function. Similarly for the NLoS BS,

$$f_N^{\wedge}(x) = \left(2\pi\lambda_2 x(1-\mathfrak{P}_{LoS}(x))\, exp\left(-2\pi\lambda_2\int_0^x(1-\mathfrak{P}_{LoS}(t))\,t\,dt\right)\right.$$
$$\left. exp\left(-2\pi\lambda_2\int_0^{\Xi_N(x)}(\mathfrak{P}_{LoS}(t))\,t\,dt\right)\right)/\delta_{2,N}, \tag{C.13}$$

where $\Xi_L(x)$ and $\Xi_N(x)$ are given in Appendix A. Now $I_L = \widetilde{P}_2\sum_{i\in\phi^{\wedge}_{mm,L}} G_V h_{i,mm}x^{-\beta_L}$ and $I_N = \widetilde{P}_2\sum_{i\in\phi^{\wedge}_{mm,N}} G_V h_{i,mm}x^{-\beta_N}$ are the interference from LoS and NLoS BSs, respectively and $I_{LU} = \widetilde{P}_4\sum_{i\in\phi^{\wedge}_{u,L}} G_e h_{i,u}r^{-\beta_L}$ and $I_{NU} = \widetilde{P}_4\sum_{i\in\phi^{\wedge}_{u,N}} G_e h_{i,u}r^{-\beta_N}$ are the interference from LoS and NLoS UAVs. We assumed Nakagami fading, there-

fore $h_{o,m}$ is a normalized gamma random variable with parameters Ω_w.

$$
\begin{aligned}
&P_c^{2,v} = \\
&\mathbb{P}[\widetilde{P}_2 G_r^{mm} G_t^{mm} h_{o,mm} x^{-\beta_v} > \Gamma_2 \left(\sigma_2^2 + I_L + I_N + I_{LU} + I_{NU}\right)], \\
&= \mathbb{P}\left[h_{o,mm} > \frac{x^{\beta_v}\Gamma_2 \left(\sigma_2^2 + I_L + I_N + I_{LU} + I_{NU}\right)}{\widetilde{P}_2 G_r^{mm} G_t^{mm}}\right], \\
&\overset{(a)}{=} 1- \\
&\mathbb{E}\left[\left(1 - exp\left(\frac{-\rho_w x^{\beta_v}\Gamma_2 \left(\sigma_2^2 + I_L + I_N + I_{LU} + I_{NU}\right)}{\widetilde{P}_2 G_r^{mm} G_t^{mm}}\right)\right)^{\Omega_w}\right], \\
&\overset{(b)}{=} \sum_{i=1}^{\Omega_w} (-1)^{i+1} \binom{\Omega_w}{i} \\
&\mathbb{E}\left[exp\left(\frac{-i\rho_w x^{\beta_v}\Gamma_2 \left(\sigma_2^2 + I_L + I_N + I_{LU} + I_{NU}\right)}{\widetilde{P}_2 G_r^{mm} G_t^{mm}}\right)\right], \\
&\overset{(c)}{=} \sum_{i=1}^{\Omega_w} (-1)^{i+1} \binom{\Omega_w}{i} e^{\frac{-i\rho_w x^{\beta_v}\Gamma_2\sigma_2^2}{\widetilde{P}_2 G_r^{mm} G_t^{mm}}} \\
&\mathbb{E}_{I_L}\left[exp\left(\frac{-i\rho_w x^{\beta_v}\Gamma_2 I_L}{\widetilde{P}_2 G_r^{mm} G_t^{mm}}\right)\right] \mathbb{E}_{I_N}\left[exp\left(\frac{-i\rho_w x^{\beta_v}\Gamma_2 I_N}{\widetilde{P}_2 G_r^{mm} G_t^{mm}}\right)\right] \\
&\mathbb{E}_{I_{LU}}\left[exp\left(\frac{-i\rho_w x^{\beta_v}\Gamma_2 I_{LU}}{\widetilde{P}_4 G_r^{mm} G_t^{mm}}\right)\right] \mathbb{E}_{I_{NU}}\left[exp\left(\frac{-i\rho_w x^{\beta_v}\Gamma_2 I_{NU}}{\widetilde{P}_4 G_r^{mm} G_t^{mm}}\right)\right],
\end{aligned}
\tag{C.14}
$$

where (a) follows from [29] and $\rho_w = \Omega_w \left(\Omega_w!\right)^{-1/\Omega_w}, w \in \{l_m, n_m\}$, (b) is derived using binomial expansion and (c) is obtained using the independence of ϕ_L and

ϕ_N PPPs. Now $\mathbb{E}_{I_L}$ is given as,

$$\begin{aligned}
&\mathbb{E}_{I_L}\left[exp\left(\frac{-i\rho_w x^{\beta_v}\Gamma_2 I_L}{\widetilde{P}_2 G_r^{mm} G_t^{mm}}\right)\right] = \\
&\mathbb{E}_{I_L}\left[exp\left(\frac{-i\rho_w x^{\beta_L}\Gamma_2 \sum_{i\in\phi^{\wedge}_{m,L}} G_V h_{i,mm} x^{-\beta_L}}{G_r^{mm} G_t^{mm}}\right)\right], \\
&\overset{(d)}{=} exp\Bigg(-2\pi\lambda_2 \sum_{i=1}^{4} p_i \int_x^{\infty} \left(1 - E_g[e^{-i\rho_{l_m} x^{\beta_L}\Gamma_2 g \hat{a}_i t^{-\beta_L}}]\right) \\
&(\mathfrak{P}_{LoS}(t))\, t\, dt\Bigg), \\
&\overset{(e)}{=} \prod_{i=1}^{4} exp\Bigg(-2\pi\lambda_2 p_i \int_x^{\infty} \left(1 - \frac{1}{\left(i\rho_{l_m} x^{\beta_L}\Gamma_2 \Omega_{l_m}^{-1} \hat{a}_i t^{-\beta_L}\right)^{\Omega_{l_m}}}\right) \\
&(\mathfrak{P}_{LoS}(t))\, t\, dt\Bigg),
\end{aligned} \tag{C.15}$$

where Laplace transform of ϕ_L gives us C.15(d). In C.15(d), Ω_{l_m} is the parameter of a normalized gamma random variable representing channel gain g, $\hat{a}_i$ represents the gain a_i which is normalized by $G_r^{mm} G_t^{mm}$, where (5.7) contains the parameters a_i and p_i. C.15(e) is found by computing the moment generating functional of g. $\mathbb{E}_{I_N}$ can be found in a similar way as $\mathbb{E}_{I_L}$. Final expression for $\mathbb{E}_{I_N}$ is given as,

$$\begin{aligned}
&\mathbb{E}_{I_N}\left[exp\left(\frac{-i\rho_w x^{\beta_v}\Gamma_2 I_N}{\widetilde{P}_2 G_r^{mm} G_t^{mm}}\right)\right] = \\
&\prod_{i=1}^{4} exp\Bigg(-2\pi\lambda_2 p_i \int_{\Xi_L(x)}^{\infty} \left(1 - \frac{1}{\left(i\rho_{l_m} x^{\beta_L}\Gamma_2 \Omega_{n_m}^{-1} \hat{a}_i t^{-\beta_N}\right)^{\Omega_{n_m}}}\right) \\
&(1 - \mathfrak{P}_{LoS}(t))\, t\, dt\Bigg),
\end{aligned} \tag{C.16}$$

where Ω_n is parameter of a normalized gamma random variable representing

channel gain. Similarly, $\mathbb{E}_{I_{LU}}$ is given as

$$\mathbb{E}_{I_{LU}}\left[exp\left(\frac{-i\rho_w x^{\beta_v}\Gamma_2 I_{LU}}{\widetilde{P}_2 G_r^{mm} G_t^{mm}}\right)\right] = \prod_{i=1}^{4} exp\Bigg(-2\pi\alpha\lambda_4 p_i \int_x^{\infty}\left(1-\frac{1}{\left(i\rho_{l_m} x^{\beta_L}\Gamma_2\Omega_{l_m}^{-1}\hat{a}_i t^{-\beta_L}\right)^{\Omega_{l_m}}}\right) (\mathfrak{P}_{LoS}(t))\, t\, dt\Bigg), \tag{C.17}$$

and $\mathbb{E}_{I_{NU}}$ is given as,

$$\mathbb{E}_{I_{NU}}\left[exp\left(\frac{-i\rho_w x^{\beta_v}\Gamma_2 I_{NU}}{\widetilde{P}_2 G_r^{mm} G_t^{mm}}\right)\right] = \prod_{i=1}^{4} exp\Bigg(-2\pi\alpha\lambda_4 p_i \int_{\xi_L(x)}^{\infty}\left(1-\frac{1}{\left(i\rho_{l_m} x^{\beta_L}\Gamma_2\Omega_{n_m}^{-1}\hat{a}_i t^{-\beta_N}\right)^{\Omega_{n_m}}}\right) (1-\mathcal{P}_{LoS}(t))\, t\, dt\Bigg), \tag{C.18}$$

where $\mathcal{P}_{LoS}(x)$ is the LoS probability between user and UAV and x denotes the horizontal distance between the user and UAV projection on ground. By combining interference terms using linearity of integrals for $v = L$, we obtain the coverage probability for LoS. For $v = N$, coverage probability can be obtained by following similar steps.

Appendix D

DERIVATION OF LEMMA 4

The coverage probability can be evaluated separately for LoS and NLoS PPPs based on thinning theorem. Given that user is connected with UAV in ϕ_u^v where $v \in \{L,N\}$, the conditional coverage probability is computed as

$$P_c^{4,v} = \delta_{4,v} \int_0^\infty \mathbb{P}\left[\frac{\widetilde{P}_4 G_r^{uav} G_t^{uav} h_{o,m} r^{-\beta_v}}{\sigma^2 + I_{L_U} + I_{N_u} + I_L + I_N} > \Gamma_4\right] f_v(r)\, dr \tag{D.1}$$

where

$$\delta_{4,L} = 2\pi\lambda_4 \int_0^\infty x \mathcal{P}_{LoS}(x)\, exp\left(-2\pi\lambda_4 Z_1(x) - A_1(x) - B_1(x) - C_1(x)\right) dx \tag{D.2}$$

where

$$M_1(x) = \int_h^r t\mathcal{P}_{LoS}\left(\sqrt{t^2-h^2}\right) dt + \int_h^{r^{\beta_L/\beta_N}} t\left(1 - \mathcal{P}_{LoS}\left(\sqrt{t^2-h^2}\right)\right) dt \tag{D.3}$$

$$A_1(x) = \pi\lambda_1 \left(\frac{\widetilde{P}_1 x^{\beta_L}}{\widetilde{P}_4} \right)^{2/\beta_1} \tag{D.4}$$

$$B_1(x) = \pi\lambda_3 \left(\frac{\widetilde{P}_3 x^{\beta_L} exp\left(-k\left(f_{c,3}\right)x\right)}{\widetilde{P}_4} \right)^{2/\beta_3} \tag{D.5}$$

$$C_1(x) = 2\pi\lambda_2 \Upsilon(x) \tag{D.6}$$

and

$$\delta_{4,N} = 1 - \delta_1 - \delta_2 - \delta_3 - \delta_{4,L} \tag{D.7}$$

are the LoS and NLoS link probabilities of the user associated with LoS and NLoS UAV links. Now the PDF of the distance to the LoS UAV, given that user is associated with LoS UAV is given as,

$$\begin{aligned} f_{UL}^{\wedge}(r) = \Big(2\pi\lambda_4 r \mathcal{P}_{LoS}\left(\sqrt{r^2-h^2}\right) e^{-2\pi\lambda_4 \int_h^r \left(\mathcal{P}_{LoS}\left(\sqrt{t^2-h^2}\right)\right) t\,dt} \cdot \\ e^{-2\pi\lambda_4 \int_h^{\xi_L(r)} \left(1-\mathcal{P}_{LoS}\left(\sqrt{t^2-h^2}\right)\right) t\,dt} \Big) / \delta_{4,L} \end{aligned} \tag{D.8}$$

where $\mathcal{P}_{LoS}(x)$ is the LoS probability function. The PDF of the distance to the NLoS BS, given that user is associated with NLoS small cell BS is given by,

$$\begin{aligned} f_{UN}^{\wedge}(r) = \Big(2\pi\lambda_4 r \left(1 - \mathcal{P}_{LoS}\left(\sqrt{r^2-h^2}\right)\right) e^{-2\pi\lambda_4 \int_h^r \left(1-\mathcal{P}_{LoS}\left(\sqrt{t^2-h^2}\right)\right) t\,dt} \cdot \\ e^{-2\pi\lambda_4 \int_h^{\xi_N(r)} \left(\mathcal{P}_{LoS}\left(\sqrt{t^2-h^2}\right)\right) t\,dt} \Big) / \delta_{u,N} \end{aligned} \tag{D.9}$$

where $\xi_L(r) = r^{\beta_L/\beta_N}$ and $\xi_N(r) = r^{\beta_N/\beta_L}$. Now $I_{LU} = \widetilde{P}_4 \sum_{i\in\phi^{\wedge}_{u,L}} G_l h_{i,u} r^{-\beta_L}$ and $I_{NU} = \widetilde{P}_4 \sum_{i\in\phi^{\wedge}_{u,N}} G_l h_{i,u} r^{-\beta_N}$ are the interference from LoS and NLoS UAVs, respectively and $I_L = \widetilde{P}_2 \sum_{i\in\phi^{\wedge}_{m,L}} G_l h_{i,m} x^{-\beta_L}$ and $I_N = \widetilde{P}_2 \sum_{i\in\phi^{\wedge}_{m,N}} G_l h_{i,m} x^{-\beta_N}$ are the interference from LoS and NLoS BSs. We assumed Nakagami fading, therefore $h_{o,u}$ is a normalized gamma random variable with parameters Ω_w,

$$
\begin{aligned}
&= \mathbb{P}[\widetilde{P}_4 G_r^{uav} G_t^{uav} h_{o,u} r^{-\beta_v} > \Gamma_4\left(\sigma^2 + I_{LU} + I_{NU} + I_L + I_N\right)] \\
&= \mathbb{P}[h_{o,u} > \frac{r^{\beta_v}\Gamma_4\left(\sigma^2 + I_{LU} + I_{NU} + I_L + I_N\right)}{\widetilde{P}_4 G_r^{uav} G_t^{uav}}] \\
&\overset{(a)}{=} 1 - \mathbb{E}\left[\left(1 - exp\left(\frac{-\rho_w r^{\beta_v}\Gamma_4\left(\sigma^2 + I_{LU} + I_{NU} + I_L + I_N\right)}{\widetilde{P}_4 G_r^{uav} G_t^{uav}}\right)\right)^{\Omega_w}\right] \\
&\overset{(b)}{=} \sum_{j=1}^{N} (-1)^{j+1} \binom{\Omega_w}{j} \mathbb{E}\left[exp\left(\frac{-j\rho_w r^{\beta_v}\Gamma_4\left(\sigma^2 + I_{LU} + I_{NU} + I_L + I_N\right)}{\widetilde{P}_4 G_r^{uav} G_t^{uav}}\right)\right] \\
&\overset{(c)}{=} \sum_{j=1}^{N} (-1)^{j+1} \binom{\Omega_w}{j} e^{\frac{-j\rho_w r^{\beta_v}\Gamma_4\sigma^2}{\widetilde{P}_4 G_r^{uav} G_t^{uav}}} \\
&\mathbb{E}_{I_{LU}}\left[exp\left(\frac{-j\rho_w r^{\beta_v}\Gamma_4(I_{LU})}{\widetilde{P}_4 G_r^{uav} G_t^{uav}}\right)\right] \mathbb{E}_{I_{NU}}\left[exp\left(\frac{-j\rho_w r^{\beta_v}\Gamma_4(I_{NU})}{\widetilde{P}_4 G_r^{uav} G_t^{uav}}\right)\right. \\
&\left.\mathbb{E}_{I_L}\left[exp\left(\frac{-j\rho_w x^{\beta_v}\Gamma_4(I_L)}{\widetilde{P}_2 G_r^{mm} G_t^{mm}}\right)\right] \mathbb{E}_{I_N}\left[exp\left(\frac{-j\rho_w x^{\beta_v}\Gamma_4(I_N)}{\widetilde{P}_2 G_r^{mm} G_t^{mm}}\right)\right]\right]
\end{aligned}
\tag{D.10}
$$

where (a) follows from [29] and $\rho_w = \Omega_w(\Omega_w!)^{-1/\Omega_w}$,$w \in \{L,N\}$, (b) from binomial expansion and (c) from the independence of ϕ_u^L, ϕ_u^N, ϕ_m^L and ϕ_m^N PPPs. Now

for $v = L$, we have

$$\begin{aligned}
&= \mathbb{E}_{I_{LU}}\left[exp\left(\frac{-j\rho_w r^{\beta_v}\Gamma_4 \sum_{i\in\phi^{\wedge}_{u,L}} G_l h_{i,m} r^{-\beta_L}}{G^{uav}_r G^{uav}_t}\right)\right] \\
&\overset{(d)}{=} e^{-2\pi\lambda_4 \sum_{i=1}^{4} p_i \int_r^{\infty}\left(1-E_m[e^{-j\rho_L r^{\beta_L}\Gamma_4 m\hat{a}_i t^{-\beta_L}}]\right)(\mathcal{P}_{LoS}(t))t\,dt} \\
&\overset{(e)}{=} \prod_{i=1}^{4} e^{-2\pi\lambda_4 p_i \int_r^{\infty}\left(1-\frac{1}{\left(j\rho_L r^{\beta_L}\Gamma_4\Omega_l^{-1}\hat{a}_i t^{-\beta_L}\right)^{\Omega_l}}\right)(\mathcal{P}_{LoS}(t))t\,dt}
\end{aligned} \tag{D.11}$$

where (d) is obtained by taking laplace transform of ϕ^L_u and g in (d) is a normalized gamma random variable with a parameter Ω_l, $\hat{a}_i$ is the normalized gain where a_i and p_i are given by (5.15) and (e) is the result of taking moment generating functional of g, respectively. $\mathbb{E}_{I_{NU}}$, $\mathbb{E}_{I_L}$ and $\mathbb{E}_{I_N}$ can be computed in a similar manner as $\mathbb{E}_{I_{LU}}$. Final expression for $\mathbb{E}_{I_{NU}}$ is given as,

$$= \prod_{i=1}^{4} e^{-2\pi\lambda_4 p_i \int_{\xi_L(r)}^{\infty}\left(1-\frac{1}{\left(j\rho_L r^{\beta_L}\Gamma_4\Omega_n^{-1}\hat{a}_i t^{-\beta_N}\right)^{\Omega_n}}\right)(1-\mathcal{P}_{LoS}(t))t\,dt} \tag{D.12}$$

Similarly, $\mathbb{E}_{I_L}$ is given as

$$= \prod_{i=1}^{4} e^{-2\pi\lambda_2 p_i \int_x^{\infty}\left(1-\frac{1}{\left(j\rho_L x^{\beta_L}\Gamma_4\Omega_l^{-1}\hat{a}_i t^{-\beta_L}\right)^{\Omega_l}}\right)(\mathfrak{P}_{LoS}(t))t\,dt} \tag{D.13}$$

and $\mathbb{E}_{I_N}$ is given as,

$$= \prod_{i=1}^{4} e^{-2\pi\lambda_2 p_i \int_{\Omega_L(x)}^{\infty}\left(1-\frac{1}{\left(j\rho_L x^{\beta_L}\Gamma_4\Omega_n^{-1}\hat{a}_i t^{-\beta_N}\right)^{\Omega_n}}\right)(1-\mathfrak{P}_{LoS}(t))t\,dt} \tag{D.14}$$

Using Linearity of integrals and combining interference terms, we get the coverage probability.

Appendix E

DERIVATION OF LEMMA 6

The achievable data rate for a user connected with i^{th} tier is given as,

$$\begin{aligned} R_i &= \mathbb{P}\left(R_i > \Gamma_i\right) = \mathbb{P}\left(log_2\left(1+\text{SINR}_i\right) > \Gamma_i\right) \\ &= \mathbb{P}\left(\text{SINR}_i > 2^{\Gamma_i} - 1\right) \\ &= \frac{1}{ln2}\int_0^{\infty} \mathbb{P}\left(\text{SINR}_i > 2^{\Gamma_i} - 1\right) \\ &= \frac{1}{ln2}\int_0^{\infty} \frac{P_c^i(\Gamma_i)}{1+\Gamma_i}\, d\Gamma_i, \end{aligned} \tag{E.1}$$

where P_c^i is the coverage probability of tier i and Γ_i is the SINR threshold of tier i.

Bibliography

[1] X. Wang, L. Kong, F. Kong, F. Qiu, M. Xia, S. Arnon, and G. Chen, "Millimeter wave communication: A comprehensive survey," *IEEE Communications Surveys & Tutorials*, vol. 20, no. 3, pp. 1616–1653, 2018.

[2] S. Abdelwahab, B. Hamdaoui, M. Guizani, and A. Rayes, "Enabling smart cloud services through remote sensing: An internet of everything enabler," *IEEE Internet of Things Journal*, vol. 1, no. 3, pp. 276–288, 2014.

[3] S. M. Johnson, "The internet changes everything: Revolutionizing public participation and access to government information through the internet," *Admin. L. Rev.*, vol. 50, p. 277, 1998.

[4] S. Abdelwahab, B. Hamdaoui, M. Guizani, and A. Rayes, "Enabling smart cloud services through remote sensing: An internet of everything enabler," *IEEE Internet of Things Journal*, vol. 1, no. 3, pp. 276–288, 2014.

[5] I. Bor-Yaliniz and H. Yanikomeroglu, "The new frontier in ran heterogeneity: Multi-tier drone-cells," *IEEE Communications Magazine*, vol. 54, no. 11, pp. 48–55, 2016.

[6] Q. Ye, B. Rong, Y. Chen, M. Al-Shalash, C. Caramanis, and J. G. Andrews, "User association for load balancing in heterogeneous cellular networks," *IEEE Transactions on Wireless Communications*, vol. 12, no. 6, pp. 2706–2716, 2013.

[7] M. S. Omar, S. A. Hassan, H. Pervaiz, Q. Ni, L. Musavian, S. Mumtaz, and O. A. Dobre, "Multiobjective optimization in 5g hybrid networks," *IEEE Internet of Things Journal*, vol. 5, no. 3, pp. 1588–1597, 2017.

[8] H. Munir, S. A. Hassan, H. Pervaiz, Q. Ni, and L. Musavian, "Resource optimization in multi-tier hetnets exploiting multi-slope path loss model," *IEEE Access*, vol. 5, pp. 8714–8726, 2017.

[9] S. Sekander, H. Tabassum, and E. Hossain, "Multi-tier drone architecture for 5g/b5g cellular networks: Challenges, trends, and prospects," *IEEE Communications Magazine*, vol. 56, no. 3, pp. 96–103, 2018.

[10] U. Siddique, H. Tabassum, E. Hossain, and D. I. Kim, "Wireless backhauling of 5g small cells: Challenges and solution approaches," *IEEE Wireless Communications*, vol. 22, no. 5, pp. 22–31, 2015.

[11] G. Gódor, Z. Jakó, Á. Knapp, and S. Imre, "A survey of handover management in lte-based multi-tier femtocell networks: Requirements, challenges and solutions," *Computer Networks*, vol. 76, pp. 17–41, 2015.

[12] R. I. Ansari, C. Chrysostomou, S. A. Hassan, M. Guizani, S. Mumtaz, J. Rodriguez, and J. J. Rodrigues, "5g d2d networks: Techniques, challenges, and future prospects," *IEEE Systems Journal*, vol. 12, no. 4, pp. 3970–3984, 2017.

[13] H. Munir, H. Pervaiz, S. A. Hassan, L. Musavian, Q. Ni, M. A. Imran, and R. Tafazolli, "Computationally intelligent techniques for resource management in mmwave small cell networks," *IEEE Wireless Communications*, vol. 25, no. 4, pp. 32–39, 2018.

[14] C. Han and Y. Chen, "Propagation modeling for wireless communications in the terahertz band," *IEEE Communications Magazine*, vol. 56, no. 6, pp. 96–101, 2018.

[15] C. Han, A. O. Bicen, and I. F. Akyildiz, "Multi-ray channel modeling and wideband characterization for wireless communications in the terahertz band," *IEEE Transactions on Wireless Communications*, vol. 14, no. 5, pp. 2402–2412, 2014.

[16] A. Moldovan, M. A. Ruder, I. F. Akyildiz, and W. H. Gerstacker, "Los and nlos channel modeling for terahertz wireless communication with scattered rays," in *2014 IEEE Globecom Workshops (GC Wkshps)*. IEEE, 2014, pp. 388–392.

[17] S. Bhattacharyya and G. Aruna, "Outage probability analysis of snr for a mm wave beamsteered mimo-mrc system," in *2019 International Conference on Wireless Communications Signal Processing and Networking (WiSPNET)*. IEEE, 2019, pp. 246–251.

[18] S. Priebe and T. Kurner, "Stochastic modeling of thz indoor radio channels," *IEEE Transactions on Wireless Communications*, vol. 12, no. 9, pp. 4445–4455, 2013.

[19] A. R. Ekti, A. Boyaci, A. Alparslan, İ. Ünal, S. Yarkan, A. Görçin, H. Arslan, and M. Uysal, "Statistical modeling of propagation channels for terahertz band," in *2017 IEEE Conference on Standards for Communications and Networking (CSCN)*. IEEE, 2017, pp. 275–280.

[20] S. Nie and I. F. Akyildiz, "Three-dimensional dynamic channel modeling and tracking for terahertz band indoor communications," in *2017 IEEE 28th Annual International Symposium on Personal, Indoor, and Mobile Radio Communications (PIMRC)*. IEEE, 2017, pp. 1–5.

[21] X. Gao, L. Dai, Y. Zhang, T. Xie, X. Dai, and Z. Wang, "Fast channel tracking for terahertz beamspace massive mimo systems," *IEEE Transactions on Vehicular Technology*, vol. 66, no. 7, pp. 5689–5696, 2016.

[22] I. F. Akyildiz, J. M. Jornet, and C. Han, "Teranets: Ultra-broadband communication networks in the terahertz band," *IEEE Wireless Communications*, vol. 21, no. 4, pp. 130–135, 2014.

[23] C. Lin and G. Y. Li, "Adaptive beamforming with resource allocation for distance-aware multi-user indoor terahertz communications," *IEEE Transactions on Communications*, vol. 63, no. 8, pp. 2985–2995, 2015.

[24] S. A. Hoseini, M. Ding, and M. Hassan, "Massive mimo performance comparison of beamforming and multiplexing in the terahertz band," in *2017 IEEE Globecom Workshops (GC Wkshps)*. IEEE, 2017, pp. 1–6.

[25] B. Peng, Q. Jiao, and T. Kürner, "Angle of arrival estimation in dynamic indoor thz channels with bayesian filter and reinforcement learning," in

2016 24th European Signal Processing Conference (EUSIPCO). IEEE, 2016, pp. 1975–1979.

[26] A. Fitzpatrick, "The Drone Age," https://time.com/longform/time-the-drone-age, May 2018.

[27] C. Ranaweera, M. G. Resende, K. Reichmann, P. Iannone, P. Henry, B.-J. Kim, P. Magill, K. N. Oikonomou, R. K. Sinha, and S. Woodward, "Design and optimization of fiber optic small-cell backhaul based on an existing fiber-to-the-node residential access network," *IEEE Communications Magazine*, vol. 51, no. 9, pp. 62–69, 2013.

[28] M. R. Akdeniz, Y. Liu, M. K. Samimi, S. Sun, S. Rangan, T. S. Rappaport, and E. Erkip, "Millimeter wave channel modeling and cellular capacity evaluation," *IEEE Journal on Selected Areas in Communications*, vol. 32, no. 6, pp. 1164–1179, 2014.

[29] T. Bai and R. W. Heath, "Coverage and rate analysis for millimeter-wave cellular networks," *IEEE Transactions on Wireless Communications*, vol. 14, no. 2, pp. 1100–1114, 2015.

[30] J. G. Andrews, T. Bai, M. N. Kulkarni, A. Alkhateeb, A. K. Gupta, and R. W. Heath, "Modeling and analyzing millimeter wave cellular systems," *IEEE Transactions on Communications*, vol. 65, no. 1, pp. 403–430, 2017.

[31] G. Fontanesi, A. Zhu, and H. Ahmadi, "Outage analysis for millimeter-wave fronthaul link of uav-aided wireless networks," *IEEE Access*, vol. 8, pp. 111 693–111 706, 2020.

[32] M. Boschiero, M. Giordani, M. Polese, and M. Zorzi, "Coverage analysis of uavs in millimeter wave networks: A stochastic geometry approach," *arXiv preprint arXiv:2003.01391*, 2020.

[33] J. Sayehvand and H. Tabassum, "Interference and coverage analysis in co-existing rf and dense terahertz wireless networks," *IEEE Wireless Communications Letters*, 2020.

[34] A. Umer, S. A. Hassan, H. Pervaiz, L. Musavian, Q. Ni, and M. A. Imran, "Secrecy spectrum and energy efficiency analysis in massive mimo-enabled multi-tier hybrid hetnets," *IEEE Transactions on Green Communications and Networking*, vol. 4, no. 1, pp. 246–262, 2019.

[35] S. Grimaldi, A. Mahmood, S. A. Hassan, M. Gidlund, and G. P. Hancke, "Autonomous interference mapping for industrial iot networks over unlicensed bands," *IEEE Industrial Electronics Magazine*, pp. 0–0, 2020.

[36] F. Jameel, S. Zeb, W. U. Khan, S. A. Hassan, Z. Chang, and J. Liu, "Noma-enabled backscatter communications: Toward battery-free iot networks," *IEEE Internet of Things Magazine*, vol. 3, no. 4, pp. 95–101, 2020.

[37] F. Jameel, M. A. Javed, D. N. Jayakody, and S. A. Hassan, "On secrecy performance of industrial internet of things," *Internet Technology Letters*, vol. 1, no. 2, p. e32, 2018.

[38] R. I. Ansari, H. Pervaiz, S. A. Hassan, C. Chrysostomou, M. A. Imran, S. Mumtaz, and R. Tafazolli, "A new dimension to spectrum management in iot empowered 5g networks," *IEEE Network*, vol. 33, no. 4, pp. 186–193, 2019.

[39] F. Hussain, R. Hussain, S. A. Hassan, and E. Hossain, "Machine learning in iot security: Current solutions and future challenges," *IEEE Communications Surveys Tutorials*, vol. 22, no. 3, pp. 1686–1721, 2020.

[40] S. Zeb, A. Mahmood, H. Pervaiz, S. A. Hassan, M. I. Ashraf, Z. Li, and M. Gidlund, "On toa-based ranging over mmwave 5g for indoor industrial iot networks."

[41] Q. Abbas, S. Zeb, S. A. Hassan, R. Mumtaz, and S. A. R. Zaidi, "Joint optimization of age of information and energy efficiency in iot networks," in *2020 IEEE 91st Vehicular Technology Conference (VTC2020-Spring)*, 2020, pp. 1–5.

[42] S. Nawaz and S. A. Hassan, "Auxiliary beam pair enabled initial access in mmwave systems: Analysis and design insights," in *2019 IEEE International Conference on Communications Workshops (ICC Workshops)*, 2019, pp. 1–6.

[43] S. Nawaz, S. A. Hassan, and H. Jung, "Auxiliary beam pair enabled initial access for mmwave d2d networks," *Physical Communication*, vol. 39, p. 101039, 2020. [Online]. Available: https://www.sciencedirect.com/science/article/pii/S187449071930583X

[44] S. A. R. Naqvi, H. Pervaiz, S. A. Hassan, L. Musavian, Q. Ni, M. A. Imran, X. Ge, and R. Tafazolli, "Energy-aware radio resource management in d2d-enabled multi-tier hetnets," *IEEE Access*, vol. 6, pp. 16 610–16 622, 2018.

[45] R. I. Ansari, S. A. Hassan, S. Ali, C. Chrysostomou, and M. Lestas, "On the outage analysis of a d2d network with uniform node distribution in a circular region," *Physical Communication*, vol. 25, pp. 277–283, 2017.

[46] R. I. Ansari, C. Chrysostomou, S. A. Hassan, M. Guizani, S. Mumtaz, J. Rodriguez, and J. J. Rodrigues, "5g d2d networks: Techniques, challenges, and future prospects," *IEEE Systems Journal*, vol. 12, no. 4, pp. 3970–3984, 2017.

[47] U. Saleem, S. Jangsher, H. K. Qureshi, and S. A. Hassan, "Joint subcarrier and power allocation in the energy-harvesting-aided d2d communication," *IEEE Transactions on Industrial Informatics*, vol. 14, no. 6, pp. 2608–2617, 2018.

[48] R. I. Ansari, S. A. Hassan, and C. Chrysostomou, "A swipt-based device-to-device cooperative network," in *2017 24th International Conference on Telecommunications (ICT)*. IEEE, 2017, pp. 1–5.

[49] ——, "Energy efficient relay selection in multi-hop d2d networks," in *2016 International Wireless Communications and Mobile Computing Conference (IWCMC)*. IEEE, 2016, pp. 620–625.

[50] S. A. R. Naqvi, S. A. Hassan, H. Pervaiz, Q. Ni, and L. Musavian, "Self-adaptive power control mechanism in d2d enabled hybrid cellular network with mmwave small cells: An optimization approach," in *2016 IEEE Globecom Workshops (GC Wkshps)*. IEEE, 2016, pp. 1–6.

[51] A. Riaz, S. Saleem, and S. A. Hassan, "Energy efficient neighbor discovery for mmwave d2d networks using polya's necklaces," in *2018 IEEE Global Communications Conference (GLOBECOM)*. IEEE, 2018, pp. 1–6.

[52] A. Enayati, G. A. Vandenbosch, and W. De Raedt, "Millimeter-wave horn-type antenna-in-package solution fabricated in a teflon-based multilayer pcb technology," *IEEE transactions on antennas and propagation*, vol. 61, no. 4, pp. 1581–1590, 2013.

[53] T. S. Rappaport, S. Sun, R. Mayzus, H. Zhao, Y. Azar, K. Wang, G. N. Wong, J. K. Schulz, M. Samimi, and F. Gutierrez, "Millimeter wave mobile communications for 5g cellular: It will work!" *IEEE access*, vol. 1, pp. 335–349, 2013.

[54] S. Sun, T. S. Rappaport, R. W. Heath, A. Nix, and S. Rangan, "Mimo for millimeter-wave wireless communications: Beamforming, spatial multiplexing, or both?" *IEEE Communications Magazine*, vol. 52, no. 12, pp. 110–121, 2014.

[55] W. Knap, F. Teppe, N. Dyakonova, D. Coquillat, and J. Łusakowski, "Plasma wave oscillations in nanometer field effect transistors for terahertz detection and emission," *Journal of Physics: Condensed Matter*, vol. 20, no. 38, p. 384205, 2008.

[56] M. S. Vitiello, D. Coquillat, L. Viti, D. Ercolani, F. Teppe, A. Pitanti, F. Beltram, L. Sorba, W. Knap, and A. Tredicucci, "Room-temperature terahertz detectors based on semiconductor nanowire field-effect transistors," *Nano letters*, vol. 12, no. 1, pp. 96–101, 2012.

[57] A. Y. Nikitin, F. Guinea, F. García-Vidal, and L. Martín-Moreno, "Edge and waveguide terahertz surface plasmon modes in graphene microribbons," *Physical Review B*, vol. 84, no. 16, p. 161407, 2011.

[58] R. Wang, Y. Sun, M. Kaynak, S. Beer, J. Borngräber, and J. C. Scheytt, "A micromachined double-dipole antenna for 122–140 ghz applications based on a sige bicmos technology," in *2012 IEEE/MTT-S International Microwave Symposium Digest*. IEEE, 2012, pp. 1–3.

[59] V. Radisic, K. M. Leong, X. Mei, S. Sarkozy, W. Yoshida, and W. R. Deal, "Power amplification at 0.65 thz using inp hemts," *IEEE Transactions on Microwave Theory and Techniques*, vol. 60, no. 3, pp. 724–729, 2011.

[60] C. Jansen, S. Priebe, C. Moller, M. Jacob, H. Dierke, M. Koch, and T. Kurner, "Diffuse scattering from rough surfaces in thz communication channels," *IEEE Transactions on Terahertz Science and Technology*, vol. 1, no. 2, pp. 462–472, 2011.

[61] J. M. Jornet and I. F. Akyildiz, "Channel modeling and capacity analysis for electromagnetic wireless nanonetworks in the terahertz band," *IEEE Transactions on Wireless Communications*, vol. 10, no. 10, pp. 3211–3221, 2011.

[62] Z. Xiao, Q. Yang, J. Huang, Z. Huang, W. Zhou, Y. Gao, R. Shu, and Z. He, "Terahertz communication windows and their point-to-point transmission verification," *Applied Optics*, vol. 57, no. 27, pp. 7673–7680, 2018.

[63] R. S. Stansbury, M. A. Vyas, and T. A. Wilson, "A survey of uas technologies for command, control, and communication (c3)," in *Unmanned Aircraft Systems*. Springer, 2008, pp. 61–78.

[64] A. Puri, "A survey of unmanned aerial vehicles (uav) for traffic surveillance," *Department of computer science and engineering, University of South Florida*, pp. 1–29, 2005.

[65] M. Zuckerberg, "Connecting the world from the sky," 2014.

[66] K. Kamnani and C. Suratkar, "A review paper on google loon technique," *International Journal of Research In Science & Engineering*, vol. 1, no. 1, pp. 167–171, 2015.

[67] M. Mozaffari, A. T. Z. Kasgari, W. Saad, M. Bennis, and M. Debbah, "Beyond 5g with uavs: Foundations of a 3d wireless cellular network," *IEEE Transactions on Wireless Communications*, vol. 18, no. 1, pp. 357–372, 2018.

[68] Q. Wu and R. Zhang, "Common throughput maximization in uav-enabled ofdma systems with delay consideration," *IEEE Transactions on Communications*, vol. 66, no. 12, pp. 6614–6627, 2018.

[69] A. Zanella, N. Bui, A. Castellani, L. Vangelista, and M. Zorzi, "Internet of things for smart cities," *IEEE Internet of Things journal*, vol. 1, no. 1, pp. 22–32, 2014.

[70] S. Samarakoon, M. Bennis, W. Saad, M. Debbah, and M. Latva-Aho, "Ultra dense small cell networks: Turning density into energy efficiency," *IEEE*

Journal on Selected Areas in Communications, vol. 34, no. 5, pp. 1267–1280, 2016.

[71] I. Bucaille, S. Héthuin, A. Munari, R. Hermenier, T. Rasheed, and S. Allsopp, "Rapidly deployable network for tactical applications: Aerial base station with opportunistic links for unattended and temporary events absolute example," in *MILCOM 2013-2013 IEEE military communications conference*. IEEE, 2013, pp. 1116–1120.

[72] J. Lyu, Y. Zeng, and R. Zhang, "Uav-aided offloading for cellular hotspot," *IEEE Transactions on Wireless Communications*, vol. 17, no. 6, pp. 3988–4001, 2018.

[73] Y. Pang, Y. Zhang, Y. Gu, M. Pan, Z. Han, and P. Li, "Efficient data collection for wireless rechargeable sensor clusters in harsh terrains using uavs," in *2014 IEEE Global Communications Conference*. IEEE, 2014, pp. 234–239.

[74] M. Asadpour, B. Van den Bergh, D. Giustiniano, K. A. Hummel, S. Pollin, and B. Plattner, "Micro aerial vehicle networks: An experimental analysis of challenges and opportunities," *IEEE Communications Magazine*, vol. 52, no. 7, pp. 141–149, 2014.

[75] Y. Zeng, R. Zhang, and T. J. Lim, "Wireless communications with unmanned aerial vehicles: Opportunities and challenges," *IEEE Communications Magazine*, vol. 54, no. 5, pp. 36–42, 2016.

[76] T. Shima and S. Rasmussen, *UAV cooperative decision and control: challenges and practical approaches*. SIAM, 2009.

[77] H. Menouar, I. Guvenc, K. Akkaya, A. S. Uluagac, A. Kadri, and A. Tuncer, "Uav-enabled intelligent transportation systems for the smart city: Applications and challenges," *IEEE Communications Magazine*, vol. 55, no. 3, pp. 22–28, 2017.

[78] S. K. von Bueren, A. Burkart, A. Hueni, U. Rascher, M. P. Tuohy, and I. Yule, "Deploying four optical uav-based sensors over grassland: challenges and limitations," *Biogeosciences*, vol. 12, no. 1, pp. 163–175, 2015.

[79] Y. Zeng, J. Lyu, and R. Zhang, "Cellular-connected uav: Potential, challenges, and promising technologies," *IEEE Wireless Communications*, vol. 26, no. 1, pp. 120–127, 2018.

[80] O. K. Sahingoz, "Networking models in flying ad-hoc networks (fanets): Concepts and challenges," *Journal of Intelligent & Robotic Systems*, vol. 74, no. 1-2, pp. 513–527, 2014.

[81] ——, "Networking models in flying ad-hoc networks (fanets): Concepts and challenges," *Journal of Intelligent & Robotic Systems*, vol. 74, no. 1-2, pp. 513–527, 2014.

[82] N. H. Motlagh, T. Taleb, and O. Arouk, "Low-altitude unmanned aerial vehicles-based internet of things services: Comprehensive survey and future perspectives," *IEEE Internet of Things Journal*, vol. 3, no. 6, pp. 899–922, 2016.

[83] P. Sudheesh, M. Mozaffari, M. Magarini, W. Saad, and P. Muthuchidambaranathan, "Sum-rate analysis for high altitude platform (hap) drones

with tethered balloon relay," *IEEE Communications Letters*, vol. 22, no. 6, pp. 1240–1243, 2017.

[84] M. Mozaffari, W. Saad, M. Bennis, and M. Debbah, "Unmanned aerial vehicle with underlaid device-to-device communications: Performance and tradeoffs," *IEEE Transactions on Wireless Communications*, vol. 15, no. 6, pp. 3949–3963, 2016.

[85] S. T. Muntaha, S. A. Hassan, H. Jung, and M. S. Hossain, "Energy efficiency and hover time optimization in uav-based hetnets," *IEEE Transactions on Intelligent Transportation Systems*, 2020.

[86] M. A. Cheema, M. K. Shehzad, H. K. Qureshi, S. A. Hassan, and H. Jung, "A drone-aided blockchain-based smart vehicular network," *IEEE Transactions on Intelligent Transportation Systems*, pp. 1–11, 2020.

[87] R. i. Ansari, N. Ashraf, S. A. Hassan, D. G.C., H. Pervaiz, and C. Politis, "Spectrum on demand: A competitive open market model for spectrum sharing for uav-assisted communications," *IEEE Network*, vol. 34, no. 6, pp. 318–324, 2020.

[88] S. A. R. Naqvi, S. A. Hassan, H. Pervaiz, and Q. Ni, "Drone-aided communication as a key enabler for 5g and resilient public safety networks," *IEEE Communications Magazine*, vol. 56, no. 1, pp. 36–42, 2018.

[89] A. Aftab, N. Ashraf, H. K. Qureshi, S. Ali Hassan, and S. Jangsher, "Block-ml: Blockchain and machine learning for uav-bss deployment," in *2020 IEEE 92nd Vehicular Technology Conference (VTC2020-Fall)*, 2020, pp. 1–5.

[90] M. K. Shehzad, S. A. Hassan, M. A. Luque-Nieto, J. Poncela, and H. Jung, "Energy efficient placement of uavs in wireless backhaul networks," in *Proceedings of the 2nd ACM MobiCom Workshop on Drone Assisted Wireless Communications for 5G and Beyond*, ser. DroneCom '20. New York, NY, USA: Association for Computing Machinery, 2020, p. 1–6. [Online]. Available: https://doi.org/10.1145/3414045.3415936

[91] A. A. Raja, M. A. Jamshed, H. Pervaiz, and S. A. Hassan, "Performance analysis of uav-assisted backhaul solutions in thz enabled hybrid heterogeneous network," in *IEEE INFOCOM 2020 - IEEE Conference on Computer Communications Workshops (INFOCOM WKSHPS)*, 2020, pp. 628–633.

[92] M. U. Akram, U. Saeed, S. A. Hassan, and H. Jung, "Uav-based air-to-ground channel modeling for diverse environments," in *2020 IEEE Wireless Communications and Networking Conference (WCNC)*, 2020, pp. 1–6.

[93] M. A. Jan, S. A. Hassan, and H. Jung, "Qos-based performance analysis of mmwave uav-assisted 5g hybrid heterogeneous network," in *2019 IEEE Global Communications Conference (GLOBECOM)*, 2019, pp. 1–6.

[94] M. K. Shehzad, S. A. Hassan, A. Mahmood, and M. Gidlund, "On the association of small cell base stations with uavs using unsupervised learning," in *2019 IEEE 89th Vehicular Technology Conference (VTC2019-Spring)*, pp. 1–5.

[95] A. Al-Hourani, S. Kandeepan, and S. Lardner, "Optimal lap altitude for maximum coverage," *IEEE Wireless Communications Letters*, vol. 3, no. 6, pp. 569–572, 2014.

[96] M. Mozaffari, W. Saad, M. Bennis, and M. Debbah, "Efficient deployment of multiple unmanned aerial vehicles for optimal wireless coverage," *IEEE Communications Letters*, vol. 20, no. 8, pp. 1647–1650, 2016.

[97] M. Alzenad, M. Z. Shakir, H. Yanikomeroglu, and M.-S. Alouini, "Fso-based vertical backhaul/fronthaul framework for 5G+ wireless networks," *IEEE Communications Magazine*, vol. 56, no. 1, pp. 218–224, 2018.

[98] M. A. Jan, S. A. Hassan, and H. Jung, "Qos-based performance analysis of mmwave uav-assisted 5g hybrid heterogeneous network," in *2019 IEEE Global Communications Conference (GLOBECOM)*. IEEE, 2019, pp. 1–6.

[99] I. Atzeni, J. Arnau, and M. Kountouris, "Downlink cellular network analysis with los/nlos propagation and elevated base stations," *IEEE Transactions on Wireless Communications*, vol. 17, no. 1, pp. 142–156, 2018.

[100] V. V. Chetlur and H. S. Dhillon, "Downlink coverage analysis for a finite 3-d wireless network of unmanned aerial vehicles," *IEEE Transactions on Communications*, vol. 65, no. 10, pp. 4543–4558, 2017.

[101] B. Galkin, J. Kibiłda, and L. A. DaSilva, "A stochastic model for uav networks positioned above demand hotspots in urban environments," *IEEE Transactions on Vehicular Technology*, vol. 68, no. 7, pp. 6985–6996, 2019.

[102] M. S. Omar, S. A. Hassan, H. Pervaiz, Q. Ni, L. Musavian, S. Mumtaz, and O. A. Dobre, "Multiobjective optimization in 5g hybrid networks," *IEEE Internet of Things Journal*, vol. 5, no. 3, pp. 1588–1597, 2018.

[103] A. Damnjanovic, J. Montojo, Y. Wei, T. Ji, T. Luo, M. Vajapeyam, T. Yoo, O. Song, and D. Malladi, "A survey on 3GPP heterogeneous networks," *IEEE Wireless communications*, vol. 18, no. 3, pp. 10–21, 2011.

[104] H. Munir, H. Pervaiz, S. A. Hassan, L. Musavian, Q. Ni, M. A. Imran, and R. Tafazolli, "Computationally intelligent techniques for resource management in mmwave small cell networks," *IEEE Wireless Communications*, vol. 25, no. 4, pp. 32–39, 2018.

[105] E. Ghunney, S. A. Hassan, and M. A. Weitnauer, "Impact of wrong beam selection on beam pair scanning method for user discovery in mmwave systems," in *2020 IEEE 91st Vehicular Technology Conference (VTC2020-Spring)*, 2020, pp. 1–5.

[106] R. Zia-ul-Mustafa and S. A. Hassan, "Machine learning-based context aware sequential initial access in 5g mmwave systems," in *2019 IEEE Globecom Workshops (GC Wkshps)*, 2019, pp. 1–6.

[107] S. Habib, S. A. Hassan, A. A. Nasir, and H. Mehrpouyan, "Millimeter wave cell search for initial access: Analysis, design, and implementation," in *2017 13th International Wireless Communications and Mobile Computing Conference (IWCMC)*. IEEE, 2017, pp. 922–927.

[108] A. Umer, S. A. Hassan, H. Pervaiz, Q. Ni, and L. Musavian, "Coverage and rate analysis for massive mimo-enabled heterogeneous networks with millimeter wave small cells," in *2017 IEEE 85th Vehicular Technology Conference (VTC Spring)*, 2017, pp. 1–5.

[109] S. A. R. Naqvi and S. A. Hassan, "Combining noma and mmwave technology for cellular communication," in *2016 IEEE 84th Vehicular Technology Conference (VTC-Fall)*. IEEE, 2016, pp. 1–5.

[110] S. Nawaz, S. A. Hassan, S. A. R. Zaidi, and M. Ghogho, "Throughput and energy efficiency of two-tier cellular networks: Massive mimo overlay for small cells," in *2016 international wireless communications and mobile computing conference (IWCMC)*. IEEE, 2016, pp. 874–879.

[111] M. S. Omar, M. A. Anjum, S. A. Hassan, H. Pervaiz, and Q. Niv, "Performance analysis of hybrid 5g cellular networks exploiting mmwave capabilities in suburban areas," in *2016 IEEE International Conference on Communications (ICC)*. IEEE, 2016, pp. 1–6.

[112] M. S. Omar, S. A. Hassan, H. Pervaiz, Q. Ni, L. Musavian, S. Mumtaz, and O. A. Dobre, "Multiobjective optimization in 5g hybrid networks," *IEEE Internet of Things Journal*, vol. 5, no. 3, pp. 1588–1597, 2017.

[113] H. Munir, S. A. Hassan, H. Pervaiz, Q. Ni, and L. Musavian, "Resource optimization in multi-tier hetnets exploiting multi-slope path loss model," *IEEE Access*, vol. 5, pp. 8714–8726, 2017.

[114] A. Umer, S. A. Hassan, H. Pervaiz, Q. Ni, L. Musavian, and S. H. Ahmed, "Secrecy outage analysis for massive mimo-enabled multi-tier 5g hybrid hetnets," in *2018 IEEE International Conference on Communications Workshops (ICC Workshops)*. IEEE, 2018, pp. 1–6.

[115] A. Ijaz, S. A. Hassan, and D. N. K. Jayakody, "A multiple region reverse frequency allocation scheme for downlink capacity enhancement in 5g het-

nets," in *2017 14th IEEE Annual Consumer Communications & Networking Conference (CCNC)*. IEEE, 2017, pp. 905–910.

[116] H. Munir, S. A. Hassan, H. Pervaiz, Q. Ni, and L. Musavian, "Energy efficient resource allocation in 5g hybrid heterogeneous networks: A game theoretic approach," in *2016 IEEE 84th vehicular technology conference (VTC-Fall)*. IEEE, 2016, pp. 1–5.

[117] I. F. Akyildiz, J. M. Jornet, and C. Han, "Terahertz band: Next frontier for wireless communications," *Physical Communication*, vol. 12, pp. 16–32, 2014.

[118] I. F. Akyildiz, C. Han, and S. Nie, "Combating the distance problem in the millimeter wave and terahertz frequency bands," *IEEE Communications Magazine*, vol. 56, no. 6, pp. 102–108, 2018.

[119] J. G. Andrews, A. K. Gupta, and H. S. Dhillon, "A primer on cellular network analysis using stochastic geometry," *arXiv preprint arXiv:1604.03183*, 2016.

[120] M. Mozaffari, W. Saad, M. Bennis, and M. Debbah, "Unmanned aerial vehicle with underlaid device-to-device communications: Performance and tradeoffs," *IEEE Transactions on Wireless Communications*, vol. 15, no. 6, pp. 3949–3963, 2016.

[121] W. Yi, Y. Liu, E. Bodanese, A. Nallanathan, and G. K. Karagiannidis, "A unified spatial framework for uav-aided mmwave networks," *IEEE Transactions on Communications*, vol. 67, no. 12, pp. 8801–8817, 2019.

[122] X. Wang and M. C. Gursoy, "Coverage analysis for energy-harvesting uav-assisted mmwave cellular networks," *IEEE Journal on Selected Areas in Communications*, vol. 37, no. 12, pp. 2832–2850, 2019.

[123] K. Ntontin and C. Verikoukis, "Toward the performance enhancement of microwave cellular networks through thz links," *IEEE Transactions on Vehicular Technology*, vol. 66, no. 7, pp. 5635–5646, 2017.

[124] J. Kokkoniemi, J. Lehtomäki, and M. Juntti, "Stochastic geometry analysis for mean interference power and outage probability in thz networks," *IEEE Transactions on Wireless Communications*, vol. 16, no. 5, pp. 3017–3028, 2017.

[125] Boulogeorgos, "Terahertz technologies to deliver optical network quality of experience in wireless systems beyond 5G," *IEEE Communications Magazine*, vol. 56, no. 6, pp. 144–151, 2018.

[126] T. Narytnyk, "Possibilities of using THz band radio communication channels for super high-rate backhaul," *Telecommunications and Radio Engineering*, vol. 73, no. 15, 2014.

[127] A. Umer, S. A. Hassan, H. Pervaiz, L. Musavian, Q. Ni, and M. A. Imran, "Secrecy spectrum and energy efficiency analysis in massive mimo-enabled multi-tier hybrid hetnets," *IEEE Transactions on Green Communications and Networking*, 2019, doi: 10.1109/TGCN.2019.2956433.

[128] C. Lin and G. Y. Li, "Indoor terahertz communications: How many antenna arrays are needed?" *IEEE Transactions on Wireless Communications*, vol. 14, no. 6, pp. 3097–3107, 2015.

[129] L. S. Rothman, "The hitran 2008 molecular spectroscopic database," *Journal of Quantitative Spectroscopy and Radiative Transfer*, vol. 110, no. 9-10, pp. 533–572, 2009.

[130] A. A. Raja, H. Pervaiz, S. A. Hassan, S. Garg, M. S. Hossain, and M. J. Piran, "Coverage analysis of mmwave and thz-enabled aerial and terrestrial heterogeneous networks," *IEEE Transactions on Intelligent Transportation Systems*, 2021.

[131] B. Galkin, J. Kibilda, and L. A. DaSilva, "Backhaul for low-altitude uavs in urban environments," in *2018 IEEE International Conference on Communications (ICC)*. IEEE, 2018, pp. 1–6.